ASSESSING MECHANICAL PROPERTIES OF THE CARDIOVASCULAR SYSTEM

A Dissertation

presented to

the Faculty of the Graduate School

at the University of Missouri-Columbia

In Partial Fulfillment

of the Requirements for the Degree

Doctor of Philosophy

---

by

MOUAYED HASSAN ZIADA AL-TOKI

Dr. Noah Manring, Dissertation Supervisor

December 2020

The undersigned, appointed by the dean of the Graduate School, have examined the dissertation entitled

ASSESSING MECHANICAL PROPERTIES OF THE CARDIOVASCULAR SYSTEM

presented by Mouayed Hassan Ziada AL-Toki

a candidate for the degree of doctor of philosophy and hereby certify that it is worthy of acceptance.

Professor Noah D. Manring

Professor Roger Fales

Professor Yuyi Lin

Professor Craig A. Emter

Professor Giovanna Guidoboni

ACKNOWLEDGEMENTS

First, I would like to give gratitude to God Almighty for helping me and always being with me everywhere.

Second, I would like to express many thanks to my excellent supervisor Dr. Noah D. Manring whom God sent him into my life to teach, support, and help me.

Third, I would like to give thanks to my lovely mother for being the secret to my lifelong success and for all the sleepless nights that I have caused her.

Fourth, I would like to extend my love and thanks to my wonderful father, loving wife and children for their support.

Fifth, I would like to express my deep appreciation for my wonderful friends, Joe Parmele, Jeanne Taylor, and Silvia Wyatt, David Lee Sowers, Benjamin Nathan Wellsand, and Linda Messimer who helped me learn English.

TABLE OF CONTENTS

LIST OF FIGURES

LIST OF TABLES

LIST OF ABBREVIATIONS

A	local cross-sectional area of the aorta
C	total cardiovascular capacitance
D	outside diameter of the aorta
D_o	outside diameter of the aorta when the blood pressure is zero
d	inside diameter of the aorta
d_o	inside diameter of the aorta when the blood pressure is zero
dv	an infinitesimally small volume of fluid
E	modulus of elasticity
h	thickness of the vessel wall
L	length of the aorta
P	blood pressure
P_d	diastolic pressure
P_m	mean arterial-pressure
P_s	systolic pressure
PWV	pulse wave velocity
Q	volumetric flow rate from the left ventricle, into the aorta
$\bar{Q}$	average volumetric flowrate across the aortic valve during the ejection period
R	total peripheral resistance
r	radius of the vessel
T	heartbeat period

T_e	ejection period
t	time
V	volume of blood in the aorta
u	blood velocity vector
ρ	density of blood
α	coefficient of radial expansion for the aorta
w	wall thickness of the aorta
δ	radial deflection of a thick-walled cylinder without capped ends
v	poisson's ratio
ΔP	pulse pressure
ΔT	delay time
ΔV	stroke volume

ABSTRACT

The elasticity of wall of the arteries plays a significant role in cardiovascular system. Capacitance of the aorta is predicative of cardiovascular events[1]. To get better understanding the function of the cardiovascular system, special attention should be paid to digest the traditional two-element Windkessel model. Because the Windkessel model provides information of cardiovascular function and which may be useful for prevention and diagnosis of hypertension. Our research presents a series of in vitro experimental studies of compliance, peripheral resistance, and pulse waves.

In this thesis, several studies have been achieved: 1) a mathematical model for the capacitance of the aorta is derived based upon the conservation of mass, and a specialized test device provided by BDC Laboratories is used to simulate the aorta by employing an arched silicone-rubber tube with a known capacitance. 2) applied and compared arterial compliance determined from blood pressure, arterial compliance determined from PWV, and mechanical capacitance in flexible tubes and animal calf aortae. 3) investigated using sensitivity analysis as the analytical technique to determine parameters which. 4) develop a new technique which based on blood pressure diagram of flexible tubes and animal aortas.

In the first study corresponding to chapter five, that the entire blood-pressure state may be plotted on a single blood-pressure diagram using three nondimensional groups. This diagram illustrates the impact of altering the capacitance and ejection period on the pulse pressure that exists within the aorta.

In the second study corresponding to chapter six, the sensitivity analysis that has been used to figure out sensitivity coefficients with the largest magnitude is based on the most sensitive parameter that can be adjusted if we want to alter a pressure.

In the third study corresponding to chapter seven, arterial compliance determined from blood pressure is more straightforward approach than arterial compliance determined from PWV to measuring the arterial stiffness. By that allowing hypertension to be managed.

In the last study corresponding to chapter seven, it is figured out that total cardiovascular capacitance plays a significant role in determining the risk factors for cardiovascular disease, and the systolic and diastolic pressures during the cardiac cycle. In addition to cardiovascular capacitance other parameters that contribute to creating blood pressure include total peripheral resistance, stroke volume, ejection period, and heartrate.

In conclusion, this research, combined with additional support may permit the realization for measuring arterial stiffness in the home setting. This research may make significant paradigm changes in prognosis and diagnosis of arterial stiffness and other cardiovascular events.

CHAPTER 1. INTRODUCTION

1.1. Introduction

Hypertension is defined as high blood pressure, which may shorten life if left untreated [2]. Changing in the mechanical properties of the large arteries induce hypertension. Why is it important to know the mechanical contributors to high blood pressure? While we were looking for a detailed answer, we found out that there are many reasons to be interested in knowing about arterial stiffness. How can we properly diagnose cardiovascular disease if we do not know what to measure, and why we measure it? This work helps us to reduce the negative effects of arterial stiffness, which is the underlying cause of a range of cardiovascular diseases including stroke, coronary disease, vascular disease, and heart failure [3]. Cardiovascular disease is listed as the leading cause of death about one-third of all deaths in the United States [4]. The most common type of these diseases is aortic stiffness that is a serious disease causing hypertension [5]. This is the reason why we have studied aortic stiffness.

Worldwide, there are many people who suffer from at least one type of cardiovascular disease that related to either the heart or vessel networks. The most common type of these diseases is aortic stiffness; that is a serious disease cause hypertension which is a kind of the high blood pressure that is known as the silent killer because the patient may not have any noticeable symptoms [6]. Blood pressure numbers are considered within normal range when these numbers of less than 120/80 mm Hg according to Table-1 which categorizes blood pressure in a guideline.

Hypertension is abnormally arterial high blood pressure; in other words, it is an increase in total peripheral resistance and a decrease in arterial compliance. Hypertension is one of the most important modifiable risk factors for cardiovascular disease which it is recognized as of the leading risk factors for human mortality.

Table 1-1. Blood pressure range [2].

Blood Pressure Category	Systolic Pressure (mm Hg)		Diastolic Pressure (mm Hg)
Normal	Less than 120	and	less than 80
Evaluated	120 -129	and	less than 80
Hypertension			
Hypertension Stage 1	120 – 139	and/or	80 – 89
Hypertension Stage 2	Higher than 140	and/or	Higher than 90

1.2 Cardiovascular System

Introducing the important aspects of the cardiovascular system is necessary for the understanding leading purposes of the presented work. Briefly speaking, the human cardiovascular system is composed of the blood, heart and two networks of vessels. To get a better understanding, according to the anatomical and operating principles of the biological circulating system [7], the circulatory system may be regarded as a hydro-mechanical scheme of the human circulating system shown in Fig. 1-1. This figure explains the concept of the cardiovascular system in term of a closed-loop hydraulic system.

We can consider the heart as being represented by four pumps: the right atrium, right ventricle, left atrium and left ventricle. The right atrium pumps the blood to the right ventricle which pumps it to the pulmonary circuit. The left atrium pushes the blood to the

left ventricle and the left ventricle has a much bigger job to do by pushing the blood to all the systems of the body periodically. The left ventricle works six times harder than the right ventricle [8], and both the right and left ventricle normally contract or beat at the same time and the same rate. Normal heart beats 70 to75 beats/min at rest and also each pump ejects about 5 liter/min at rest [1].

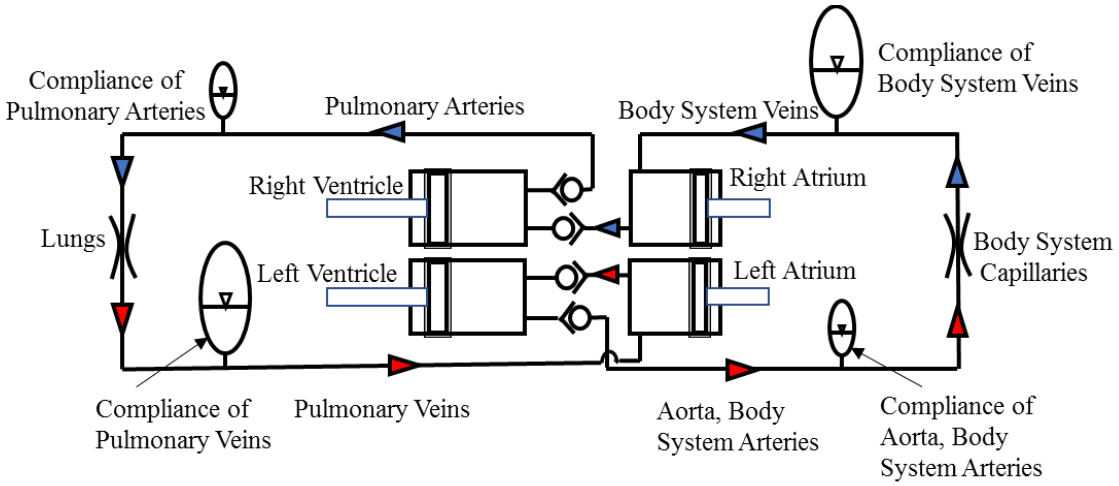

Figure 1-1. Modified hydro-mechanical scheme of the human circulatory system [9].

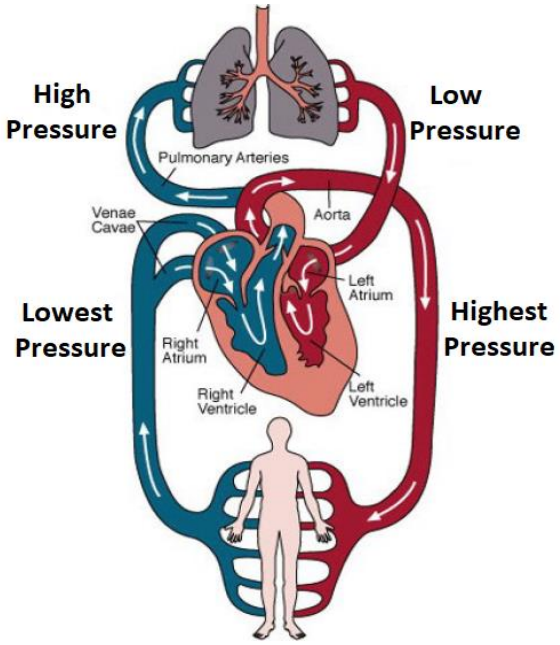

Figure 1-2. Schematic description of the circulatory system of the human body [1].

The first network as shown in Fig. 1-2 is the systemic network that stems from the aorta and then branches gradually into the thin wall vessels. These vessels are the capillary beds which eventually connect to the vena cava and the pulmonary network. The pulmonary network is shown in Fig. 2, which starts from the right ventricle to the lungs and then returns to the left atrium.

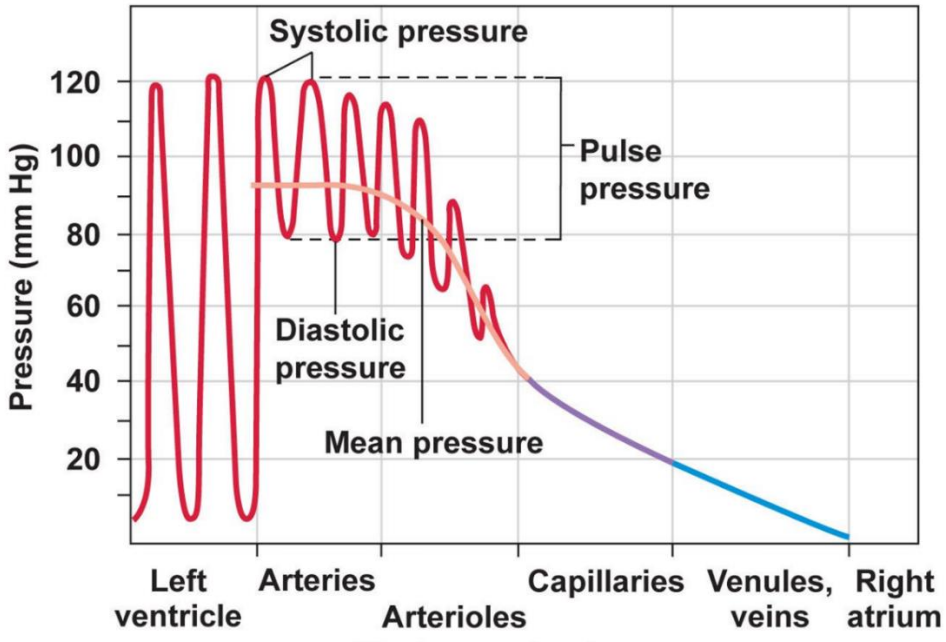

Figure 1-3. Normal blood pressure in the different the circulatory system [1].

Figure 1-3. illustrates how the change in the blood pressure in the large arteries varies between the systolic pressure (the peak pressure during heart contraction) and diastolic pressure (the minimum pressure when the heart expands and refills). We see from this figure that the blood pressure is highest in the aorta, and slightly reduces in the small arteries. The largest pressure drop occurs in the arterioles and capillaries, because they have the largest resistance. The high blood pressure stays in the aorta, and large arteries, so the compliance of these plays important role in maintaining the blood pressure in these arteries.

1.3 Elementary Hemodynamics

Blood flow through its vessels depends on the principles of fluid mechanics such as the conservation of mass despite complex physiological relations.

1.3.1 Compliance, Pressure, and Volume

The stored blood volume V (mL) in a vessel depends on the pressure difference across the vessel wall. Compliance is the mechanical property of a vessel wall that expresses a change of volume with respect to a change of pressure as

$$C \equiv \frac{dV}{dP} \quad . \tag{1.1}$$

The heart beats so it induces a wave along the aorta and arterial tree. This wave leads to expansion and contraction in the aorta and arterial tree. The change in the elasticity causes high pulse wave pressure.

1.3.2 Peripheral Resistance, Pressure, and Flowrate

Blood pressure difference ΔP (mm Hg) along a blood vessel determines the rate of blood flow Q (mL/s). Peripheral resistance is a hydraulic resistance due to blood viscous effects generated by the inner surface of the blood vessels. Peripheral resistance is dependent on the wall shear stress between the blood flow and inner blood vessel surface.

Total peripheral resistance to blood flow has a significant effect on the circulation system, and this resistance is the resistance to blood flow. According to Poiseuille's law with assuming laminar flow peripheral resistance mainly depends on the three

parameters; (1) vessel radius (2) vessel length (3) blood viscosity. Poiseuille's law states that:

$$R = \frac{8\mu L}{\pi r^4} \quad . \tag{1.2}$$

where R (*mm Hg.s/mL*) is peripheral resistance, μ (*mm Hg.s*) is the viscosity of blood, L (*cm*) is the vessel length, and r (*cm*) is the vessel diameter.

A vessel radius represents the most important parameter because a small change in the vessel radius causes a large change in the peripheral resistance because it has fourth power. The body has the ability to change the resistance to blood flow by constriction or dilation the vessels, so the constriction decreases the radius of the vessels and increases the resistance causing less blood to flow through these vessels, while the dilation produces the opposite effect.

Hagen-Poiseuille law was supposed to compute blood flow. It describes the linear relation between blood pressure drop and blood flow rate and is valid for circular flow passages undergoing laminar flow.

The flow rate between two places in a vessel is proportional to the pressure difference between the two locations.

$$Q = \frac{\Delta P}{R} \quad . \tag{1.3}$$

Where Q (*mL/s*) is the rate of blood flow, and ΔP (*mm Hg*) is the blood pressure difference along a blood vessel.

1.4 Blood Flow

There are two ways to study the blood flow in the aorta: distributed modeling and lumped parameter modeling. Distributed modeling has been conducted using computational fluid dynamics [5], while most often, lumped parameter arterial modeling has been done using the Windkessel model [10].

In 1899, the first lumped parameter arterial model was proposed by German physiologist Otto Frank as a mathematical model for simulating the blood pressure in the aorta [10]. He considered that the systemic arterial system as a closed hydraulic system and resembled the heart's pulsatile flow as a traditional fire engine hose as shown in Fig. 1-4. According to this model, the arterial system consists of a flexible reservoir composed of a flexible aorta and large arteries and inflexible small arterioles and capillaries with peripheral resistance to the blood flow.

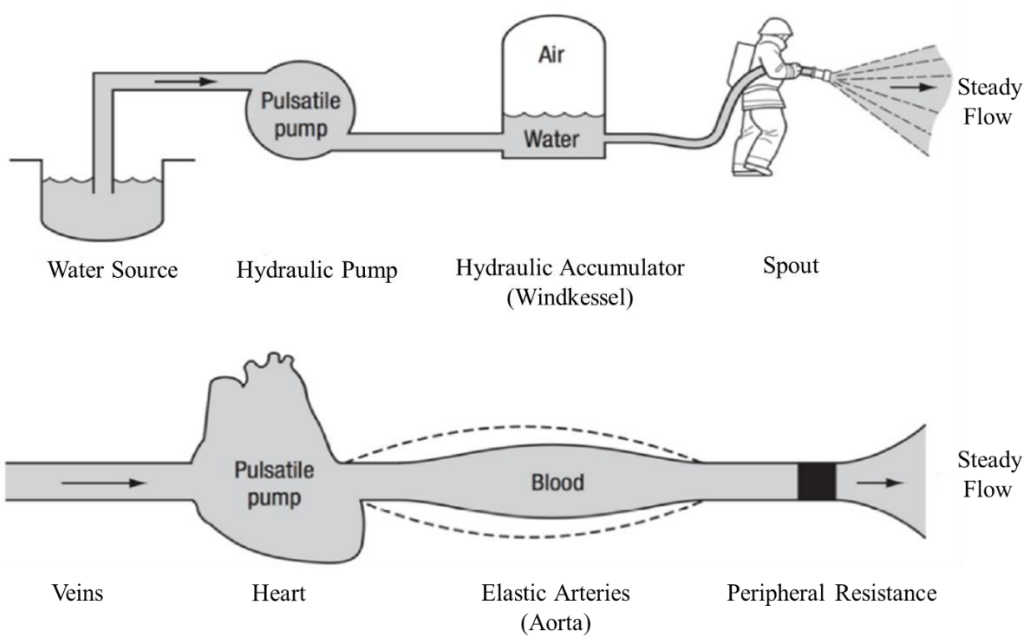

Figure 1-4. Modified diagrammatic representation of the Windkessel Model [11]. The hydraulic accumulator is the actual Windkessel and the large arteries act as the Windkessel, while the fire hose nozzle represents the peripheral resistance.

1.5 Arterial Stiffness

Arterial stiffness is a term that refers to reducing efficacy of the large arteries, but in hydraulic systems stiffness refers to increasing its efficacy. Large arteries work to dampen the heart's pulsatile flow to approximately continuous flow in capillaries (peripheral resistance), and to carry oxygen-rich blood away from the heart to the rest of the body. Arterial stiffness initiates and indicates several kinds of cardiovascular diseases.

Arterial stiffness can be measured noninvasively, and there are many methods that have been suggested for estimating arterial stiffness. These methods can be categorized into the local and global groups [11].

Local estimations can be measured directly using echo tracking (ultrasound device) and making resonance imaging (MRI), while regional estimations are commonly estimated from models of the pulse wave velocity (PWV).

The Pulse Wave Velocity (PWV) may be assessed by simultaneously recording the pressure waveform at two different sites in the arterial tree [12]. These measurements are typically taken using noninvasive methods. The distance between the two arterial segments is then divided by the time delay between the two waveforms. This calculated velocity of the blood pressure wave is called the PWV and is intended to be an indirect measure of the capacitance with the arterial tree. The carotid-femoral PWV is assessed by measuring the pressure waveform in the carotid artery in the neck, and comparing this to the pressure waveform in the femoral artery near the groin. The distance between these two pressure measurements must be assessed accurately to obtain a good PWV result.

PWV test is one that produces a result of 4 to 6 m/s for healthy person. A PWV that exceeds 13 m/s is considered to be a strong predictor of cardiovascular mortality [13].

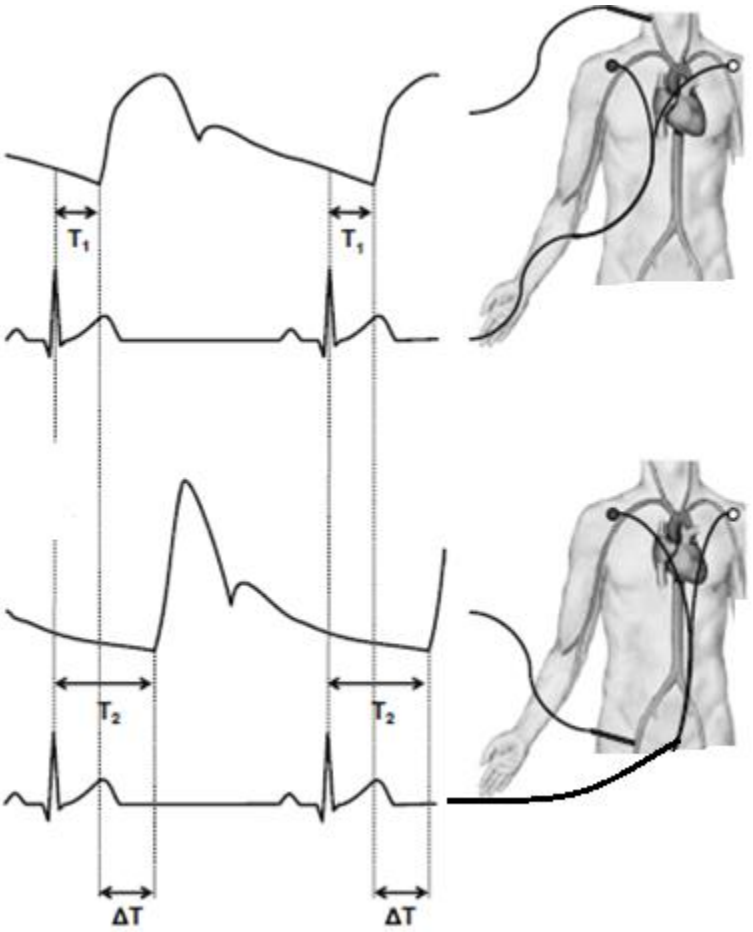

Figure 1-5. Carotid-femoral pulse wave velocity [12].

The PWV is the propagation speed of pressure wave along the arterial tree.

$$PWV = \frac{\text{Distance}}{(T_2 - T_1)} = \frac{\text{Distance}}{\Delta T} \quad . \tag{1.4}$$

In 1878, Moens and Korteweg presented their equation for thin walled vessel with homogenous elastic properties [14]. The Moens-Korteweg Equation describes the following relation between PWV and stiffness.

$$PWV = \sqrt{\frac{Eh}{2r\rho}} \quad . \tag{1.5}$$

Where E is the elastic modulus of the vessel, h is the thickness of the vessel wall, r is the radius of the vessel, and ρ is the density of blood. This method has several limitations because assuming constant and homogeneous vessel dimensions along the traveling path of the blood wave propagation. In this respect, blood pressure increases both vessel diameter and circumferential stress causing decrease vessel wall thickness. In other words, elastic modulus, diameter, and wall thickness depend on mean pressure [15].

1.6 Motivation

The motivation behind this study is to increase the understanding of underlying causes of hypertension and develop a new method for estimating the most sensitive parameters that affect blood pressure and to consider the particular influence of aortic capacitance. In our research, we developed a mathematical model for the capacitance of the aorta based on fluid mechanics (not the electrical analogy of the Windkessel model).

1.7 Hypothesis

Based upon the literature review thus far, the following hypothesis has been formulated for our research: That the mechanical properties of the blood pressure problem may be extracted using a fluid dynamics, lumped parameter model; that sensitivity analysis may be used to identify the properties that have the greatest impact on adjusting blood pressure characteristics.

1.8 Thesis Objectives

In this present study a novel approach is proposed to improve understanding of mechanical properties to high blood pressure. More specifically, this study is divided into six parts:

1- Reviewing the existing literature related to arterial compliance and map out research directions.

2- Developing and validating a mathematical model for the capacitance of the aorta is derived based upon the conservation of mass, and a specialized test device provided by BDC Laboratories is used to simulate the aorta using an arched silicone-rubber tube with a known capacitance.

3- Estimating the most sensitive parameters that affect blood pressures.

4- Using a method of in-vitro experimentation to demonstrate that the total cardiovascular capacitance may be reasonably obtained using known values of stroke volume, ejection period, heartrate, systolic pressure, and diastolic pressure. All five of these parameters are available from a fully exploited echocardiogram. If a reliable assessment of cardiovascular capacitance may be obtained in this way, certain advantages over the current “gold standard” of PWV testing may be achieved.

5- Comparing simulation results with experimental results.

6- Assessing PWV from waveform pressures and distance between two measured pressure sites.

7- Establishing the novel correlation between the arterial compliance and mean arterial pressure.

8- To experimentally apply and compare three different methods for computing arterial capacitances.

1.9 Thesis Outline

The work presented is organized into seven chapters. Chapter one gives the physiological description of the cardiovascular system with a brief introduction to the subject of the mathematical model of the cardiovascular system.

Chapter Two – The literature review will provide an extensive review of existing literature on arterial stiffness, peripheral resistance, and Windkessel models to determinate the mechanical behavior of the aorta. Each chapter is presented with its own individual introduction methodology, results and discussion.

Chapter Three – Analysis and Modeling Cardiovascular System. The objective of this chapter is to analyze and model an introduction to the development lumped parameter model (two-element Windkessel model) to simulate aortic pressure. This model helps to depict how blood pressure changes when different variables of cardiac are changed.

Chapter Four – An in-vitro experimental approach is used to validate the findings of our computational study in chapter three. We examine the results of the experimental data and compares it with mathematical model results.

Chapter Five – Blood Pressure Diagram. This chapter introduces deriving a non-dimensional number with the verified mathematical model that can be useful as a diagnostic tool when used to draw a blood pressure diagram to characterize the systemic cardiovascular system for any mammal having a cardiovascular structure similar to that

of swine. Although not yet shown, this diagram may one day enable physicians to diagnose various cardiovascular diseases and to quantify the impaired balance between the total peripheral resistance and arterial compliance.

Chapter Six- Sensitivity Analysis is performed to describe the sensitivity coefficients and to account for the effect of the main model parameters that play an important role in hypertension.

Chapter Seven – Vascular Stiffness. This chapter increases understanding of the arterial stiffness and presents the different powerful and implementable tools for the non-invasion assessment of the arterial capacitance.

Chapter Eight– Conclusion and Future Work. This chapter summarizes the dissertation's findings along with suggestions for future efforts.

CHAPTER 2. LITERATURE REVIEW

2.1 Introduction

This chapter reviews previous works that have been done related to blood pressure. Blood pressure measuring techniques date back to William Harvey (1578-1657) who is the first person studied the cardiovascular system and successfully discovered blood circulation [16]. After that, Giovanni Bernoulli (1608-1677) studied the contraction of the heart and explained the capacitive effect of the elastic arteries (now known as the Windkessel effect) [17]. After Giovanni, the Reverend Stephan Hales (1677-1746) found a similarity between arterial system and fire system which provide steady flow because an air compression chamber damps the pressure oscillations and provides a nearly steady flow. Hales also published a series of papers illustrating how blood pressure is altered by the elasticity of arteries [6]. The originality of the pulse velocity in physics developed by Isaac Newton (1642-1726), and later in the early 1800s, Thomas Young defined pulse wave velocity in terms of the change in pressure and volume of the vessel. Additionally, Moens and Korteweg (1878) presented their equation for thin walled vessel with homogenous elastic properties as the expression of pulse wave velocity in terms of dimensions and arterial elasticity [14].

Hale's concept was further expounded upon by Otto Frank to describe the elastic effects of the arterial system. Otto Frank presented the first mathematical to give a further description of the cardiovascular system in 1899. Later, this model became known as the Windkessel model. This model represents a hydraulic circuit that consists of a water pump working as a heart that has systole and diastole phase. He considers the arterial

system as an electrical analog of the parallel combination of peripheral resistance and compliance in parallel to simulate the cardiovascular system and to find parameters for this mathematical model.

Development in computer technology has made it possible to apply more sophisticated models and numerical analysis techniques to the description of arterial system function.

The two-element Windkessel was developed to describe the ventricular dynamics with systemic and pulmonary arteries. In order to study modeling effects of medication that change capacitance and resistance of vessel and modeling grafts that their resistance and capacitance lower than normal, there are many kinds of study the cardiovascular system. Therefore, we have used several keywords to do the search about literature review, for example, the Windkessel model to study arterial stiffness and peripheral resistance, left ventricular and EKG, wave propagation, and using the finite difference to study the cardiovascular system.

Capoccia, M. [18] reviewed a mathematical models for the arterial Windkessel to analyze a blood pressure and flow in the cardiovascular system relying on the conservation equations of mass, momentum and energy and applying them in electrical circuits. There are different kinds of the arterial Windkessel models in this article such as two, three, and four-element WK model. The two-element WK model is simple lumped parameter model and consists of parallel connection of resistor and capacitor only. Resistor R represents total peripheral resistance and capacitor C represents compliance of veins to predict diastolic pressure, but Fourier analysis of pressure and flow signals shows the weakness of this model.

In the three-element WK, the impedance R_c was connected in series with the two-element WK model to get more realistic aortic pressure and flows and it is widely used. In order to reduce the errors in the low frequency range, the four-element WK was found by connecting an inertial element L in parallel or series with impedance R_c.

Żyliński, M. et al [19] explain a pulse wave propagation phenomena which was employed to describe the change of pulse wave of arterial pressure which was obtained from finger and arterial flow velocity by using a mathematical model. The researchers explained that the shape of the pulse pressure graph of the carotid is similar to the shape of pulse pressure of the aortal. Also, they used the Modelflow method to compute the volume stroke and total peripheral resistance which is produced by blood viscosity and depends on the geometry of the vascular bed.

Kamoi, S. et al [20] employed mathematical models to estimate the ventricular stroke volume by using the three-element Windkessel Model (impedance, peripheral resistance, and compliance) which fixed one of the three Windkessel parameters at optimal value and evaluating the accuracy of stroke volume estimation from the aortic pressure waveforms. The experiments were achieved by using three healthy pigs. They get changes in stroke volume by changing of the thoracic cavity pressure, because expanding lungs directly affect on the stroke volume and arterial waveform. When the theoretical results were compared with experimental results, researchers found accurate stroke volume.

Charlton, P. et al [21] assessed cardiac output which is the flowrate (ml/min) from heart. Cardiac output equals (beat/min)×(ml/beat) and can also be estimated by observing the atrial blood pressure wave based on two-element Windkessel model during changes

in vascular tone. They used conservation of mass in analytical approaches to get stroke volume from pulsatile pressure from onset to end of the beat by using reduces assumptions for stroke volume to a function of pulsatile pressure and a constant of proportionality which is obtained by calibration with reference measurement. The stroke volume is proportional to the cardiac output, and also dissipated power.

Ruel, J., & Lachance, G. [22] in a mathematical model, differential equations used to get results to compare experimental data which was obtained from three actual bioreactors. In this paper, researchers built three hydraulic systems to mimic a human cardiovascular system and theoretical results were compared to experimental results of these hydraulic systems. This comparison was about the flow rate and pressure waveforms, and they got good coefficients of correlation between theoretical and experimental curves of flow rate. However, they got different values of coefficient of correlation for the pressure waveforms.

Hlaváč, M., & Holčík, J. [23] briefly described three Windkessel models by using MATLAB mathematical modeling computer program to do three things; to estimate values of Windkessel model parameters, to compare between these three models, and to know about a contribution of different arterial properties to the heart load. Propagating pressure and flow waveforms and the input impedance of these models were predicted minutely. In this paper, there is a recommendation that the four-element Windkessel model is a good method to know time dependency of blood pressure and using the two-element Windkessel if we want to get only the values of systolic and diastolic pressure.

Tsanas, A. [24] derived and used a comprehensive computational model in a created two-element Windkessel model to predict the arterial pressure and the cardiac

output of humans. The created model was derived using a method similar to the Kirchhoff law for electrical resistance and capacitance which gave more sense about blood pressure resistance and blood vessel capacity. This model has many benefits such as being an easy, cost-effective estimation of the arterial pressure serving non-experts. In this study, the researchers used real data from a treadmill test of 208 patients of men and women who had different ages. Some of them were smokers and either had systemic hypertension or high cholesterol. The others were healthy. Some factors were used for model input like, age, sex, used drug, fitness, and habits. They concluded that his model offers a good agreement (5% error) as compared with physiological observations of arterial pressure.

Choudhury, A. et al [25] estimated human blood pressure by the photoplethysmographic method using two-element that reduces the number of unknown variables which are internal parameters that affect human blood pressure as they are studied in the three or four-element Windkessel which is a high accuracy. This methodology outperformed pervious two researches because it obtained better results more than the standard methodologies which directly estimate blood pressure from photoplethysmography.

Guan, D., Liang, F., & Gremaud, P. A [26] [5, 25] focused on four points to do comparison between the four-element Windkessel model and the structured tree model in this study for a one dimensional atrial tree model. These points are namely the difference between the two models is wave reflection properties for the same equivalent resistance, compliance and inductance. In low frequency less than 100 Hz, for the WK model, the impedance was very sensitive, but frequencies for ST model higher 500 Hz the

impedance exhibited stronger dependence on the compliance. For the aortic impedance, pressure and flow waves, there are no large discrepancies between two models when they were compared with the vivo data. The last point of the two models under aging is; there is no a big difference between.

Ortiz-León, G. et al [27] used MATLAB Simulink R2013a that containing toolbox that is based on the SimPowerSystems to simulate six mathematical models that are WK2, WK3, WK4, WK coupled to the left ventricle, Systemic and pulmonary circulation (2V2A), and Ferreira's model (calculates the instantaneous arterial pressure in the same way as the Windkessel models) of flow and pressure in the cardiovascular system. The researchers studied the effects of different illnesses conditions and compared with reference hemodynamic parameters obtained at specialized laboratories. The most important parameters that were used to compare simulations are the cardiac output, aortic flow and the arterial pressure. When comparing between these six model, we the Systemic and pulmonary circulation (2V2A) computes higher number of parameters than other models that have less precision, and also the 2V2A model can show the pressure-volume loops that can be used to calculate the stroke volume of the left ventricle to see how much increasing the volume of blood in the left ventricle to pump the same volume of blood per beat.

Stergiopulos, N. et al [28] used a mathematical model and an electrical model to represent a heart parameters and the three-Windkenssel which used to resemble the arterial load. Researchers tested these models by using available experimental data of the isolated cat heart which was loaded by the three-element Windkessel. From this prediction test, good results were obtained when compared with experimental data

applying the model on human cardiovascular system to describe sensitivity systolic and diastolic pressure and stroke volume, the research used some equations which were derived for the human and checked it with empirical formula of the isolated cat experiments. They found a big difference for the elastance during this check between human and cat.

Fazeli, N., & Hahn, J. O [29] proposed a Windkessel method that used mean arterial blood pressure equation to estimate cardiac output (CO) and total peripheral resistance (TPR). This equation approximates the aortic flow single as a train of squire wave, and the area under each square wave equals to stroke volume. They approximated the aortic flow as square waves and assumed the pressure depends on arterial compliance as opposed to the standard Windkessel model. The proposal Windkessel model performs better than the standard Windkessel model according to a comparison between them and the experimental data that was obtained from anaesthetized pigs.

Baumgartner, B. et al [10] designed four controllers for Extra-Corporal Circulation (ECC) machine which represented the Westerhof model (three-element Windkessel). ECC is a technique that temporarily takes over the function of the heart and lungs during a surgery. These four controllers are a PI-Controller, a H∞ –Controller, a Model Reference Controller and a PI-Fuzzy Controller. They varied the peripheral resistance in fast (1 second to target) and slow (10second) to compute an error measure by using the Integral Absolute Error (IAE). When they did a comparison between each one to the other controllers, they found the best one is PI controller because the PI controller reaches the target values faster without overshooting or oscillations.

Kokalari, I. et al [30] reviewed 40 papers regarding CVS modeling and simulation and excluded the repetitive and similar researches to describe the proper dimensions from zero to three dimensional and compare modeling techniques for the study of cardiovascular dynamics according to their applications such as 0D represents pressure and flow changes in local areas of circulation, 1D represents the pulsed wave reflection effect in systemic circulation, ---etc. Researchers recommended that the 0-dimensional models are still largely used. They explained WK models at researches from the simple to complex WK model. This paper tells us that we cannot name a bad or good model, but evaluating model depends on the certain purpose of its use.

Maksuti, E. et al [31] dealt with the aging stage that is after middle age to determine parameter contributed in blood pressure changes by using two models that are four-element Windkessel model to represent the arterial system and the time-varying elastance model for the heart. These parameters are resistance and compliance. The structural changes cause compliance decreasing with age which is estimated from pulse wave velocity. For the age period from 20 to 80 years, the systolic pressure increases from 100 to 151 mmHg while diastolic aortic pressure decreases from 76 to 69 mmHg. When these values of pressures were compared to the population data of the Framingham Study, it was close to the population data. The aortic flow for this age period decreases because hypertrophy that is an increased muscle cross sectional area of left ventricular, also hypertrophy increases the blood pressure.

Choudhury, A. et al [25] estimated human blood pressure by the photoplethysmographic method using two-element that reduces the number of unknown variables which are internal parameters that affect human blood pressure as they are

studied in the three or four-element Windkessel which is high accuracy. This methodology outperformed pervious two researches because it has better results than the standard methodologies which directly estimate blood pressure from photoplethysmography.

Ghasemalizadeh, O.et al [32] designed an electrical circuit to simulate the human cardiovascular to compute aorta pressure. This circuit consists of three parts: heart, hands and carotids, and thoracic aorta and feet. They used amplifiers to generate the required current as a blood flow. The paper's graphics show calculated pressures for right and left ventricles are close to real pressure, and also calculated pressure for the ascending aorta is close to real pressure ascending aorta. In the other words, the results are in complete agreement with experimental data. The results reveal sensitive relationships among the important parameters during systole and diastole periods as the pressure is sensitive for compliance at the end systole and end diastole.

Chen, B. et al [33] presented an electrical human arterial system , for the left upper human limb, which was built and modeled to simulate the pressure and flows at the aortic root in the brachial artery. The amplitude of the impedance approaches to characteristic valve while increasing the frequency. The model reveals the defects of the three-element Windkessel model that is no variation in the middle frequency band. Therefore, researchers derived impedance curve in the middle frequency band. At the constant value of the heart rate, the increasing stroke volume leads to increase systolic pressure and diastolic pressure, but when fixing the value of the stroke volume and increase the heart rate that leads to increase the heart beat because three causes: shorten

diastolic period, reduce the peripheral blood flow, and remain more blood in the aorta at the end diastolic period. These results agree with the results of pervious literatures.

Du, T. et al [34] suggested a new model (CWK model) to improve the three-element Windkessel by adding a complex capacitance to get accurate capture of the fundamental-frequency time lag between the blood pressure and flow rate that means reducing the model error of the pulse wave in large arteries by extracting parameters from the impedance. They used mass and momentum equation of conservation law in the one-dimensional fluid dynamic for this. The Structured Tree (ST) model was employed to achieve the comparisons which were carried out among these three models each one to another based on impedance. The findings of these comparisons showed good agreements.

de los Reyes, V. A. A. [35] presented a mathematical model of the cardiovascular system to study the behavior of blood pressures under various conditions such as during rest or exercise conditions to predict the pulsatile pressures. The model was formulated in terms of an electric circuit analog. The aorta compartment was incorporated to indicate pressure changes detected by the baroreceptors which act as sensors in the cardiovascular system. The main objective of this paper is to develop a global pulsatile lumped compartment that predicts pressures pulmonary circulation as well as the pulsatile pressures in the finger arteries.

Wu, Y. et al [36] in order to approximate the response of human cardiovascular circulatory system, the dynamic model was developed by using a MATLAB Simulink. The resistance of blood vessels is critical time-varying parameter to estimate the aortic pressure for physiologic control by using nonlinear function of the pump head to meet the

physiologic need. To test the designed physiologic control system using different physiologic conditions, the adaptive optimal physiologic controller consists of three parts: an adaptive parameter estimation scheme to estimate the total peripheral resistance, an adaptive state observer using the estimate of the total peripheral resistance, and an optimal PI controller also using the estimate of the total peripheral resistance for controller parameter selection. The results of simulation and experiments show there is a small error in the aortic pressure estimation.

Parlikar, T. et al [37] estimated cardiac output and total peripheral resistance by observing arterial blood pressure waveforms. We know how to calculate a cardiac output from cardiac stroke volume and heartbeat, but here they compute the cardiac output from mean arterial pressure divide by total peripheral resistance but it differs from traditional method to compute cardiac output because it did not neglect variable pressure change in beat-to-beat ($\Delta P_n/T_n$). A least-square-error solution was used to achieve a calibration.

Gul, R., & Bernhard, S. [38] for anastomosis which is an interconnection between two vessels researchers utilized a computational model to compute sensitive parameters, finite difference a sensitivity analysis method which used two approaches norms and finite difference to compute sensitivity coefficients, and to study the effects of viscous flow resistance and terminal impedance on pressure and flow through anastomosis in two cases that (with and without anastomosis). They derived their model from the Navier-Sockes equation, and shell- equation for thin walled linear elastic tubes. At end systolic and at end diastolic and P_{max}, the results reveal that the compliance is most sensitive while the compliance has low sensitivity at P_{min} which shows a clear agreement with Ohm's law of hydrodynamics. The results reveal that pressure is sensitive for

compliance at end systole and end diastole while the pressure is sensitive for resistance and blood inertia at early systole and early diastole. Also, the flow is sensitive for resistance at early systole and early diastole. The comparison between the sensitivity analysis results and the norms results shows that the diameter and length of vessel have the most influential parameters.

Roy, R., et al [39] developed mathematical models of blood flow in an artery at steady and unsteady components to study the axial velocity field, pressure gradient, impedance and wall shear stress in the stenosis zones because these zones lead to higher blood pressure in the artery and the gradient pressure is not even at these zones, but outside the gradient pressure is constant. Models interpret a wall shear stress at critical height is higher than at the stenosis throat and this value of the wall shear stress be higher with increasing of stenosis size. Also, the models illustrate a difference in the value of the impedance increases with the stenosis height between Newtonian and non-Newtonian fluid. The models can measure the flow rate of blood, which in turn implies that is a good indication to diagnose and treat heart attack and strokes.

Srivastava, V. et al [40] investigated in the effects of the stenotic region, stenosis throats and stenosis critical height in an artery on the blood flow characteristics to show the value of the impedance increases with the stenosis size (height, length) and with small increasing values of the Casson fluid parameter (non-Newtonian behavior) which have more sensitive to stenosis than Newtonian. The magnitude of a shear stress at stenosis throats is higher than the stenosis critical height. The researcher saw similarity variations of impedance and shear stress at throats and critical height of stenosis.

Shah, S. et al [41] investigation about blood flow through stenosed artery was carried out by Power-law fluid model which describes two fluids: non-Newtonian fluid in the core region and Newtonian fluid for peripheral plasma. This model dealt with variation of wall shear stress with stenosis size for different values of stenosis length and with stenosis length for different values of stenosis shape parameter. The model also describes variation of resistance to flow with stenosis size for different values of stenosis shape parameter and with stenosis length for different values of stenosis size. The resistance to flow decreases due to stenosis shape parameter increases while it increases due to stenosis size and peripheral layer viscosity increases. The outcomes of the peripheral layer viscosity profiles were compared with the experimental data and previous known results.

Manring, N. D. [42] the effective bulk modulus was computed by cheap approach to help the engineers or others to measure the effective bulk modulus at high accuracy by using any component of a hydraulic system such as pump, valve, and actuator. In this study, hydraulic motor was used to compute the effective bulk modulus depending on the definition of fluid bulk modulus, equation of conservation of mass (continuity equation) at constant temperature (50 ^{o}C) of the fluid. A Newton-Raphson method was used to get the results. Manring approved that there is strong relationship between the mass density and the bulk modulus. Also, there is linear change between the effective fluid bulk modulus and pressure within a hydrostatic transmission. The bulk modulus results can only be trusted within ±337 MPa.

Tsai, W., & Savaş, Ö. [43] built a circulatory model to simulate vascular flow. He replicated three waveforms (sinusoidal, carotid, and coronary flow) by using two positive

displacement pumps (gear, and piston) in series, and distilled water was used as a hydraulic. He employed software to get acceptable response to an input signal by adjusting the gain settings and recording over 15 waveforms to compare with the input signal. He used the root mean square deviation between the input and the mean output measurement. The presenting steep changes leads to the greatest deviation, and validation tests show good agreement between the input and outlet waveforms.

Chen, T. et al [44] built a heart model in Simulink to model both diseased and normal rhythms of the heart as a network (an accurate fine-grained heart model) of communicating input-output hybrid automata that works directly with cell action potential to represent the voltage of cardiac cell signal to know the timing of the effective refractory period and relative refractory period. There is delay at AV node when electrical signal passes from SA node to AV node allowing the ventricles to fill fully using these delays to model various diseases. If any abnormality in passing electrical signal happens, the rhythm will change.

Taura, L. et al [45] used continuity equation to explain the mechanism that uses to achieve a balance between the output (cardiac output) of left ventricle and right ventricle because a heart consists of two pumps that are connected in series connection. The change from rest to exercise the stroke volume increased in this transition to reach up to steady state. The researcher interpreted the Frank-Starling mechanism by experiment and analysis, but they neglected the elastic of the vascular beds.

Gohean, J. [46] used a computational model to get an insight investigation about a simple comparison between two distinct models. The first model is an assist device for a synchronized valveless pulsatile left ventricular. Valveless, dual piston positive

displacement pump was used for that purpose. The second is an assist device for a continuous flow left ventricular. The comparison was done at the same level of flow rate. The researchers used vive porcine data in order to verify the validity of the suggested model as well. Also, they developed the computational model for human dynamic cardiovascular system to simulate native heart conditions for the two models above. Some results were compared with some real experimental data for a vivo porcine. It was concluded that the pulsatile pump produces higher cardiac output and cardiac pulsation than the continuous flow model and the suggested model work well for dynamic heart simulation.

Creigen, V.et al [47] the axial rotary pump was used between the aortic valves of the human heart that a patient with coronary artery disease. Researchers carried out an empirical model and developed a mathematical model for the cardiovascular dynamics to estimate some parameters. They used the first order differential equation to describe the pressures, volumes, and flow, and also to measure the resistances, and compliances for normal blood flow or calibrated to fit the model. Results point to there are no too much deviations from the normal blood flow values the model was examined with constant pump speed but it needs to thoroughly investigate under extreme circumstances to show the relationship between the pressure and flow.

Pironet, A. et al [48] cardiovascular was modeled by the multi-scale model that consists of seven model chamber seven resistances: systemic, pulmonary, mitral, aortic, tricuspid, pulmonary valves, and resistance of the proximal section of the pulmonary vein. The model describes three roles of the atrium: reservoir, conduit and pump. To

prevent flow through valve electrical diodes were used. The used governing equations are the Poiseuille's law to compute the flow and the continuity equation. Researchers focused on three main points: First, the left atrium and left ventricle which described by using widespread time-varying elastance. Second, the flow through mitral valve and final point is a simulation of preload reduction experiments. The cardiovascular model was compared with reference curves for dogs published in the previous literatures. The results reveal good agreements between experimental and simulated values.

Aurelio A. de los Reyes [49] presented numerical simulations to predict pulsatile pressure in a cardiovascular during rest and exercise conditions. In other word he focusses on the on left ventricle elastance and pressure during these conditions. Increasing heart rate leads to increase maximum elastance value and decrease the time of elastance curve peak. The used exercise was a bicycle-ergmeter with a workload of 50 W.

de los Reyes V, A., & Kappel, F [50] built a mathematical model by combining two models which are non-pulsatile global model and a simplified pulsatile left heart model. This mathematical model was formulated in an electrical analog. The blood pressure difference was represented as a voltage, the compliances were represented as capacitors, and resistances were resistances. They interpreted a ventricular elastance to measure a contractile state of the ventricle for rest and exercise conditions. There is a sigmoidal relationship between the maximum elastance and the heart rate. They compute a time-varying ventricular elastance to show an increasing ventricular elastance which depends on the time for start of diastolic relaxation and the time for systolic duration.

Gregory, S et al [51] built a mathematical model and Mock Circulation Loop to represent cardiovascular system in order to a cost of validation of cardiovascular assist

devices that need an expensive animal and clinical trials. In physical rig, they used pneumatic power to adjust the ventricular and atrial compliance chambers. MATLAB Simulink program which used to develop the mathematical model and get results that compared with the physical system. This comparison of results showed differences in some parameters that were fixed some of them.

Chaudhary, R. et al [52] comparison was carried out in this paper between a normal person EKG heart signals with different arrhythmic heart signals by using MATLAB program to see how much differences between them and where that are happened to diagnose heart abnormalities for example if there is no visible P wave in the CKG recordings and QRS complex and T wave are merged that means ventricular flutter. Also, this method helps to see the effects of drugs or devices which used to regular the heart. Also, this approach can involve identifying other heart disorders. Researchers did a comparison between the amplitude of normal EKG signal and abnormal signal.

AL-Ziarjawey, H. et al [6] presented a software package that is an easy approach to read EKG signal by designing a graphical user interface through using MATLAB program to analyze P wave, QRS wave and T wave. While the earlier methods use the numerical manipulation of signals (DSP technique). This software load EKG recordings from the source and then the software deals with these data to get such as get analysis data of EKG to detect PQRST values and selects which one needed to print out or specific samples. Also, the software helps physicians and engineers working together to solve heart problems.

Lillie, J. et al [53] examined the accuracy of the pulse wave velocity (PWV) which is generated by systolic contraction, and propagates along an atrial tree. PWV has

an important index for diagnosing the cardiovascular diseases because it is considered a measure of atrial stiffness. When atrial stiffness changes with age, cardiovascular diseases may lead to clear change of a vessel wall. The researchers used mathematical model to compare the accuracy in the prediction of PWV between single layer thick wall and multilayer wall. They mentioned that single thick layer model is sufficient to predict PWV.

Morris, P. et al [54] presented the benefits of using three dimensions in silico computational fluid mechanics (CFD) to model the cardiovascular system in health and disease in order to access a virtual physiological human representation that leads to reduce the risk related to clinical trials. This model can compute hemodynamic parameters that cannot previously be measured. In silico testing reduces risk to human, cost, time-consuming. In recognition of this, the US Food and Drug Administration (FDA) issued draft guidance in 2014 on the use of modeling to support regulatory submissions.

Petrescu, S., & ENACHE, V. [55] studied the possibility of modeling the cardiovascular using the concept and approach of the Finite Speed Thermodynamics (FST). FST is based on the expression of combined first and second law of thermodynamics for processes with finite speed. Researcher used the concept of the Stirling machine to represent the cardio-respiratory-vascular system and compared to thermodynamic machine because substances such as oxygen, carbon dioxide, and nutrients transport. They used pressure-volume diagrams to draw diagnose heart conditions diagram that represents the aortic pressure and atrial pressure and also when

mitral and aortic close or open. This look likes the Wigger diagram that is physicians have been used.

Cascaval, Radu C. et al [56] the effects of variable external conditions on propagation flow and pressure of the systemic circulation was studied by using the 55 largest arteries in an arterial network to collect flow and pressure data and put it in simulation model to get a dynamic illustrations of the 55 network edges in order to describe the dynamics of network during presence and absence of the changes.

Gharahi, H. et al [57] used a magnetic resonance imagining (MRI) to achieve investigated study of blood flow in carotid arterial with different viscosities to get four different viscosity models, Newtonian, Power-law, Carreau-Yasuda, and Casson. A comparison was carried out between these models and MRI results to know a relationship between shear stress and viscosity. There is also another comparison was performed between MRI measurements and CFD (Ansys Fluent) results in order to determine major drawbacks associated with program, but the combination of MRI with CFD analysis gets many benefits.

Nithiarasu, P. [58] used finite element flow algorithms which were proposed for 63 arterial segments of a systemic circulation. Researchers used computational robust that is Locally Conservative Galerkin (LCG) to get more accurate, faster and stabile in order to overcome the main drawbacks of the previous approaches such as Taylor-Galerkin method which including the time step. The advantage this proposed method (LCG) is no limitation on the time step and easy may be due to the matrix size. Also, when they studied the effect of three meshes refinements on the accuracy, they found approximately the same results, but the higher degree is faster.

Gul and Bernhard [59] studied the sensitivity of the cardiovascular parameters to identify subset sensitive parameters to find optimal measurement locations in the carotid bifurcation and optimal time regions in the pressure and flow waves. They used three variances based on the global sensitivity analysis methods; Sobol, FAST and a sparse grid stochastic collocation technique. Results appear most sensitivity of parameters was found in early systole, peak systole and end diastole, and also show compliance of vessels and blood inertia are sensitive only at right common while pressure ,flow resistance diameter and length of the vessel are sensitive within right common, right internal carotid and external carotid.

Gul and Bernhard [60] derived computational cardiovascular model for the arm arteries from the Navier-Stokes equation, continuity equation and shell-equation for thin walled and linear elastic tubes to analysis behavior of vascular network by using parameter sensitivity analysis. The results show that elastic and thickness of the arterial wall are a much lower while the pressure and flow was found strong dependence onto a variation in vessel diameter and wall. In other words, the flow resistance and diameter of the vessel are most sensitive parameters while wall thickness and elastic modulus are less sensitive. They got a good agreement by using norms to compare the variation in state variables according to parameter changes.

Cameron, K.,et al [61] explained the blood viscosity effect appears when a heart transplantation was carried out. Cameron, et al. presented a mechanical flow loop model to investigate the theoretical results of previous works for researchers. The model uses two types of fluid; Newtonian fluid (water) and non-Newtonian fluid (polyacrylamide) which compared based on non-dimensionalized centerline velocity, non-dimensionalized

velocity profiles and vector maps at five times steps during one pump cycle. The results give excellent agreement with theoretical finding of previous theoretical works.

He, F., et al [62] there are variations between commercial compliance grafts that need to study. In this paper researchers studied effects of compliance graft mismatch on flow distributions, wall stress and deformation of mechanical properties by presenting experimental artery model that helps in the selection of arterial grafts. They presented a model consisted of three segments had the same diameter with different wall stiffness was constructed to simulate arterial compliance mismatch in order to investigate the effects of compliance mismatch. The results show that wall shear stresses and wall strains are higher while wall stresses are lower at the more compliant section.

Bhavya S., et al [18] measured the blood velocities and blood pressure in arteries at any part of the body and also in difficult places as brain by replacing each segment of the artery by analogous electrical circuit with current source which represents incoming blood velocity. These lumped electrical models are validated with ultrasound images of the carotid artery of different patients. The value accurate of results of these simulations up to 5%.

Xiao, N., et al. [63] investigated the differences in computational prediction of flow and pressure between the 1-D and 3D. The made the physical dimensions, vessel wall properties, and inflow and outflow boundary conditions to be consistent between the 1-D models and their 3-D counterparts, and they used equivalent constitutive laws in 1-d and 3-d formulations. Results show a good agreement for this comparison especially during diastole and the largest differences occur in systole.

Segers, P., et al. [64] derived mathematical expressions for systolic, diastolic pressure and stroke volume to describe and apply any mammal cardiovascular as a function of six dimensionless cardiovascular parameters that were gotten from nine dimensions parameters by using Buckingham π theorem to describe the same problem. The nine-dimension parameters consist of four arterial parameters and five heart-related parameters. The study carried out on six intact sheep and they got cardiac output as derived from stroke volume. They got a good correlation between measured and predicted values.

Campo, A. [65] explained one of the most important characteristics need to be seriously considered is the Arterial stiffness because it is very good indications about cardiovascular screening. The sooner the detection, the safer for a patient. In their research, Adriaan Campo, et al, have compared between two ways to measure stiffness, displacement, and the velocity. They compared between pulse wave velocity (PWV) and ultrasound-based pulse wave imaging (PWI). They used Laser Doppler vibratory (LDV) to estimate the pulse wave speed. They have tested whether the phantom structure can be established using LDV for a vessel which some got hardening (increasing in the stiffness). Non-parametric Spearman relation and the analysis (Spearman- ρ =1 and p <0.05) and Bland–Altman analysis with a mean bias of -0.63 m/s between 0.35 and -0.90 m/s for limit agreement) were used in this research Four points of laser beam was selected for the test and velocity measurements. It was noted that the two results presented close results and they showed good agreement between them. They concluded that both methods were not able to estimate wave speed and the location of the inclusion.

Obeid, H., et al. [66] created a very simple technique to measure the Arterial stiffness which considered as one of the most important parameters in indicating the cardiovascular screening. This technique is simply mix results from Carotid–femoral pulse wave velocity (PWV), (cf-PWV) and Finger–toe PWV (ft-PWV). The last method was determined depending on a height chart using 66 patient's information. The main idea of the technique is to take the advantage of the second derivative of the running pulse wave by taking its maximum value and adding it to a wave was already processed using a suitable signal processing algorithm. They concluded that, the accuracy of the ft-PWV) can be increased by selecting the maximum value of the second derivative and added to optimized signals. However, it is just an estimation because the distance of the carotid to-femoral was estimated depend on the weights.

JIA-JUNG WANG et al. [67] studied the relationship between the radial vessel volume and the radial arterial pressure to determine the global compliance of the radial arterial wall in the normotensive subjects, and to establish the arterial compliance to pressure relationship in the ascending portion of arterial pressure waveform. To measure the radial arterial compliance, an arterial tonometer designed was used to register both the radial blood pressure and volume simultaneously for ten young subjects (male, 19~21 years) with normal systolic pressure of (110 6 mm Hg) and diastolic pressure of (65 5 mm Hg). Compliance of an artery is simply defined as the ratio of change in vessel volume and change in pressure. In the study, they assume the arterial blood pressure is logarithmically related to the arterial volume. The radial arterial blood pressure and vessel volume change in the ten subjects were measured with the tonometer. They conclude that The arterial global compliance, calculated as the ratio of maximum change

in arterial volume and pulse pressure, may be a convincing parameter for characterizing the arterial stiffness, although pressure-dependent.it is suggested that when we would like to make a comparison between two arterial wall compliances in different physiological situations, they should be determined at the level of mean arterial pressure.

Z. Keshavarz-Motamed et al. [68] presented a Model for the impact of concomitant aortic stenosis and coarctation of the aorta on left ventricular workload The objective of this work was to develop a lumped parameter model allowing the investigation of the respective impacts of AS and COA on the left ventricular load. For this purpose, a formulation for instantaneous net pressure gradient through the COA was proposed and validated by comparing the results against in vitro experiments. The suggested model was then applied to calculate the LV work for different severities of AS and COA. Further validations were performed by comparing the flow rate through COA with in vivo MRI measurements published in the literature. This model includes three different sub-models: (1) left heart arterial model; (2) AS model; (3) COA model.

They conclude that the lumped parameter model is able to estimate left ventricular stroke work using non-invasive data, which makes it suitable for clinical practice. It can be used to guide the choice of the optimal operative procedure (aortic valve replacement and/or COA repaired surgery) by providing potential outcomes of surgery in such patients. This is an important issue since the benefit of a single procedure can be limited by the remaining overload from the untreated pathology. The interesting results obtained through this study need, however, to be further validated using in-vivo animal experiments to investigate the effects of physiologic parameters such as heart rate

variation, anatomical differences, collaterals and upper body on pressure, flow and ventricular function.

McCombie et al. [69] developed a method to estimate pulse wave velocity as it relates to blood pressure using peripheral PPG measurements and to present a means of calibrating those measurement to peripheral arterial blood pressure. In-line PPG sensors were placed at a fixed distance to measure PWV using the fact that PWV will be equal to the difference of the distance traveled over the difference of the time to travel. Blood pressure equations were derived using PWV. They show that PWV is experimentally and possibly measured using two PPG sensors located at the wrist and finger. Experimentation has shown that it is possible to observe the alterations in PWV measurements produced by varying inter-arterial hydrostatic pressure.

2.2 Summary:

The literature review presented above is intended to support this thesis by describing the role of the aorta in adjusting the blood pressure. In recent years, one of the common objective of many the aforementioned research project was to fully understand the correlation between the reduction of the arterial compliance and the hypertension, so researchers have become increasingly interested in estimating the peripheral resistance and arterial compliance (arterial stiffness) in order to solve the problem of high blood pressure. As previously noted, it can be noticed that some works have relied on either the Windkessel models [18, 20-23] or computational fluid dynamics [46, 54, 55]. Some of researchers have enhanced their studies by experimental data [28, 29, 48, 62]. Researchers have concluded that arterial stiffness plays an important role as does the

peripheral resistance in the cardiovascular system, and clinicians are currently seeking ways to estimate these values noninvasively[19, 31, 36, 37, 50]. Arterial stiffness can be measured noninvasively by estimating the compliance. Several different approaches to estimating and describing arterial stiffness as aortic pulse wave velocity, aortic augmentation index, and central systolic pressure have been used [53, 69], or local determination. PWV is the velocity of the pulse wave traveling through an artery that is a function of the compliance of the artery that means the compliance of an artery can be indirectly observed by PWV in the artery while local determination that can be measured by using techniques of ultrasound or magnetic resonance imaging (MRI) devices [57].

Ultrasound devices have limited resolution and difficult to detect small changes in vessel diameter that relies on the ability of the operator to image the vessel wall. Although MRI has the advantage of being noninvasive it remains expensive and the availability of scanning facilities is limited. Therefore, the role of this technique in clinical practice is doubtful although it continues to be used in research. Sensitivity analysis techniques have been used to estimate cardiovascular model parameters that are most sensitive and play as the key is used to diagnosis the cardiovascular problems. Researchers [38, 58-60], who worked on or used sensitivity analysis for their researches stated that sensitivity analysis was very helpful to get an insight into how sensitive parameters affect cardiovascular.

Finally, to the best my knowledge, no one has worked on pressure rise rate equation to plot a blood pressure diagram and get sensitive parameters for cardiovascular from this equation. The study focuses specifically on the feasibility of non-invasively

estimating compliance through the pressure rise rate equation and how much agreement with results.

CHAPTER 3. MODELING AORTIC PRESSURE

3.1 Introduction

Prediction and diagnosis of cardiovascular diseases are an increasingly growing interest, and different mathematical models have been developed and applied. We used a lumped parameter model to account for a strong correlation between high blood pressure and reduction in arterial compliance. It is important to identify the mechanical factors that contribute to hypertension.

The first aim of this chapter is dedicated to analysis and modeling the cardiovascular behavior which have been developed to characterize the elastic properties of arteries by characterizing hemodynamic properties of interest include blood pressure, stroke volume, heartrate, ejection period, peripheral resistance, and arterial capacitance. Each of these properties has been used to diagnose patient health and to suggest clinical treatments for cardiovascular disease; however, at least four of these six markers are not easily measured without using invasive methods.

The second aim of this chapter is to find an expression for each mean arterial pressure, pulse pressure, total peripheral resistance and arterial compliance relying on the hemodynamic properties.

3.2 Heartbeat Schematic

With the purpose of developing the mathematical model that follows, we first present a description of the hemodynamic terms that will be used later. Figure 3-1 shows a schematic of the blood pressure within the aorta and the volume changes that occur

within the left ventricle during a single heartbeat. In this figure, the duration of the heartbeat is shown by time T, and the ejection period is shown by the symbol T_e. During the beginning of the ejection period, the blood pressure in the left ventricle increases just above the pressure in the aorta thus opening the aortic valve to facilitate blood flow. The blood that is displaced from the left ventricle is pushed into the aorta, causing the pressure in the aorta to increase. The stroke volume that is displaced during the ejection period is shown in Fig. 3-1 by the symbol ΔV. Toward the end of ventricular systole, the blood pressure in the left ventricle begins to drop below the pressure in the aorta, causing the aortic valve to close. As shown in Fig. 3-1, the closing of the aortic valve occurs at time $t = T_e$. During ventricular diastole, and while the aortic valve is closed, blood in the aorta continues to flow across the body capillaries to the vena cava on the right side of the heart.

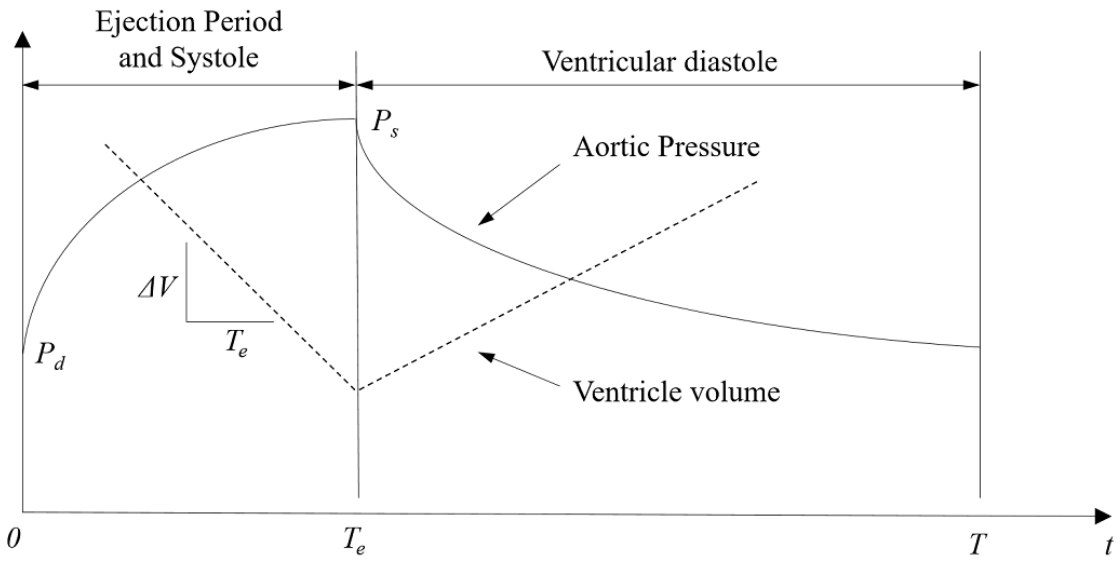

Figure 3-1. A schematic of aortic pressure and the stroke volume that is displaced by the left ventricle during a single heartbeat.

During this time period, the fluid pressure in the aorta decreases until the aortic valve opens again to facilitate flow from the left ventricle. Once this flow is facilitated by the aortic valve, the pressurization cycle for the aorta repeats itself for another heartbeat.

Four pressure characteristics in the aorta are of primary interest: 1) the systolic pressure, 2) the mean arterial pressure, 3) the diastolic pressure, and 4) the pulse pressure. The systolic pressure is shown in Fig. 3-1 by the point labeled S and the diastolic pressure is shown by the points labeled D in two places. The mean arterial pressure is not labeled in Fig. 3-1 but is roughly halfway between the systolic and the diastolic pressure. The pulse pressure is simply the difference between the systolic and diastolic pressure.

3.3 Governing Equation and Boundary Conditions

Blood pressures in the aorta can be mathematically be described using fluid dynamic equations in order to derive the governing equations that describe blood pressures in the aorta, we start from the basic law of fluid mechanics and take into account certain assumptions. The fluid dynamics of the aortic flow associated with systolic and diastolic pressures it can be depicted in Fig. 3-2. The aortic flow can be summarized as the aortic expanding with blood, contracting it through the body and expanding back again to start a new cycle. During these expansions some of blood flow through the body.

The systolic action is when blood is ejected from left ventricle to the aorta and diastolic action is when the left ventricle refilled with blood and relaxes. The aortic pressure may be described using the Windkessl Mode that relies on the pressure-rise equation.

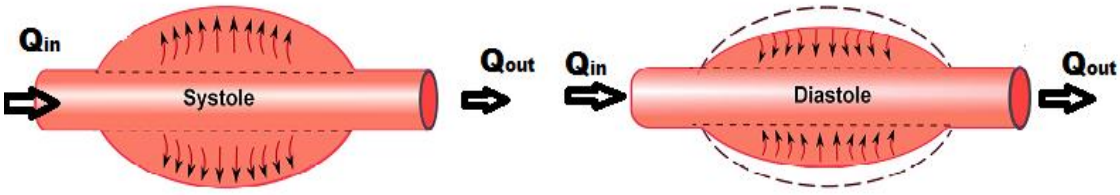

Figure 3-2. Blood flow through the aorta modified [70].

3.3.1 Pressure-Rate Equation

Pressure rise rate equation is one of the most useful equation that has been using in analysis and modelling in hydraulic control system [71]. This equation is ordinary

differential equation (ODE) that describes the dynamics of pressure within the aorta as shown in Fig. 3-2 blood pressure behavior in the aorta.

$$\frac{dP}{dt} = \frac{\beta}{V}\left(Q_{in} - Q_{out}\right) \quad . \tag{3.1}$$

where P is the blood pressure in the aorta, t is time, V is the volume of the aorta, β is the bulk modulus of blood, Q_{in} is the volumetric flow-rate of blood across the aortic valve into the aorta, and Q_{out} is the volumetric flow-rate of blood out of the aorta.

The flow out of the aorta faces a resistance.

$$Q_{out} = \frac{1}{R}P \quad . \tag{3.2}$$

If we have a perfect close system with no blood losses, we may say that the rate of storage equals to the difference inflow and outflow. Thus,

$$\frac{V}{\beta}\frac{dP}{dt} = Q_{cardiac} - \frac{1}{R}P \quad . \tag{3.3}$$

Thus,

$$C\frac{dP}{dt} = Q_{cardiac} - \frac{1}{R}P \quad . \tag{3.4}$$

This equation is a fluid mechanics version of the traditional two-element, Windkessel model that represents a perfect system with no fluid losses, and we assumed the pressure inside atrium equals zero. Where P is the blood pressure in the aorta, t is time, C is the capacitance of the aorta which describes the change in the aortic volume with respect to pressure, $Q_{Cardiac}$ is the volumetric flow-rate of blood across the aortic valve into the aorta, and R is the peripheral resistance of the body as depicted in Fig 3-3.

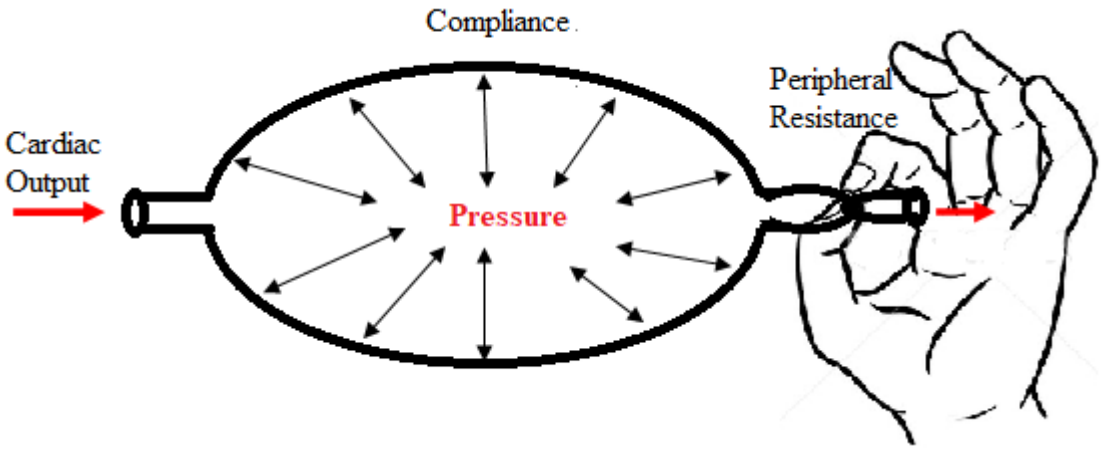

Figure 3-3. Depiction of the pressure-rise-rate equation.

If the pressure-volume relationship is linear, the compliance will be a constant while if the pressure-volume relationship is nonlinear, the compliance will be not constant but depends on the level of the pressure.

3.3.1 Modelling of Systolic and Diastolic Pressures

Blood pressure is the blood force against blood vessels during blood flow. There are two components in blood pressure reading: systolic blood pressure is the higher number that indicates to heart contacting and to the highest level of blood force against the artery wall. Diastolic pressure is the lower number that indicates to heart relaxing and to the lowest level of blood force against the artery wall. The blood force is crucial to make the blood flow.

The average volumetric flowrate across the aortic valve during the ejection period as

$$\bar{Q} = \begin{cases} \dfrac{\Delta V}{T_e} & 0 < t < T_e \\ 0 & T_e < t < T \end{cases} , \tag{3.5}$$

Where ΔV is the stroke volume for the left ventricle during the ejection period T_e. From an analytical perspective, it would be convenient if Eq. (3.5) could be used to model the cardiac output $Q_{Cardiac}$ that is the ejection flow rate Q since this lends itself to the development of a closed-form expressions for the blood-pressure state.

Using Eqs. (3.4) and (3.5), where Q is modeled as $\bar{Q}$, a piecewise solution for the blood pressure may be obtained for the two regions of pressure.

For the ejection period, where $0 < t < T_e$, the pressure in the aorta we get a linear first order differential equation:

$$\frac{dP}{dt} + \frac{P}{RC} = \frac{\Delta V}{CT_e} \quad , \tag{3.6}$$

Integrate, at $t = 0,\ P = P_D$ and at $t = T_e,\ P = P_S$.

$$\int_{P_D}^{P_S} \frac{RCT_e}{\Delta VR - PT_e} dP = \int_0^{T_e} dt, \tag{3.7}$$

Eq. (3.7) has a solution of the form

$$-\frac{RCT_e}{T_e} ln(\frac{\Delta VR - P_S T_e}{\Delta VR - P_D T_e}) = T_e, \tag{3.8}$$

This result can next be written as;

$$\frac{\Delta VR - P_S T_e}{\Delta VR - P_D T_e} = e^{-\frac{T_e}{RC}}, \tag{3.9}$$

That means

$$P = \frac{R\Delta V}{T_e} - \left(\frac{R\Delta V}{T_e} - P_D \right) e^{\left(\frac{-t}{RC}\right)} \quad . \tag{3.10}$$

The systolic pressure during the ejection period, where $0 < t < T_e$

During diastole, there is no blood flow from the left ventricular, so, for normally operating aortic valve that leads to vanish the right-hand side of Eq. (3.6).

$$\frac{dP}{dt} + \frac{1}{RC} P = 0 \quad , \tag{3.11}$$

A direct integration yield,

$$-\int_{P_S}^{P_D} \frac{RC}{P} dP = \int_{T_e}^{T} dt, \tag{3.12}$$

We get

$$-RC \ln(\frac{P_D}{P_S}) = T - T_e, \tag{3.13}$$

That means

$$P = P_S e^{\left(\frac{-(t-T_e)}{RC}\right)} \quad . \tag{3.14}$$

Eq. (3.14) expresses an exponential decay equation which describes the drop in blood pressure and depends on the peripheral resistance and compliance.

Result can be rearranged and written as;

$$P_D = P_S e^{\frac{-(T-T_e)}{RC}} \quad . \tag{3.15}$$

Substituting Eq. (3.15) into Eq. (3.9)

$$\Delta VR - P_S T_e = \Delta VR.e^{\frac{-T_e}{RC}} - P_S T_e.e^{\frac{-T}{RC}}, \tag{3.16}$$

We get the systolic pressure equation

$$P_S = \frac{\Delta VR}{T_e}\left(\frac{1-e^{\frac{-T_e}{RC}}}{1-e^{\frac{-T}{RC}}}\right) \quad . \tag{3.17}$$

Substituting Eq. (3.17) into Eq. (3.15) we get diastolic pressure during ventricular diastole, when $T_e < t < T$.

$$P_D = \frac{\Delta V R}{T_e}\left(\frac{1-e^{\frac{T_e}{RC}}}{1-e^{\frac{T}{RC}}}\right) \quad . \tag{3.18}$$

This diastolic equation is an exponential decay equation that shows the drop-in blood pressure during the diastolic phase. In other words, diastolic pressure equation is exponentially decreasing depending on the peripheral resistance and compliance.

We can conclude that five parameters (stroke volume, heart rate, ejection period, total peripheral resistance, and arterial compliance) are sufficient to accurately describe systolic and diastolic pressure.

Eqs. (3.17) and (3.18) the first presentation of a closed-form solution for the systolic and diastolic pressure is given in the literature. It may be shown from this form that the peripheral resistance and the stroke volume are expected to scale all pressure terms. It may also be seen from Eqs. (3.17) and (3.18) that the resistance and capacitance provide a first-order time constant for describing how quickly the blood pressure changes. A small value of the product RC produces a faster response of the system. This is a well-known property for the time response of RC electrical circuits, which hearkens back to the electrical analogy of the Windkessel model.

Equations (3.17)and (3.18) illustrate that an increase in the stroke volume will increase all pressures proportionally, including the pulse pressure.

3.3.2 Modeling of Pulse Pressure

Pulse pressure may be calculated as the numeric difference between systolic and diastolic pressure as shown in Fig. 3-4. It is a useful predictor of heart attacks or other cardiovascular diseases and it a good approach to elevate a stiffness of the aorta [5].

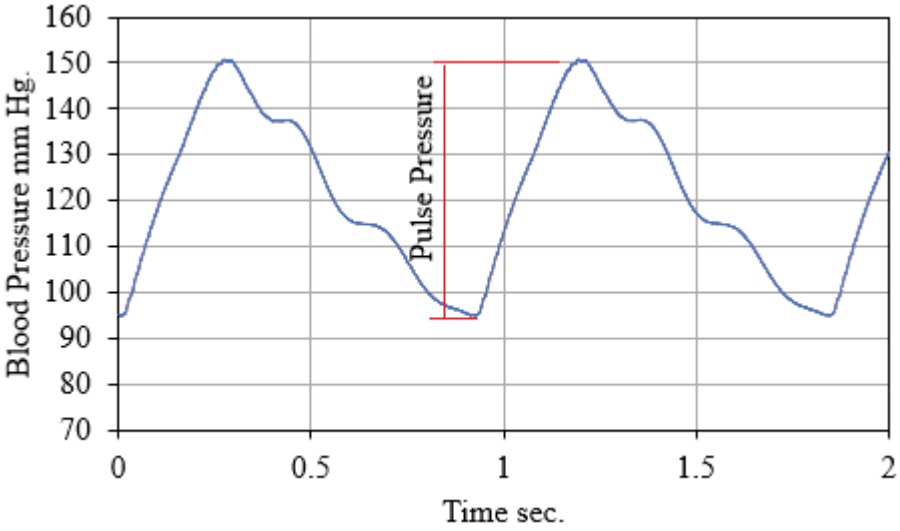

Figure 3-4. Example of a pulse pressure recorded by aortic simulator machine.

$$\Delta P = P_S - P_D \quad . \tag{3.19}$$

Substitute Eq. (3.18) into (3.19)as

$$\Delta P = P_D e^{\left(\frac{T-T_e}{RC}\right)} - P_D, \tag{3.20}$$

Rearranging,

$$\Delta P = P_D \left[e^{\left(\frac{T-T_e}{RC}\right)} - 1 \right] \quad . \tag{3.21}$$

Substituting Eq. (3.18) into Eq. (3.21) as

$$\Delta P = \frac{R\,\Delta V}{T_e}\ \frac{1-e^{\left(\frac{T_e}{RC}\right)}}{1-e^{\left(\frac{T}{RC}\right)}}\left[e^{\left(\frac{T-T_e}{RC}\right)}-1\right]\ . \tag{3.22}$$

Pulse pressure brings in set of variables which are related to the elastance of the aortic wall, peripheral resistance, stroke volume and the proportion of time in systole and diastole.

3.3.3 Modeling of Mean Arterial Pressure

Mean arterial pressure is the average of the blood pressure throughout arteries that is used by physician to access a patient's hemodynamic status. Using Eqs. (3.6) and (3.11) a piecewise integral may be used to obtain the mean arterial pressure within the aorta as follows:

$$P_M = \frac{1}{T}\int_0^T P\,dt\ , \tag{3.23}$$

The integration consists of two portion that are systolic and diastolic portion.

$$P_M = \frac{1}{T}\int_0^{T_e} P dt + \frac{1}{T}\int_{T_e}^{T} P dt \tag{3.24}$$

After integration we get expression of the mean arterial pressure

$$P_M = P_D\,\frac{T_e}{T}\ \frac{1-(P_S/P_D)^{\frac{T}{T-T_e}}}{1-(P_S/P_D)^{\frac{T_e}{T-T_e}}}\ . \tag{3.25}$$

$$P_M = \frac{\Delta V}{T}\times R\quad . \tag{3.26}$$

The reader will note that Eq. (3.26) is simply the average cardiac output $\Delta V / T$ multiplied by the peripheral resistance R. Equation (3.26) represents a common

understanding of the mean arterial pressure. As an average quantity, the mean arterial pressure is not dependent upon the capacitance in the aorta.

The simplicity of this result will be included in the blood-pressure diagram that follows. If we consider an ideal ejection period, such that $T_e / T = 1/3$, then Eq. (3.25) may be reduced to the following ideal form:

$$P_M = \frac{P_S + P_D + \sqrt{P_S\ P_D}}{3} \quad . \tag{3.27}$$

This result may be used for a quick approximation of the mean arterial pressure when the ejection period is not known exactly.

3.3.4 Modeling of Total Peripheral Resistance

Left ventricle has main function that pushes blood to all parts of the body through different kind of blood vessels, and blood flow faces an impedance that named peripheral resistance causes rising blood pressure.

Total peripheral resistance is a most important cardiovascular parameter. The physicians defined as the ratio of mean arterial pressure to cardiac output.

For steady state, there is conventional correlation among mean arterial pressure, cardiac output and total peripheral resistance that is.

$$P_M = \frac{\Delta V}{T} \times R \tag{3.28}$$

Where P_M is the time-averaged arterial blood pressure over a single cardiac cycle of period *T*.

The Eq. (3.23) is simply the average cardiac output $\Delta V / T$ multiplied by the

peripheral resistance R. Equation (3.23) represents a common understanding of the mean arterial pressure. As an average quantity, the mean arterial pressure is not dependent upon the capacitance in the aorta, or the ejection period.

$$R = \frac{P_M}{\Delta V / T} \quad . \tag{3.29}$$

An estimate of total peripheral resistance allows physicians to conclude the effect of the medications on cardiovascular system. Substituting Eq. (3.29) into Eq. (3.28) as

$$R = \frac{P_D T_e}{\Delta V} \frac{1-(P_S / P_D)^{\frac{T}{T-T_e}}}{1-(P_S / P_D)^{\frac{T_e}{T-T_e}}} \quad . \tag{3.30}$$

For the normal condition where $T_e / T = 1/3$, it may be shown that the peripheral resistance is given by

$$R = \frac{P_S + P_D + \sqrt{P_S P_D}}{3} \frac{T}{\Delta V} \quad . \tag{3.31}$$

3.3.5 Modeling of Compliance from Cardiovascular Parameters

The function of the arterial compliance is to store part of blood ejected from heart during systolic phase, and then to release it during diastolic phase. There is a strong link between arterial compliance and hypertension [72], so many researchers have been focusing on this topic in order to present better understanding for this link that may help treating hypertension.

Compliance is the ability for arteries to expand and contract under an applied pulse pressure. After we got equations for the systolic and diastolic pressure that help us to figure out approach to estimate the arterial compliance based on the two-element

Windkessel Model assuming a pressure in left atrium is zero and using exponential shape of the diastolic pressure decay that is represented by Eq. (3.15).

$$\frac{P_D}{P_S} = e^{\frac{-(T-T_e)}{RC}} \quad . \tag{3.32}$$

Take the natural log of both sides to simplify the Eq.

$$\ln\left(\frac{P_D}{P_S}\right) = \ln\left(e^{\frac{-(T-T_e)}{RC}}\right) \quad . \tag{3.33}$$

We assume the time interval T_e to T in diastole is constant.

Rearranging,

$$\ln\left(\frac{P_D}{P_S}\right) = \frac{-(T-T_e)}{RC} \quad . \tag{3.34}$$

Rearranging,

$$RC = -\frac{T-T_e}{\ln\left(\frac{P_D}{P_S}\right)} \quad . \tag{3.35}$$

The left term of the Eq. (3.35) is call time constant. We obtain the expression for the compliance

$$C = \frac{T-T_s}{R\ln\left(\frac{P_S}{P_D}\right)} \quad . \tag{3.36}$$

Substituting Eqs. (3.25)and (3.30) into Eq. (3.36) as

$$C = \frac{\Delta V}{P_D}\ \frac{T-T_e}{T_e}\ \frac{1}{\ln(\frac{P_S}{P_D})}\ \frac{1-(P_S/P_D)^{\frac{T_e}{T-T_e}}}{1-(P_S/P_D)^{\frac{T}{T-T_e}}} \quad . \tag{3.37}$$

Obtaining *C*, operationally define by the Eq. (3.37) requires P_S , P_D , ΔV , T_e and T that quantities can be conveniently measured in humans.

Again, for the normal case where $T_e / T = 1/3$, the aortic capacitance is simply

$$C = \frac{\Delta V}{P_S + P_D + \sqrt{P_S P_D}} \frac{2}{\ln(P_S / P_D)} \quad . \tag{3.38}$$

Equations (3.30) and (3.37) are significant results, in that they describe the mechanical properties of resistance and capacitance in terms of five cardiovascular parameters: stroke volume ΔV , heartbeat period T , ejection period T_e , systolic pressure P_S , and diastolic pressure P_D . In other words, if these five cardiovascular parameters are known the peripheral resistance and the aortic capacitance may be calculated using Eq.s (3.30) and (3.37). Three of these five parameters are routinely measured in the clinic (heartbeat period, systolic and diastolic pressure). The other two parameters must either be estimated or measured using an echocardiogram

3.3.2 Modeling of Capacitance from Mechanical Parameters

This is the second way to compute a compliance from mechanical parameters, so blood flow and blood pressure are causing stresses in the vessels and then these mechanical stresses can result in strain in the radial direction of the vessels. Let us study a cylindrical vessel as depicted in Fig. 3-5.

$$V = \frac{\pi}{4} d_o^2 L \quad . \tag{3.39}$$

Where V is the blood volume inside the vessel, d_o is the vessel diameter and L is the vessel length.

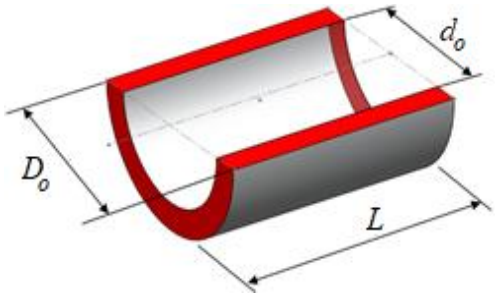

Figure 3-5. Section of a simulated aorta.

We assume that the vessel expands only in the radial direction, then the expanded vessel volume may be expressed as

$$V = \frac{\pi L}{4}\left(d_o + 2\delta\right)^2 = \frac{\pi}{4} L d_o^2 \left[1 + 4\left(\frac{\delta}{d_o}\right) + 4\left(\frac{\delta}{d_o}\right)^2\right] \quad . \tag{3.40}$$

Where d_o is the original diameter of the vessel, and δ is the radial deflection.

Simplify

$$V = \frac{\pi L}{4}\left(d_o^2 + 4\delta d_o + 4\delta^4\right) \quad . \tag{3.41}$$

Derive the volume

$$dV = \pi L d_o d\delta + 2\pi L \delta d\delta \quad . \tag{3.42}$$

The derivative of this expression with respect to the pressure P is then

$$\frac{dV}{dP} = \pi L d_o \frac{d\delta}{dP} + 2\pi L \delta \frac{d\delta}{dP} \quad . \tag{3.43}$$

From a strength of material textbook [73], we get that radial deflection of a thick-walled cylinder without capped ends is given by

$$\delta = \frac{d_o}{2}\frac{P}{E}\left(\frac{D_o^2 + d_o^2}{D_o^2 - d_o^2} + \nu\right) \quad . \tag{3.44}$$

Where P is the blood pressure, E is the tensile modulus of elasticity for the vessel, D_o and d_o are the nominal outside and inside diameters of the vessel respectively, and ν is Poisson's ratio for the vessel material.

From Pressure-Vessel Analysis, By definition the capacitance of a pressurized vessel is given by the change in volume, divided by the change in pressure. Mathematically this is expressed

$$C = \frac{dV}{dP} \quad , \tag{3.45}$$

which is essentially the constitutive equation presented in Eq.

Substituting Eq. (3.44) into (3.43)

$$\frac{dV}{dP} = \frac{\pi L d_o^2}{2E}\left(\frac{D_o^2 + d_o^2}{D_o^2 - d_o^2} + \nu\right) + \frac{\pi L d_o^2 P}{2E^2}\left(\frac{D_o^2 + d_o^2}{D_o^2 - d_o^2} + \nu\right)^2 \quad . \tag{3.46}$$

Compliance is defined as dV / dP where V and P are systemic arterial blood volume pressure respectively then

$$C = \frac{\pi L d_o^2}{2E}\left(\frac{D_o^2 + d_o^2}{D_o^2 - d_o^2} + \nu\right)\left[1 + \frac{P}{E}\left(\frac{D_o^2 + d_o^2}{D_o^2 - d_o^2} + \nu\right)\right] \quad . \tag{3.47}$$

If it is assumed that $P/E << 1$, then the compliance may be closely approximated as

$$C = \frac{\pi L d_o^2}{2E}\left(\frac{D_o^2 + d_o^2}{D_o^2 - d_o^2} + \nu\right) \quad . \tag{3.48}$$

α is a nondimensional geometry and material factor given by

$$\alpha = \frac{D_o^2 + d_o^2}{D_o^2 - d_o^2} + \nu \quad . \tag{3.49}$$

Using Eqs. (3.48) and (3.49) the mechanical capacitance equation for the blood vessels may be written as

$$C = \frac{\pi L d_o^2}{2E} \alpha \quad . \tag{3.50}$$

Using thick-wall pressure vessel analysis it may be shown that the inside volume of a pressurized circular-vessel is given by

$$V = V_o \left(1 + \alpha \frac{P}{E} \right)^2 \tag{3.51}$$

where V_o is the unpressurized volume of the vessel, P is the uniform pressure inside the vessel, E is the modulus of elasticity for the vessel material.

$$\alpha = \frac{D_o^2 + d_o^2}{D_o^2 - d_o^2} + \nu \quad . \tag{3.52}$$

Taking the derivative of Eq. (3.51) with respect to pressure produces the following expression for the capacitance of the circular vessel:

$$C = 2\alpha \frac{V_o}{E} \left(1 + \alpha \frac{P}{E} \right) \quad . \tag{3.53}$$

This applied pressure to the fluid is dimensionally significant, especially for an aorta with a high capacitance, and increases the PWV as shown in the equation. In order to obtain the mean arterial-capacitance for the aorta, in Eq. (3.53) the mean cross-sectional area of the aorta should be used for A and the mean arterial-pressure should be used for P. Note: AL is the nominal blood volume within the aorta. As shown in

Eq.(3.53), an increase in pressure will tend to increase the aortic capacitance but is only significant if $P/(\rho\,\mathrm{PWV}^2) > 1/10$. For a healthy human $\mathrm{PWV} \approx 6.5$ m/s and it can be shown that the pressure within the aorta can become a significant contributor to the capacitance in this case. Pulse wave velocity makes the pressure dependence for the capacitance fairly insignificant over a reasonable range of pressures. This will be discussed later.

3.3.3 Modeling of Capacitance from PWV

Figure 3-6. shows a schematic for an infinitesimal control volume within a segment of the aorta. The dashed line indicates the control volume which has a length shown by the symbol δx. The local pressure and blood velocity within the aorta are given by the symbols P and u respectively. The local cross-sectional area of the aorta is shown by the symbol A and the total length of the aorta segment is given by the symbol L. The aorta is a type of a hydraulic transmission line where the pressure varies as a function of time t and location in the *x*-direction. The wave equation for the pressure within the transmission line is classically known to exist in the following form [74, 75].

$$\frac{\partial^2 P}{\partial t^2} = c^2 \frac{\partial^2 P}{\partial x^2} \quad . \tag{3.54}$$

where c is the propagation speed of the pressure wave within the aorta. This speed is also known as the Pulse Wave Velocity (PWV) and the focus of this analysis is to derive an expression for this quantity as a function of all physically relevant parameters.

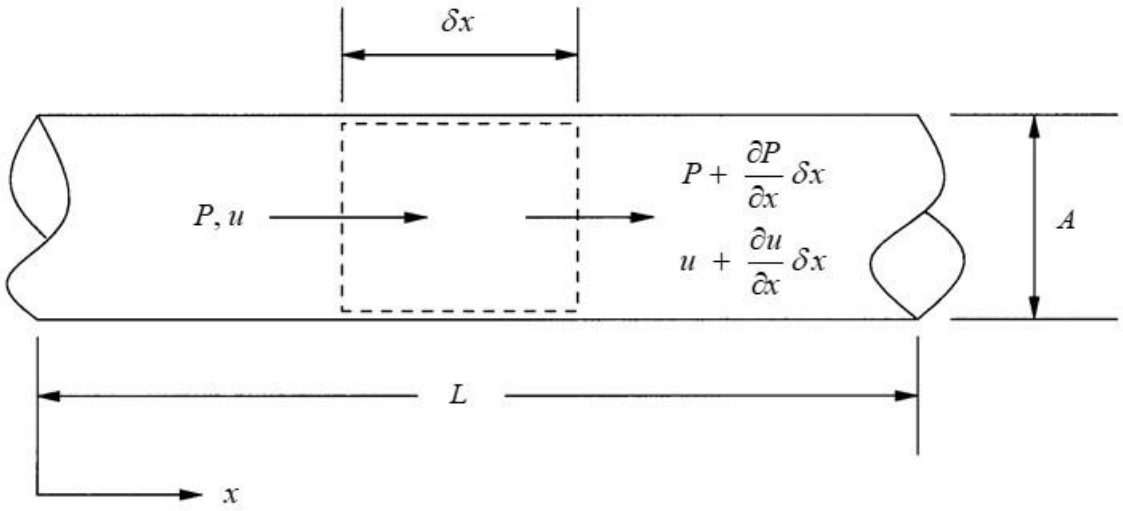

Figure 3-6. Schematic for an infinitesimal control volume within a segment of the aorta.

Using the Reynolds Transport Theorem, the conservation of mass for the control volume shown in Fig. 3-6 is given by

$$0 = \underbrace{\frac{\partial}{\partial t}\int_{cv} \rho \, dv}_{\substack{\text{Time rate-of-change} \\ \text{of mass within the} \\ \text{control volume}}} + \underbrace{\int_{cs} \rho \, (\mathbf{u}\cdot\hat{\mathbf{n}}) \, da}_{\substack{\text{Inflow of mass across} \\ \text{the control-volume boundary.}}} \quad . \tag{3.55}$$

In this expression ρ is the fluid density, dv is an infinitesimally small volume of fluid, $\mathbf{u}$ is the blood velocity vector, $\hat{\mathbf{n}}$ is a unit vector that points normally outward from the control surface across which blood is passing.

If we treat the blood as incompressible fluid, the fluid density in Eq. (3.55) may be cancelled from the expression and we are left with the following form for the conservation of mass:

$$0 = \frac{\partial}{\partial t}\int_{cv} dv + \int_{cs} (\mathbf{u}\cdot\hat{\mathbf{n}})\, da \quad . \tag{3.56}$$

The first integral in Eq. (3.56) may be expressed as

$$\frac{\partial}{\partial t}\int_{cv} dv = \frac{\partial}{\partial t}\left(\bar{A}\,\delta x\right) = \frac{\partial A}{\partial t}\delta x \quad , \tag{3.57}$$

where the average cross-sectional area of the control volume is given by

$$\bar{A} = \frac{1}{2}\left(A + A + \frac{\partial A}{\partial x}\delta x \right) \ . \tag{3.58}$$

and where quadratically small terms have been neglected in Eq.(3.57). The second integral in Eq. (3.56) may be evaluated to show

$$\begin{aligned} \int_{cs} (\mathbf{u}\cdot\hat{\mathbf{n}})\, da &= -u\,A + \left(u + \frac{\partial u}{\partial x}\,\delta x \right)\left(A + \frac{\partial A}{\partial x}\,\delta x \right) \\ &= -u\,A + u\,A + A\frac{\partial u}{\partial x}\,\delta x + u\frac{\partial A}{\partial x}\,\delta x + \frac{\partial u}{\partial x}\frac{\partial A}{\partial x}\,\delta x^2 \quad . \end{aligned} \tag{3.59}$$

$$\begin{aligned} \int_{cs} (\mathbf{u}\cdot\hat{\mathbf{n}})\, da &= -u\,A + \left(u + \frac{\partial u}{\partial x}\,\delta x \right)\left(A + \frac{\partial A}{\partial x}\,\delta x \right) \\ &= -u\,A + u\,A + A\frac{\partial u}{\partial x}\,\delta x + u\frac{\partial A}{\partial x}\,\delta x + \frac{\partial u}{\partial x}\frac{\partial A}{\partial x}\,\delta x^2 \quad . \end{aligned} \tag{3.60}$$

Neglecting quadratically small terms, this expression may be written as

$$\int_{cs} (\mathbf{u}\cdot\hat{\mathbf{n}})\, da = \frac{\partial (A\,u)}{\partial x}\,\delta x = \frac{\partial Q}{\partial x}\,\delta x \tag{3.61}$$

where it has been recognized that A times u is equal to the volumetric flow rate Q. Substituting Eq.s (3.57) and (3.61) into Eq. (3.56)produces the following expression for the conservation of mass:

$$0 = \frac{\partial A}{\partial t} + \frac{\partial Q}{\partial x} \quad , \tag{3.62}$$

where the axial length of the control volume δx has conveniently cancelled out. This

form of the conservation of mass will be used later to develop the pressure-wave equation for the aorta.

Similarly, using the Reynolds Transport Theorem, the conservation of momentum for the control volume shown in Fig. 3-6. is given by

$$\frac{D\mathbf{p}}{Dt} = \underbrace{\frac{\partial}{\partial t}\int_{cv} \rho\,\mathbf{u}\,dv}_{\substack{\text{Time rate-of-change}\\ \text{of momentum within the}\\ \text{control volume}}} + \underbrace{\int_{cs} \rho\,\mathbf{u}\,(\mathbf{u}\cdot\hat{\mathbf{n}})\,da}_{\substack{\text{Inflow of momentum across}\\ \text{the control-volume boundary.}}} \quad . \tag{3.63}$$

where $D\mathbf{p}/Dt$ is the material derivative of the fluid momentum vector $\mathbf{p}$.

As it turns out for the blood-pressure problem within the aorta, dimensional analysis may be used to shown that the inflow of momentum across the control-volume boundary is negligible compared to the time rate-of-change of momentum within the control volume. For this reason, the second term on the right-hand-side of Eq. (3.63) will be neglected and the conservation of momentum will be written as:

$$\frac{D\mathbf{p}}{Dt} = \frac{\partial}{\partial t}\int_{cv} \rho\,\mathbf{u}\,dv \quad . \tag{3.64}$$

According to Newton's second law, the time rate-of-change for the fluid moment must be equal to the forces that are acting on the surfaces of the control volume. If we neglect shear stress at the inside wall of the aorta and only consider the pressures acting to push the control volume in the positive *x*-direction, the left-hand-side of Eq. (3.64) may be written as:

$$\begin{aligned}\frac{D\mathbf{p}}{Dt} &= P\,A - \left(P + \frac{\partial P}{\partial x}\delta x\right)\left(A + \frac{\partial A}{\partial x}\delta x\right)\\ &= P\,A - P\,A - A\frac{\partial P}{\partial x}\delta x - P\frac{\partial A}{\partial x}\delta x - \frac{\partial P}{\partial x}\frac{\partial A}{\partial x}\delta x^2 \quad .\end{aligned} \tag{3.65}$$

Neglecting quadratically small terms produces the following result for the time rate-of-change for the fluid momentum within the aorta:

$$\frac{D\mathbf{p}}{Dt} = -\frac{\partial(P\,A)}{\partial x}\delta x \quad , \tag{3.66}$$

where the vector direction of this result is in the positive *x*-direction. Note: It is here where previous developments for the PWV equation have taken a different turn, treating A as a constant rather than considering this parameter to vary with respect to x. For example, see Reference [76]. This is inconsistent with the development of the conservation-of-mass equation presented in Eq. (3.62). It can also be shown that if the cross-sectional area is assumed to be independent of x at this point of development, the final PWV result will be independent of pressure and a significant physical contributor will be neglected.

If we consider the fluid density to be constant, and we assume that the fluid velocity within the control volume is uniform and average in the positive x-direction, the time rate-of-change of the fluid momentum within the control volume may be written as

$$\frac{\partial}{\partial t}\int_{cv}\rho\,\mathbf{u}\,dv = \rho\,\frac{\partial}{\partial t}\left(\bar{u}\int_{cv}dv\right) = \rho\,\frac{\partial}{\partial t}\left(\bar{u}\,\bar{A}\,\delta x\right) = \rho\,\frac{\partial Q}{\partial t}\delta x \tag{3.67}$$

where the average velocity of the fluid within the control volume is given by

$$\bar{u} = \frac{1}{2}\left(u + u + \frac{\partial u}{\partial x}\delta x\right) \tag{3.68}$$

and where the average cross-sectional area of the control volume $\bar{A}$ is given in Eq.(3.58) . Note: Quadratically small terms have been neglected in Eq. (3.67).

Substituting Eq.s (3.66) and (3.67) into Eq. (3.64) produces the following expression for the conservation of momentum:

$$0 = \frac{\partial Q}{\partial t} + \frac{1}{\rho}\frac{\partial (P\,A)}{\partial x} \tag{3.69}$$

where, again, the axial length of the control volume δx has conveniently cancelled. This form of the conservation of momentum will be used later to develop the pressure-wave equation for the aorta.

Equations (3.62) and (3.69) represent the conservation of mass and momentum respectively, for the blood flow passing through the aorta shown in Fig. 3-6. Taking the derivative of the conservation of mass with respect to time, and the derivative of the conservation of momentum with respect to the spatial coordinate x, the following equations may be written:

$$-\frac{\partial}{\partial t}\left(\frac{\partial Q}{\partial x}\right) = \frac{\partial^2 A}{\partial t^2} \quad \text{and} \quad -\frac{\partial}{\partial x}\left(\frac{\partial Q}{\partial t}\right) = \frac{1}{\rho}\frac{\partial^2 (P\,A)}{\partial x^2} \quad . \tag{3.70}$$

Because differentiation is a linear operator, we recognize that

$$\frac{\partial}{\partial t}\left(\frac{\partial Q}{\partial x}\right) = \frac{\partial}{\partial x}\left(\frac{\partial Q}{\partial t}\right) \quad . \tag{3.71}$$

Using Eqs. (3.70) and (3.71) the wave equation for the blood flow problem may be written as

$$\rho\frac{\partial^2 A}{\partial t^2} = \frac{\partial^2 (P\,A)}{\partial x^2} \quad . \tag{3.72}$$

This is the basic form of the wave equation that will be further developed in the following paragraphs using a constitutive model for the cross-section area A as a function of blood pressure P.

Equation (3.72) shows that the wave equation is dependent upon the local cross-sectional area A. For the circular geometry of the aorta, the cross-sectional area is given

by

$$A = \pi\left(r + \alpha P\right)^2 \tag{3.73}$$

where r is the local radius of the aorta when the blood pressure P is zero, and α is the coefficient of radial expansion for the aorta. Using pressure vessel analysis [73] it may be shown that the local coefficient-of-expansion for the aorta is given by

$$\alpha = \frac{\delta C}{2\pi r\, \delta x} \quad , \tag{3.74}$$

where δC is the local capacitance and δx is shown in Fig. 3-6.

By substituting Eqs. (3.73) and (3.74) into Eq. (3.72) and neglecting small terms, the wave equation may be written as:

$$\frac{\partial^2 P}{\partial t^2} = c^2 \frac{\partial^2 P}{\partial x^2} \quad \text{where} \quad c^2 = \frac{1}{\rho}\left(\frac{\delta V}{\delta C} + 2P\right) \quad . \tag{3.75}$$

In this equation c is the propagation speed of the pressure wave within the aorta. and $\delta V = \pi r^2 \delta x$, which is the unpressurized volume of blood at a specific location within the aorta.

The wave equation presented in Eq. (3.75) has been developed to describe the blood pressure at a specific time and location within the aorta. By rearranging terms in Eq. (3.75) it may be shown that the local capacitance within the aorta is

$$\delta C = \frac{\delta V}{\rho c^2 - 2P} \quad . \tag{3.76}$$

Using this form, we may consider the overall capacity of the aorta to be

$$C = \frac{V_o}{\rho \mathrm{PWV}^2 - 2P_m} \quad . \tag{3.77}$$

where V is the volume of blood in the aorta when the pressure is zero, P_m is the mean arterial pressure, and PWV is the Pulse Wave Velocity of the blood as measured by the methods that been previously discussed for the carotid-femoral PWV measurement. Note: A significant difference exists between this expression for the PWV, and other expressions that have been presented in the literature [76-79] namely, Eq. (3.77) contains a pressure term whereas previous PWV results have not. This applied pressure to the fluid is dimensionally significant, especially for an aorta with a high capacitance, and increases the PWV as shown in the equation.

3.4 Summary

Understanding systolic and diastolic pressure is crucial to guiding diagnosis and would improve prognosis of cardiovascular diseases. The objectives of this chapter are to introduce a new method that used in two-element Windkessel model enables us to analyze the effect of the arterial compliance reduction that is relevant for hypertension. Additionally, the two element Windkessel model was used to predict aortic pressure.

The truly big challenge is to move the cardiovascular system to the level of its corresponding mechanical analog instead of electrical analog. We believe that our model is more appropriate to offer valuable insight into adjusting the adjustable parameters that affect arterial compliance. This will be useful to identify which parameter is responsible for high blood pressure.

Arterial capacitance is a measure of the stiffness of the aorta which corresponds to arteriosclerosis and high pulse-pressures that may lead to dissections. But capacitance is a difficult parameter to quantify, and so methods of measuring the blood-pressure pulse-

wave velocity have been introduced [70] and different approaches are being developed and used to estimate arterial compliance. A high arterial compliance redaction has been shown to be a strong predictor of cardiovascular mortality. Prediction of arterial compliance would be very helpful for clinicians to predict cardiovascular risk. Compliance is a pressure-dependent parameter [80], and also compliance can be determined by the mechanical properties of the arterial wall or by pressure and geometry volume of the arterial vessels.

The arterial compliance and peripheral resistance are two arterial parameters that have effect for instance a small value for product RC (time constant) produces a faster response of the system. These parameters may determine the systolic and diastolic pressure values while the stroke volume, ejection period and heart rate are heart (cardiac) parameters, so this study shows that both arterial and heart parameters contribute to the blood pressure changes. The changes in arterial parameters initiate a systolic pressure increase so both the arterial compliance and the total peripheral resistance are load that cause blood pressure. The arterial parameters change with age based on the literature review that lead to increase the systolic, mean arterial and pulse pressures and decrease diastolic pressure.

The new mathematical models of determination of compliance need in vitro experiments to validate them. Therefore, the following chapter explains the experiments.

CHAPTER 4. EXPERIMENTS

4.1 Introduction

Before going in deep to describe the aortic simulator a short introduction depicts the role of technology that aims to build in vitro model system that has shown great potential for mimicking the function of the organ. It provides significative insight and gives the possibility to examine the system behavior under various conditions. That could not be obtained through some animal or human studies. In this chapter, description of the hardware and software parts of the experimental aortic simulator was reported.

4.2 Physical Model

In order to achieve the proposed objectives, we used experimental hemodynamics simulation. The simulator uses pulsatile pump that gives the possibility to examine the simulated hydrodynamic system behavior under various conditions. In other words, the control stroke volume, heartrate, and ejection percent could be controlled independently and variably which is difficult to perform in an in-vivo animal setting.

4.2.1 Experimental Setup

In our study, the experimental setup of the laboratory rig was designed based on a hydro-mechanical model by BDC Laboratories Company. The laboratory rig, also called pulsatile pump, consists of main devices such as a linear servo motor, single piston-in cylinder pump, programmable servo controller. The combination of the linear motor servo and single piston-in cylinder pump, controlled by the programmable servo

controller enable adjustable stroke volume, heartrate and systolic ratio. The pulsatile pump has physical and dynamical properties similar to a left ventricle and aorta that is suitable for this study under various test conditions.

The pulsatile pump replicates flow waveforms with reasonable accuracy into two pattern groups: steady flow in a single direction and oscillatory flow. In our work, the programmable servo controller is represented in a computer, two pressure transducers, temperature sensor and data acquisition. The programmable servo controller uses a software that was developed and implemented by BDC Laboratories Company. This software controls the linear motor motion and manages the output data. Initially, we setup the values of stroke volume, heartrate and ejection period. The general scheme experimental setup is shown in Fig. 4-1and Fig. 4-2 shows a picture of the experimental setup.

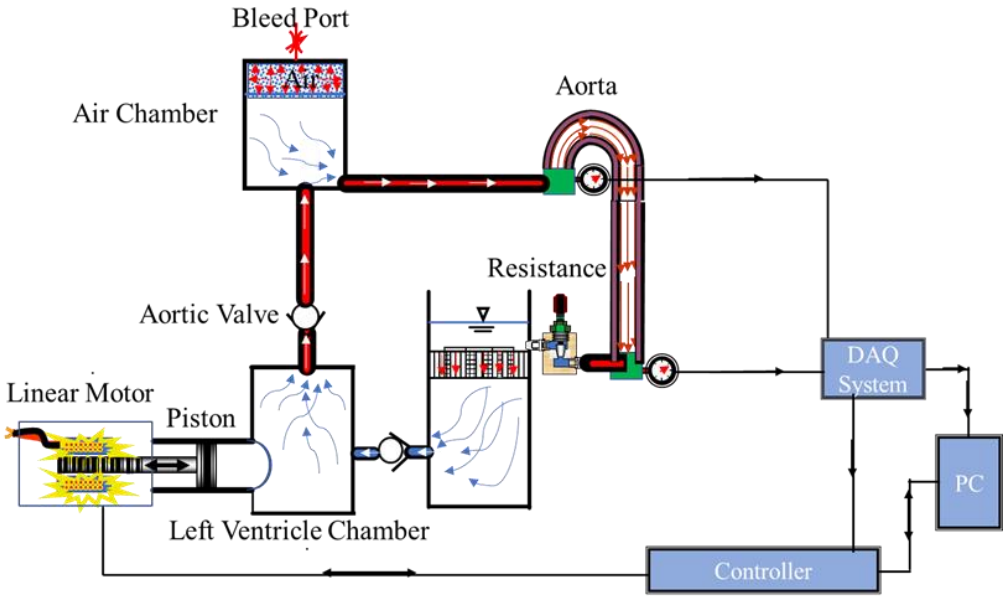

Figure 4-1. A schematic of general experiment setup.

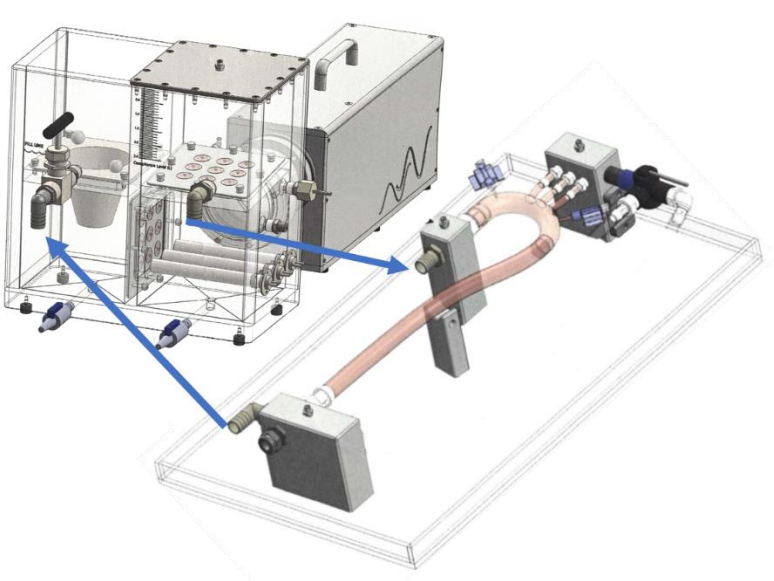

Figure 4-2. Scheme of the main components of the experimental workbench (BDC Laboratories).

A metallic heater is placed in the ventricle chamber and is controlled by a temperature controller to create a closed loop that permits a constant temperature of circulating water. All experiments were performed at room temperature and a distillate water was used as blood, because water is a fluid similar to the blood, in terms of density and viscosity. The arrows describe the water direction and the different parts are labeled to easily understand the function. The simulated aorta was put horizontally in transparent plastic tray to collect leaked circulating water.

4.2.1.1 Linear Motor

The linear motor differs from traditional rotary electrical motors in that it has much higher accuracy with good dynamic control, ability to provide a constant force and high efficiency because of its low friction and minimal moving parts.

The linear motor represents an artificial left ventricle and moves the working water that pushes the diaphragm inside the ventricle chamber and the whole system works as a double direction pump that reproduces the pulsatile heart flow. The armature of the motor moves forward to represent the systolic phase while it moves backward to represent the diastolic phase.

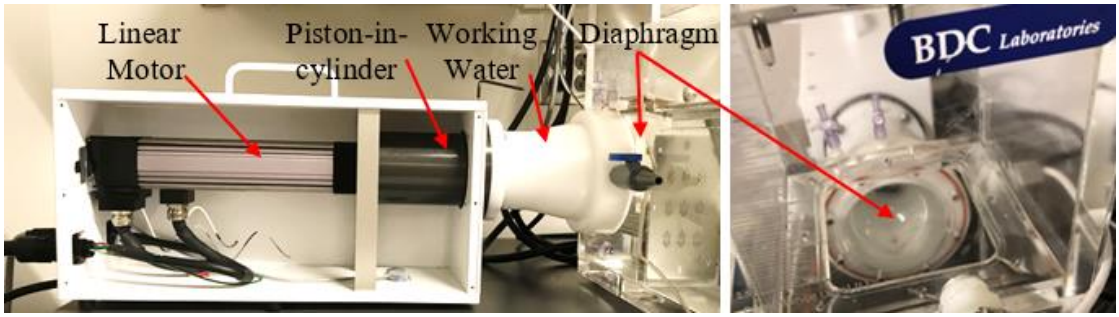

Figure 4-3. Linear motor.

4.2.1.2 Chambers

The hydraulic pump is attached with a left ventricle chamber that is one of four compacted cubical chambers (left ventricle chamber, air compliance chamber, left atrium chamber, and arterial reservoir chamber). Each chamber was made from a transparent Plexiglas that has inside dimension 6x6x6 inches and 10 mm thickness.

The left ventricle chamber is located under the air compliance chamber and beside atrium chamber. The left ventricle chamber has two one-way valves; the mitral valve plate is an entrance valve to let water in the left ventricle chamber and is located in

vertical position between the left ventricle and atrium chamber. The aortic valve plate is an exit valve to allow for pumping water out the left ventricle chamber and is located in the horizontal position in the top of the left ventricle chamber. The left atrium chamber is filled passively from the arterial reservoir chamber while the left ventricle chamber hydraulically pumps water. The arterial reservoir chamber that was open to the atmosphere

The linear motor has connected a single piston pump that consists of a single piston in a Teflon cylinder filled with water. Its end has a diaphragm that expands inside the ventricle chamber to push the circulating water through the aortic valve to the rest of the system.

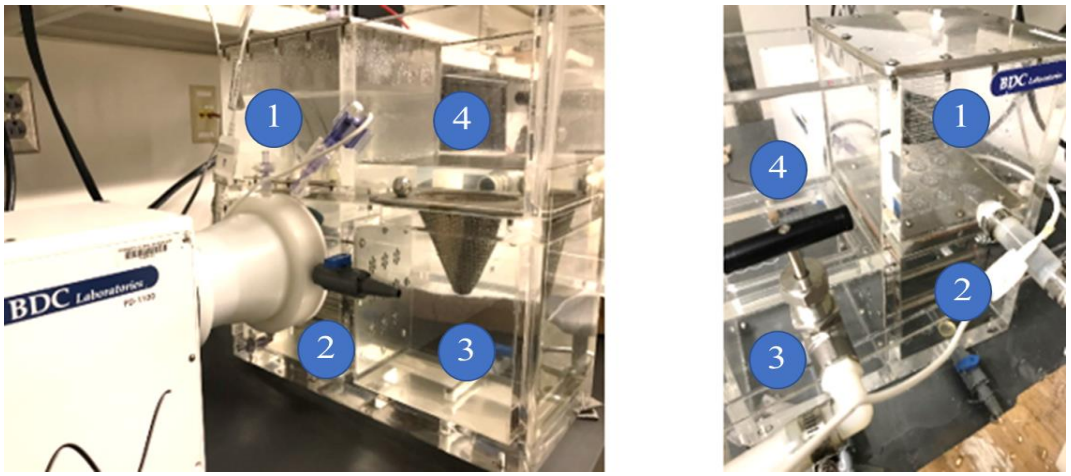

Figure 4-4. The scheme shows the component of the aortic simulator. Numbers are 1- Air compliance chamber, 2- Left ventricle chamber, 3- Atrium chamber, 4- Arterial reservoir chamber.

4.2.1.3 Aorta

The aorta is the biggest elastic artery in the body that is carrying oxygenated blood and vital nutrients to different organs of the body, and temporarily storing blood

during the systole and then pushing to the rest of the body. The shape and elasticity of the aorta plays a crucial role in the arterial system.

This work helps to further our understanding of the elasticity's role in the hypertension. The human aorta shape is similar to a walking stick. In our research, we have studied artificial aorta and different kinds of animal aorta.

4.2.1.3.1 Simulated Aorta

In our study, we investigated different artificial aortas to simulate the expected effects of increasing or decreasing the arterial compliance. We expect that an artificial aorta could be a feasible candidate for treating hypertension. In our experiments, elasticity properties were considered when synthetic materials were selected for forming aortas that are to meet the different experimental conditions. Artificial aortas were formed into the shape that developed by the BDC Laboratories Company. Synthetic materials are as a silicone, latex, and polyurethane (PMC 770).

Aorta were modeled in relevant size that the thickness of the tube was set at 1.7 mm thick, an inner diameter of 2.8 cm and a length of 55 cm. The geometry was simple as shown in Fig.4-3 and similar to this BDC Laboratories Company.

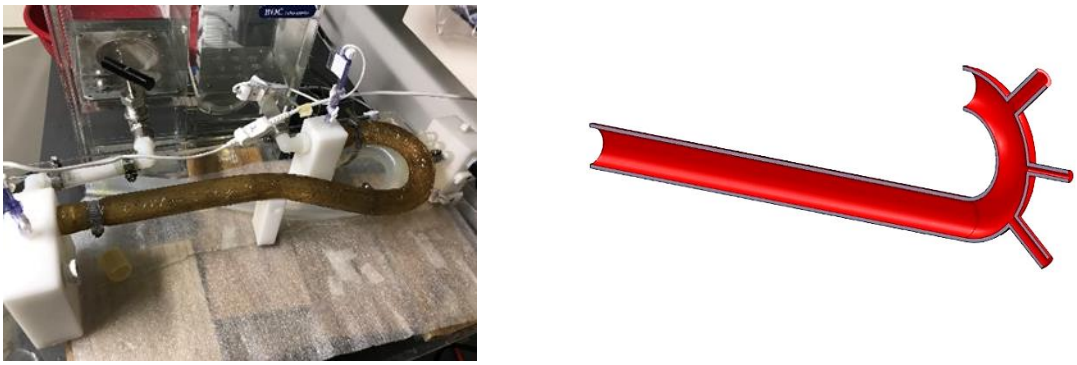

Figure 4-5. Cross section of the simulated aorta.

In this project, different molding techniques were adapted to manufacturing different compliance using different materials with keeping the tube dimensions constant. Those molding techniques were chosen as low cost and repeatable procedure. The molding process was to first choose a pipe with a 1-inch outer diameter and rotating the pipe between two fixture centers at appropriate speed.

The Smooth-On silicone first required mixing the two pots with mixing ratio by volume 1:1 at room temperature and then putting the mixture in a vacuum chamber as shown in Fig. 4-4. When removing air bubbles, the mixture was poured lightly, and straight ruler was used to determine the thickness of the poured silicone. After finishing pot time, the ruler was put away and the left pipe rotated for one hour. A mold release was not used to assure that the poured silicone stuck on the pipe surface; therefore, molded aorta was extracted from the pipe using pressurized water five hours after finishing cure time.

The final step in manufacturing aorta was extraction of simulated aorta from the tube using pressurized water. When bending the tube to make the arch during the cure life, the bending portion was thicker on one side than the other, and a little thickness variance occurred along the tube. In manufacturing, it is difficult to attain the exact

thickness. The wall thickness was measured carrying out with digital caliper at several points. The simulated aorta was lied horizontally in transparent plastic tray to reduce the vibration transmission and to collect leaked circulating water as shown in Fig. 4-5.

The different experimental setups have been performed under different stroke volume, heartrate, and ejection percent rates, and the pressure data was measured at inlet and outlet of the simulated aorta. The pressure data was collected for 15 seconds and experiment was repeated at least three times.

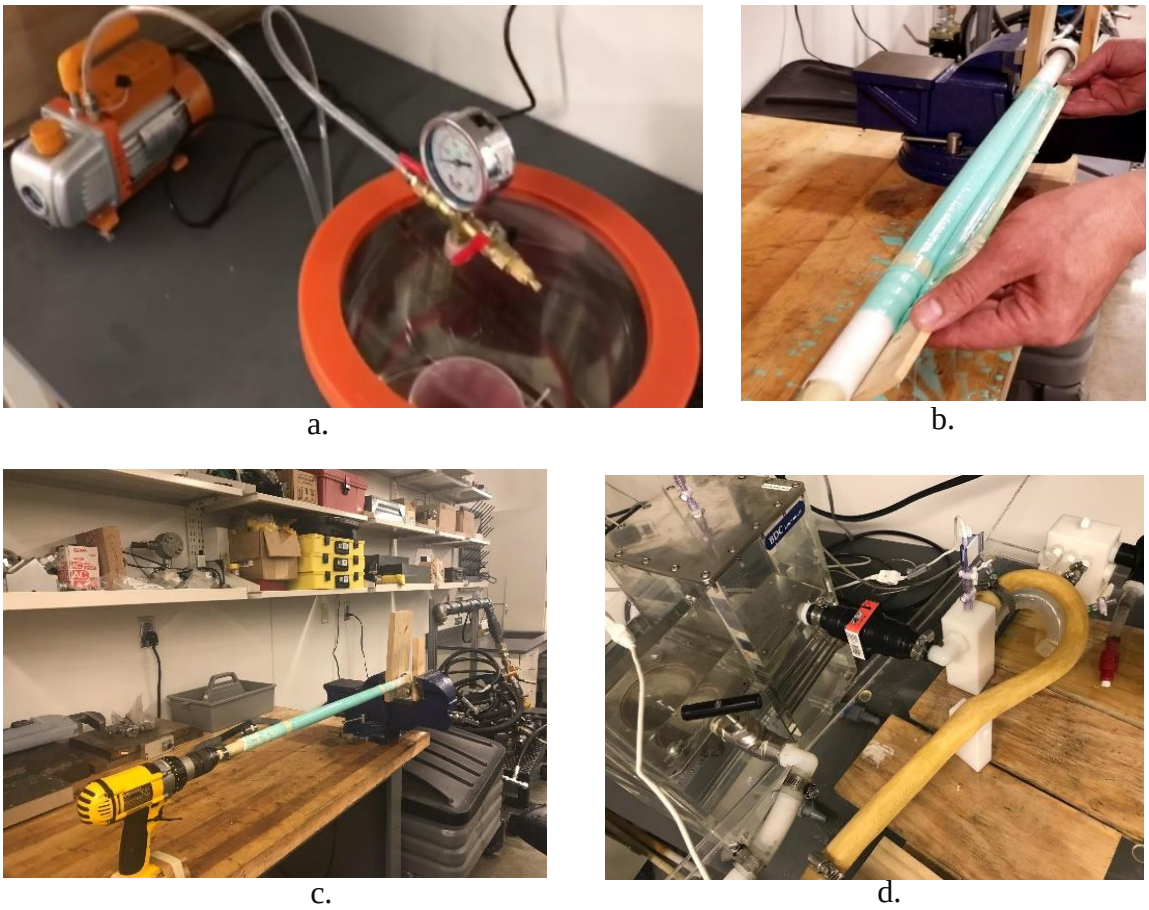

a. b. c. d.

Figure 4-6. Manufacturing the simulated aorta. a- Vacuum chamber, b, c, and d- Ways of manufacturing the simulated aorta.

4.2.1.3.2 Animal Aortas

To gain a better insight regarding the blood pressure diagram, different fresh animal aortas were tested with the pulsatile machine that is elucidated further in Fig, 4-7. Fresh aortas were obtained from different donor animals such as ox, cow, pig, sheep, and goat. Experiments were carried out on the same day of extracting them.

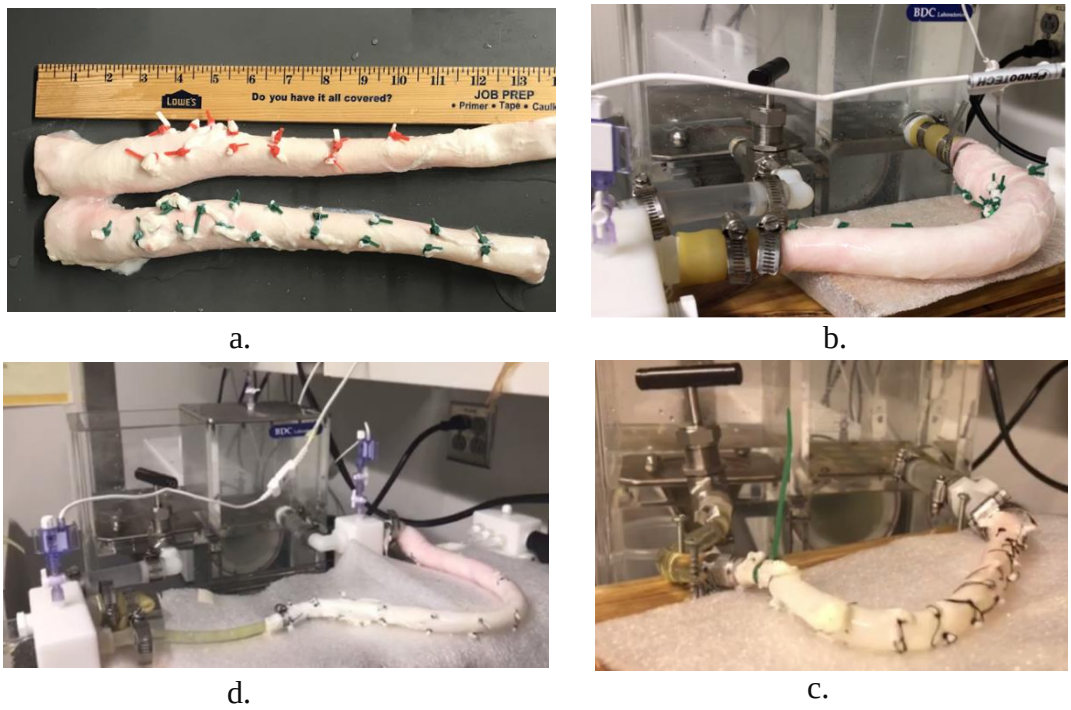

Figure 4-7. Testing a fresh ox aorta.

All branches were sewed closed at their roots using a suture to provide leakages. During experiments that were performed to draw the blood pressure diagram, each dissection aorta was subjected to different heartrates, stroke volume, ejection period and peripheral resistances. The setup of animal aortas was horizontal and air bubble-free.

For example, the stroke volume was maintained at a certain value of 70 mL/ stroke. The systemic pressure was varied by adjusting the peripheral resistance, heartrate, and ejection period.

Figure 4-8 shows the waveforms results for systemic pressure at 80 BPM heartrate and 70 mL/stroke with an ejection period of 0.3.

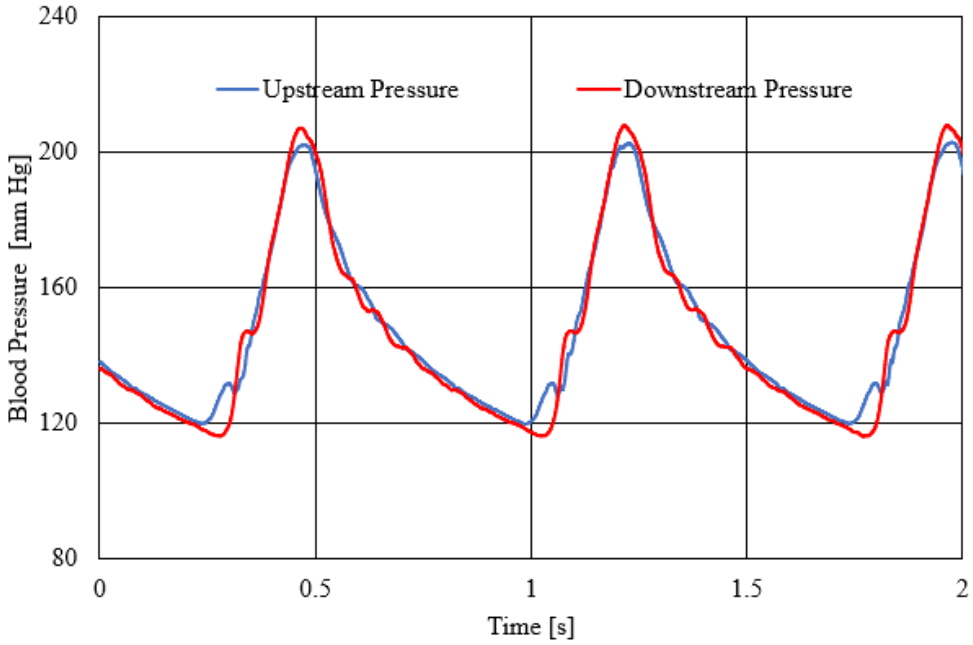

Figure 4-8. Aortic blood pressure waveforms in the Ox#6.

Several problems arose before and during animal data collection. The most serious of these was the difficulty to close the root of aorta's branches by sewing and tethering. The mechanical properties of the aortas were extremely influenced by sewing and tethering the root of aorta's branches, but this way gives a great opportunity to do the ultimate laboratory experiments to measure aortic capacitance.

4.2.1.4 Peripheral Resistance

At the outflow of the simulated aorta, a needle valve was used to mimic a peripheral resistance of the system as shown in Fig.4-9. This valve is made up of Stainless steel with ½ inch size. The valve makes it possible to increase or decrease both

systolic and diastolic pressure. It provides flow restrictions and a relatively large pressure drop that helps to obtain the desired aortic pressure.

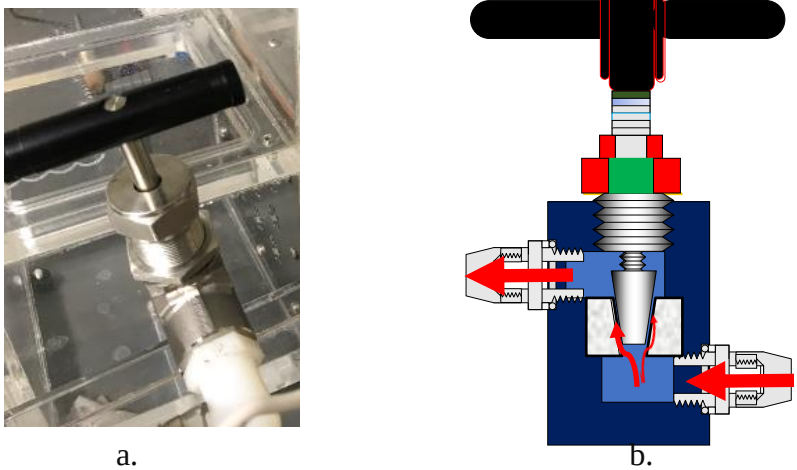

a. b.

Figure 4-9. The peripheral resistance, a- picture of the valve, and b- scheme of the valve.

4.2.1.5 Circulating water

The blood was replicated by distillate water which approximately replicates the blood in the aorta in terms viscosity and density. The distillate water has density of 997 kg/m^3, and dynamic viscosity of 0.89×10^{-3} $kg/(m.\ s)$, whereas the human blood is an incompressible fluid that has an average density of 1050 kg/m^3 and a dynamic viscosity of $3\text{-}4\times10^{-3}$ $kg/(m.\ s)$. The blood has a density approximately similar to water, but its dynamic viscosity is twice more than water.

4.2.1.6 Measuring System

For monitoring and controlling a system, proper measurements are needed to involve collecting information in order to take corrective action. Sensors work as parts of the interface between the physical phenomenon and the electronics. Sensors are electronic devices that turn physical phenomenon changes into measurable electrical signals (voltages). The characteristics of a good sensor chosen for our experiments are small size, quick response, and low power consumption.

4.2.1.6.1 Pressure Transducer

The definition of pressure is force per area. A pressure transducer is a device that converts physical pressure phenomena into a low electrical voltage signal as shown in Fig. 4-10a. This signal is linear proportional to the physical pressure and it needs an amplifier to make it measurable. The data acquisition system collects sensor information and provides driving signals to pulsatile pump system. Before sending acquired signals to the data acquisition system, acquired signals are necessarily filtered, amplified as shown in Fig. 4-10b and converted from analog into digital by using a signal condition. The signal condition is an interface between sensors and system measurements, in other words it is a crucial process for making signals more suitable for the data acquisition system.

Figure 4-10. a-Pressure transducer, b- picture of the SCC-SG24 Wheatstone bridge and amplifier.

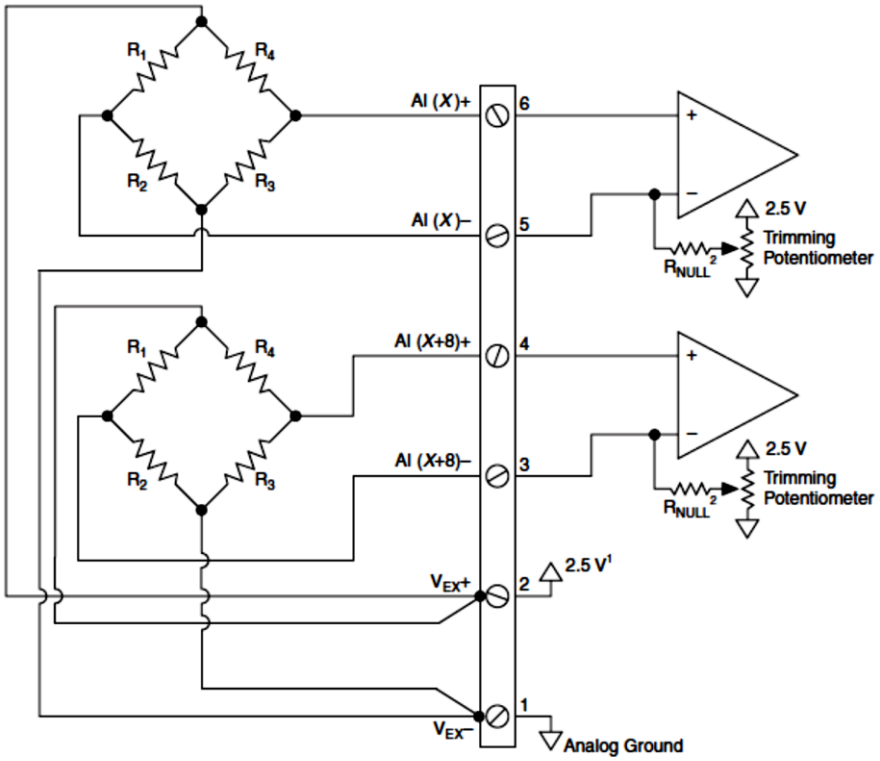

Figure 4-11. Diagram of the SCC-SG24 Wheatstone bridge and amplifier (National Instruments).

To provide an excitation voltage to the strain gage of the pressure transducer, the two wires are connected to points 1 and 2. Two wires of the strain gages are connected to point 3 and 4 as shown in Fig. 4-11.

4.2.1.6.2 Thermostat

To mimic the physiological blood temperature a metallic heater with an electronic temperature sensor was placed in the ventricle chamber. This permits a good control of the temperature of circulating water by creating a closed loop.

4.2.2 Software

Statys software is a graphical program that has been used to accurately simulate and adapt cardiovascular applications. The software has optional data collection and a wide set of tools for acquiring, analyzing, displaying and storing data. The front panel of the software is the user interface for PID control and indicators and displays the results.

BDC Laboratories developed the Statys software that enables full system control and test monitoring through a simple interface that gives interactive control of the software system. A dashboard of the software has control buttons to simulate the desired waveform during loop operation as shown in Figs. 4-12 and 4-13. This software provides sufficient real-time performance analysis during system operation.

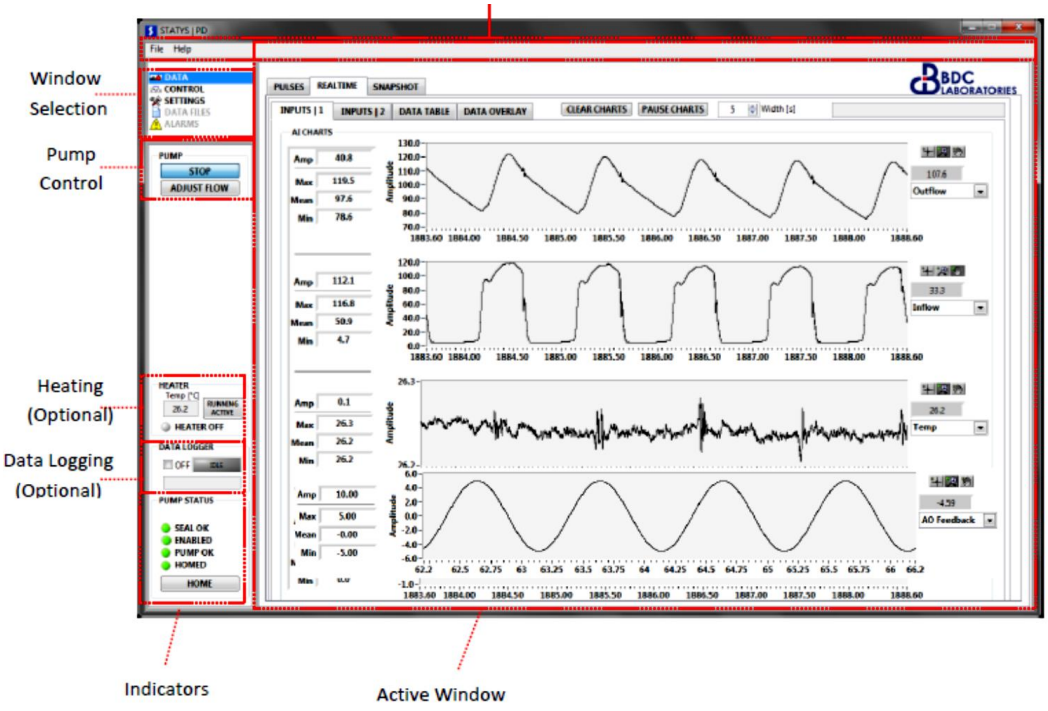

Figure 4-12. Statys control dashboard.

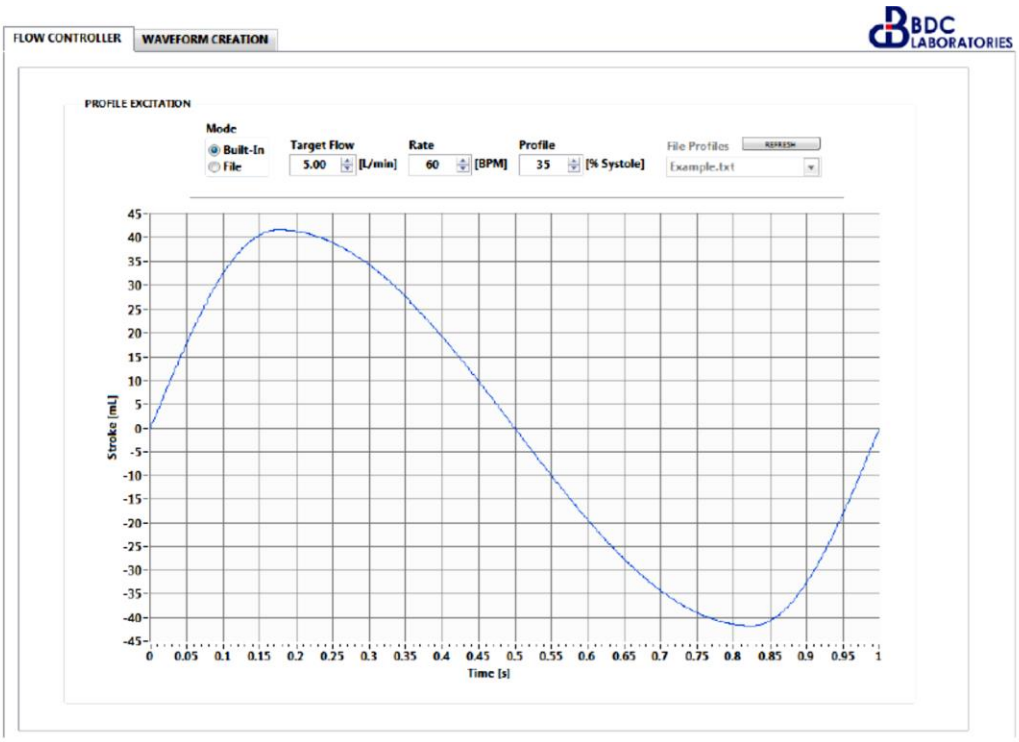

Figure 4-13.Piston's movement path.

4.2.3 Control Unit

Control unit manages the operation of the linear electrical motor by communicating with the computer and receiving the signal feedbacks by sensors as shown in Fig 4-15. To govern motor via remote software, the control unit developed by BDC Laboratories represents a fundamental element for improving the pulse duplicator efficiency. Looking at the front panel it is possible to monitor the correct status of the communication between the driver and the PC. The outputs are cables for the motor control, for the relays monitoring, and a bus connection to the master PC.

The board manages the different signals to and from the engine and guarantees a correct translation of commands via the servo drive system. Three principal parts characterize the control unit: the power supply circuit that ensures a correct energy to all different parts, the on board PC and linear drive as in the Fig 4-14.

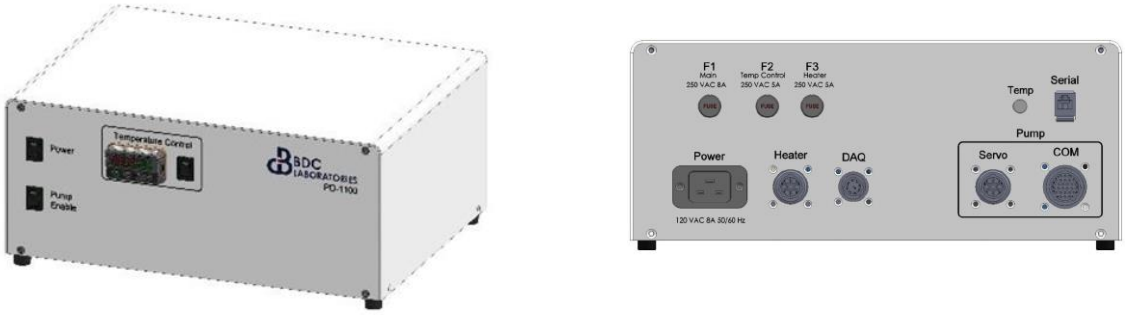

Figure 4-14. The control unit.

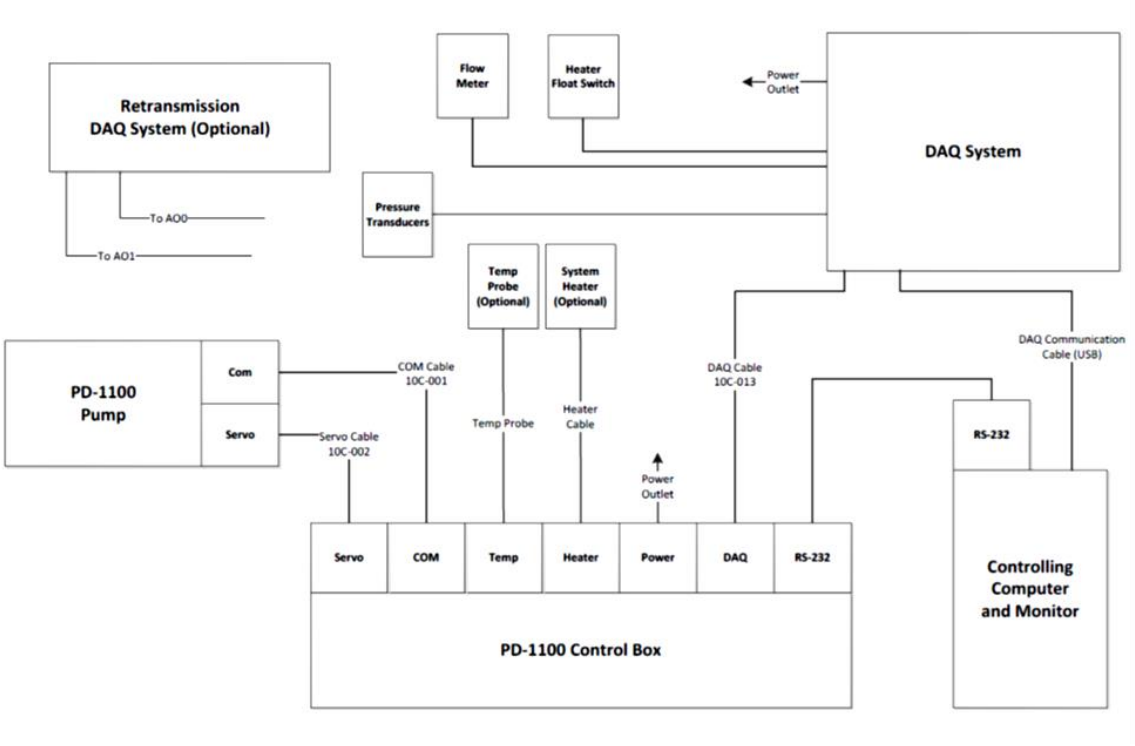

Figure 4-15. Electrical connection diagram.

4.2.4 Experimental Procedures

In this study, we investigated an artificial aorta, to simulate the expected effect of increasing or decreasing the total arterial compliance. We anticipate that technology could be a feasible candidate for treating hypertension.

The basic idea of the simulator system mechanism is based on the left ventricle function. The workbench was designed to use two fluids: the working fluid that is the water between the piston of the linear motor and the ventricle chamber. This water is responsible to transfer the pulse transmission to the ventricle chamber. The second kind of the fluid is test water passing through the simulated aorta. A flexible silicon membrane separates the two fluids and transmits the pulse motion from the working fluid in the hydraulic cylinder of the piston to the test fluid in the ventricle chamber. During the

ejection phase, the piston moves forward and the membrane will expand inside the ventricle chamber. This leads to increased pressure inside the ventricle chamber and the mitral valve remaining closed while the aortic valve opens. When the pressure in the chamber becomes greater than that aortic pressure the aortic valve will open to allow the water out to the aorta. When the pressure in the chamber falls below that in the aorta, the piston moves back, the aortic valve closes, which means that both the mitral and aortic valves are closed again. This is called relaxation, a phase that precedes water filling and represents the onset of diastolic. Falling ventricle chamber pressure below the atrium pressure opens the mitral valve and allows the test fluid to enter in the atrium chamber.

A needle valve was connected between the outflow of the aorta and the aterial tank to mimic the peripheral resistance. The needle valve has responsibility for increasing systemic pressure. During the experiments three flow parameters were varied: stroke volume and heart rate and systolic percentage at room temperature without air bubbles in the aorta.

4.3 Material Characterization

In order to estimate the Young's Modulus for the tube used as a simulated aorta, tensile testing machine was used. Tensile test specimens were molded in shape and size according to ASTM D638 standard test method for tensile properties of plastics [81] as shown in the Fig. 4-6. Several specimens were molded at a time, allowing one full set of specimens for each kind of plastic material according to the ASTM testing standard.

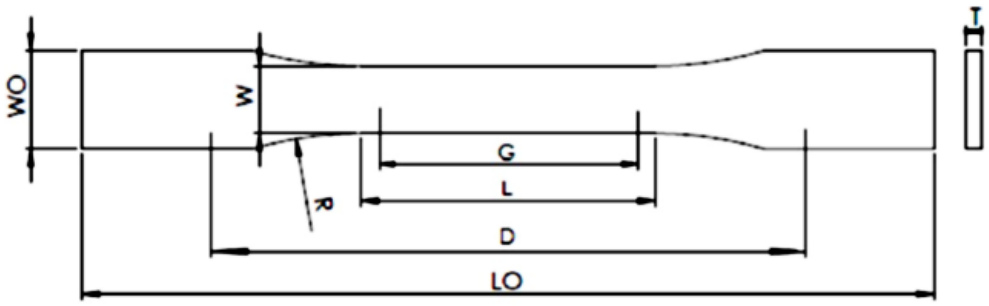

Variable	Description	Dimension (mm)
W	Width of narrow section	13 ± 0.5
L	Length of narrow section	57 ± 0.5
WO	Width overall, min	19 + 6.4
LO	Length overall, min	165 (no max)
G	Gage length	50 ± 0.25
D	Distance between grips	115 ± 5
R	Radius of fillet	76 ± 1
T	Thickness	3.2 ± 0.4

Figure 4-16. The dimension of the specimens according to ASTM D638.

The tensile test is universally well-known technique for mechanical characteristics. The tensile testing machine pulls the sample from both ends and measures the force required to pull the specimen and how much the sample stretches.

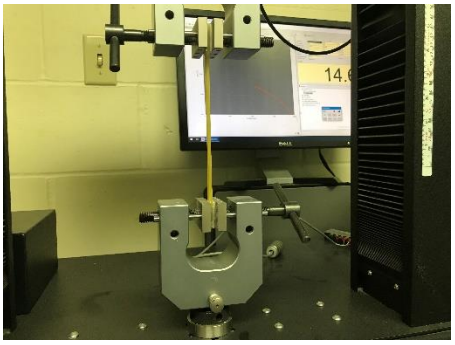

a.

b.

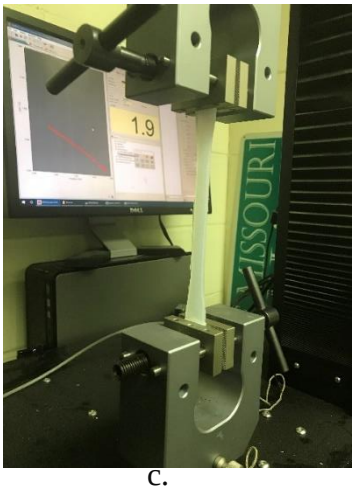

c.

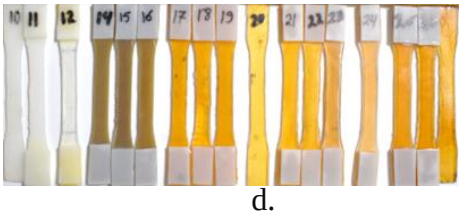

d.

Figure 4-17. a, b, and c - Grips for specimen test, d -specimen setup in the tensile test machine.

Nylon flat blocks were glued on specimens to secure grip with no slipping. Testing speed was 5 *mm/min* based on the recommendation in the ASTM D638 standard test method for tensile properties of plastic. The test run up to 5 *Ib* load, and displacement was automatically collected. The data was then post -processed in Excel and the Young Modulus calculated for each specimen. Then an average was determined as shown in Fig.4-17. The load versus extension curve and the stress strain for PMC simulated aorta which diameter is 2-8 cm, wall thickness is 1.7 *mm* were plotted.

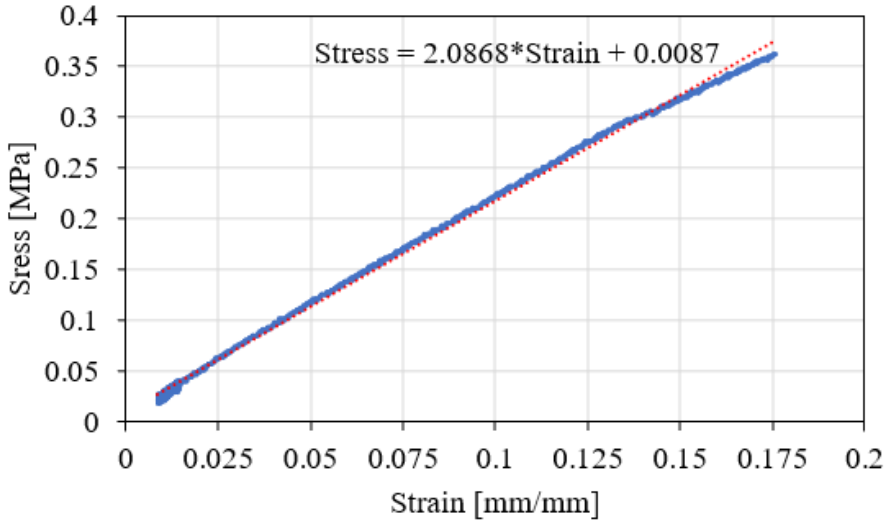

Figure 4-18. Stress vs. strain profile of the PMC770 specimen.

From the given stress and strain values obtained from tensile test as shown in Fig. 4-18, we can calculate the Young's Modulus that was calculated using Eq.

$$E = \frac{\sigma}{\epsilon}. \tag{4.1}$$

where σ is stress (MPa/m^2) and ϵ is strain (no unit).

4.4 Summary

The intended goal of this chapter was to focus on the realization of an experimental laboratory for cardiovascular studies. It is not possible to gain this information from a medical clinic because it is difficult to measure.

A detailed description of hardware and software of the aortic simulator machine was presented with manufacturing techniques of aortic prototypes. This study gave the chance to focus on in vitro test using the aortic simulator machine to assess the hydrodynamic performance of an artificial aorta.

In order to study this type of hydraulic systems in our research, we considered somethings such as positive reciprocating pump for water handling as a left ventricle, needle valve as peripheral resistance, elastic tube or air chamber for mimicking arterial compliance. During manufacturing the artificial aorta, we faced a problem that was how to determine the desired tube elasticity or inner and outer diameter of the tube. The solution of this problem was adopting the mechanical capacitance equation for calculation of tube sizing and elasticity. This equation is clearly simplification of the reality of the behavior of the atrial compliance, but it provides a design guidance.

The model aorta was used to simulate wall aortic compliance to ascertain that decreased compliance increases pulse pressure by increasing systolic pressure and decreasing diastolic pressure. In this work the experiments presented a simple and noninvasive tool for doing just that.

In the proceeding chapters, we introduce a novel approach for an interpretation treating resist hypertension.

CHAPTER 5. THE PRESSURE DIAGRAM

5.1 Introduction

Cardiovascular diseases are one of the biggest problems in medicine today. In the U.S. alone, it is the number cause of death claiming 635,260 lives in 2016 [70] and the numbers of patients continue to increase. To diagnose the reason for each this diseases, blood pressure and pulse oximeter, which measures blood oxygen levels. Both are common inexpensive quick-assessment tools. Chest pain is usually followed up with an electrocardiogram (EKG). EKG is a noninvasive method that records your heart's electrical activity and detect an abnormal rhythm as well as myocardial infraction (heart attack) or a dangerous arrhythmia. However, many preliminary test results have been misclassified lead to patients' unnecessary treatments and expense. For example, some cardiovascular medications decrease peripheral resistance, but they may affect the total arterial compliance, so the blood pressure measurement itself does not identify the specific cause for the high blood pressure reading. These considerations emphasize the need to explore blood pressure characteristics in more detail. Diagnoses based on blood pressure are determined by a combination of mechanical properties within the cardiovascular system including the stroke volume of the left ventricle, the ejection period of the heart, the peripheral resistance of the body, and the capacitance of the aorta. There is evidence of correlation between increased blood pressure, increased peripheral resistance, and decreased compliance. To clarify the physical characteristics of the blood pressure pulse, a non-dimensional blood pressure diagram is developed and the impact of altering the arterial parameters and cardiac parameters is discussed.

5.2 Non-Dimensional Parameters

Any physical problem can be defined by an analysis of the relationship between different physical quantities. Heart problem are based on the physical dependencies of aortic pressure are blood pressure P, stroke volume ΔV, peripheral resistance R, arterial capacitance C, ejection period T_e, and heartrate T. This analysis is named dimensional analysis while nondimensional parameters have been created to help us to understand the physical significance associated with the physical problem. By focusing on the basic function of the left ventricle, we have been able to reduce the problem to three nondimensional groups that are able to describe the blood-pressure problem completely by using the Buckingham Pi Theorem to arrive at a basis set of dimensionless parameters for the aortic pressure.

5.2.1 Buckingham Pi Theorem

The Buckingham Pi Theorem has been used to find mathematical relationships between variable physical quantities in an equivalent form of a set of independent dimensionless products composed of the relevant physical parameters. The Buckingham Pi Theorem states that the minimum of non-dimensional groups is found from the number of physical dependencies minus the number of fundamental units. The Pi terms can be written in-one physically meaningful form to one another to describe the whole problem. Describing a problem by using the Buckingham Pi Theorem depends upon the careful selection of parameters; however, the Pi Theorem does not tell how to select the significant parameters [44], but it provides us information that helps to select the parameters needed to plot the blood pressure diagram. The used selection of parameters

that was arranged the first nondimensional group describes each of the systolic, diastolic and mean arterial pressures as they each relate to the mean arterial pressure. The second nondimensional group describes the exponential time-constant. The third nondimensional group describes the ejection fraction that illustrates how the left ventricle pumps the blood into the aorta with each heartbeat.

Applying this theorem to the aortic pressure, the parameters can be found by forming a matrix showing the exponent of each unit for every physical quantity as shown in Table 5-1.

As shown in the previous chapter physical quantities associated with the aortic pressure are ΔV, R, C, T_e, and T where each symbol was used and described before. These quantities and units are summarized in Eq. (5.1).

$$\begin{aligned}
[P] &= \frac{kg}{m.s^2} && \text{Arotic Pressure} \\
[\Delta V] &= m^3 && \text{Stroke volume} \\
[R] &= \frac{kg}{m^4.s} && \text{Total Peripheral Resistance} \\
[C] &= \frac{m^4.s^2}{kg} && \text{Arterial Compliance} \\
[T_e] &= sec. && \text{Ejection Time} \\
[T] &= sec. && \text{Heart Rate}
\end{aligned} \tag{5.1}$$

Table 5-1. Exponents of units associated with each fundamental physical quantity.

	Physical Quantities					
Dimensions	P	ΔV	R	C	T_e	T
M	1	0	1	-1	0	0
L	-1	3	-4	4	0	0
T	-2	0	-1	2	1	1

Where *M*, *L* and *T* are the dimensional quantities of a mass, length and time respectively. The matrix formed from Table 4-1 is denoted by matrix *A* and explicitly given in Eq (5-2). where *A* is a unit exponent matrix.

$$A = \begin{pmatrix} 1 & 0 & 1 & -1 & 0 & 0 \\ -1 & 3 & -4 & 4 & 0 & 0 \\ -2 & 0 & -1 & 2 & 1 & 1 \end{pmatrix} . \tag{5.2}$$

The basis of the null space of the unit exponent matrix gives a set of parameters sufficient to describe the system. The null space for the matrix *A* in Eq. (5.2) is given in Eq. (5.3). The rank of matrix *A* is two; therefore; the null space of the unit exponent matrix is rank three, indicating that three dimensionless groups form a minimum basis to describe blood-pressure behavior.

$$Null(A) = \begin{pmatrix} 1 & 1 & 1 \\ -1 & -1 & -1 \\ 0 & -1 & -1 \\ 1 & 0 & 0 \\ 0 & 1 & 0 \\ 0 & 0 & 1 \end{pmatrix} . \tag{5.3}$$

The next step is to convert physical quantities back using the null space dimensionless basis. The null dimension basis is shown in the Eq. (5.4). The new dimensionless representations can be created combinations of the original basis as shown;

$$\frac{PC}{\Delta V} \quad , \quad \frac{PT_e}{\Delta VR} \text{ , and } \quad \frac{PT}{\Delta VR} \tag{5.4}$$

5.2.2 Three Non-dimensional Groups

The three nondimensional groups chosen to develop the blood-pressure diagram can be written in another form as:

$$\hat{P} = \frac{P\,T}{R\Delta V} \quad , \quad \hat{C} = \frac{RC}{T} \quad \text{and} \quad \hat{T}_e = \frac{T_e}{T} \quad . \tag{5.5}$$

A set of parameters can be chosen to have as few terms as possible or to have more physical meaning. The first nondimensional group describes any blood-pressure measurement divided by the mean arterial pressure. The second nondimensional group describes the exponential time-constant which is given by *RC* period divided by the heart rate. The third nondimensional group describes the ejection period divided by the heartbeat period which is effectively the percent of time spent in the systole versus diastole during a single heartbeat.

5.3 Blood Pressure Diagram

In order to illustrate the physical characteristics of the blood pressure pulse, a nondimensional blood pressure diagram is developed and the impact of altering the aortic capacitance, peripheral resistance, stroke volume, etc., is discussed. To illustrate the importance of measuring the stroke volume and the ejection period of the heart, hypothetical patient cases are presented and shown to yield a wide variety of cardiovascular conditions which produce the same blood pressure and heartrate measurements.

The blood pressure diagram is an informative and useful approach of representing the data in the graphical presentation to display data correlations.

The previous analysis shows that blood pressure is dependent on five dimensional parameters within the cardiovascular system. Mathematical expressions for the systolic, diastolic, and mean arterial pressures were derived and illustrated in Chapter 3. These results are re-presented here for convenience where:

The systolic pressure equation is

$$P_S = \frac{R\Delta V}{T_e}\,\frac{1-e^{\left(-\frac{T_e}{RC}\right)}}{1-e^{\left(-\frac{T}{RC}\right)}} \quad . \tag{5.6}$$

The diastolic pressure equation is

$$P_D = \frac{R\Delta V}{T_e}\,\frac{1-e^{\left(\frac{T_e}{RC}\right)}}{1-e^{\left(\frac{T}{RC}\right)}} \quad . \tag{5.7}$$

The mean arterial pressure equation is

$$P_M = \frac{1}{T}\int_0^T P\,dt = P_D\frac{T_e}{T}\,\frac{1-(P_S/P_D)^{\frac{T}{T-T_e}}}{1-(P_S/P_D)^{\frac{T_e}{T-T_e}}} = \frac{R\Delta V}{T} \quad . \tag{5.8}$$

However, using the Buckingham Pi Theorem it may be shown that the blood pressure problem may be more succinctly described using three nondimensional groups:

$$\frac{P\,T}{R\Delta V} \quad , \quad \frac{RC}{T} = \frac{P_M\,C}{\Delta V} \quad \text{and} \quad \frac{T_e}{T} \quad . \tag{5.9}$$

Using these groups with Eqs. (5.6), (5.7) and (5.8), the nondimensional expressions for systolic, mean and diastolic pressures may be written as

$$\text{Systolic pressure} \quad \frac{P_S T}{R\Delta V} = \frac{T}{T_e}\,\frac{1-e^{\left(\frac{-T}{RC}\frac{T_e}{T}\right)}}{1-e^{\left(\frac{-T}{RC}\right)}}$$

$$\text{Mean pressure} \quad \frac{P_M T}{R\Delta V} = 1 \tag{5.10}$$

$$\text{Diastolic pressure} \quad \frac{P_D T}{R\Delta V} = \frac{T}{T_e}\,\frac{1-e^{\left(\frac{T}{RC}\frac{T_e}{T}\right)}}{1-e^{\left(\frac{T}{RC}\right)}} \quad .$$

The characteristics of blood pressure may be completely described using the three nondimensional groups presented in Eq. (5.5), and Fig. 5-1 shows a plot of these three equations for reasonable values of the nondimensional groups shown in Eq. (5.9). The top half of the diagram describes the systolic pressure while the bottom half describes the diastolic pressure. The horizontal axis at the center describes the mean arterial pressure which simply says that $\frac{P_M T}{R\Delta V} = 1$.

The significance of Fig. 5-1 is that it captures all physical characteristics of the blood-pressure pulse in a single diagram. For instance, by examining this plot and assuming all other parameters remain constant, it may be shown that the pulse pressure decreases as the aortic capacitance increases. This phenomenon is well-known and may be physically explained by the fact that a flexible aorta is more capable of absorbing the injection of blood coming from the aortic valve as opposed to a stiff aorta, thereby keeping the pressure spikes low. It is also shown in Fig. 5-1 that an increase in the ejection period T_e has the same impact as increasing the aortic capacitance. This reduces the pulse pressure. Physically speaking, an increase in the ejection period gives the aorta more time to receive the same stroke volume of blood coming from the heart and

therefore provides a gentler delivery of flow. The blood pressure diagram in Fig. 5-1 also captures the effect of altering the peripheral resistance R and the heartbeat period T. However, a description of this impact is less straight forward as both the vertical and horizontal axes of the blood pressure diagram depend on these parameters.

Generally speaking, an increase in the peripheral resistance will raise all pressures and will tend to raise the pulse pressure slightly. An increase in the heartbeat period, corresponding to a slower heartrate, decreases the cardiac output thereby lowering all pressures while slightly lowering the pulse pressure as well. Although not obvious in Fig. 5-1, it should be noted that the blood pressure diagram is not able to describe the impact of altering the stroke volume ΔV since this quantity only scales and dimensionalizes the blood pressure; it does not physically alter the shape of the blood pressure pulse. Equations (5.6) and (5.7) illustrate this point and may be used to show that an increase in the stroke volume will increase all pressures proportionally, including the pulse pressure.

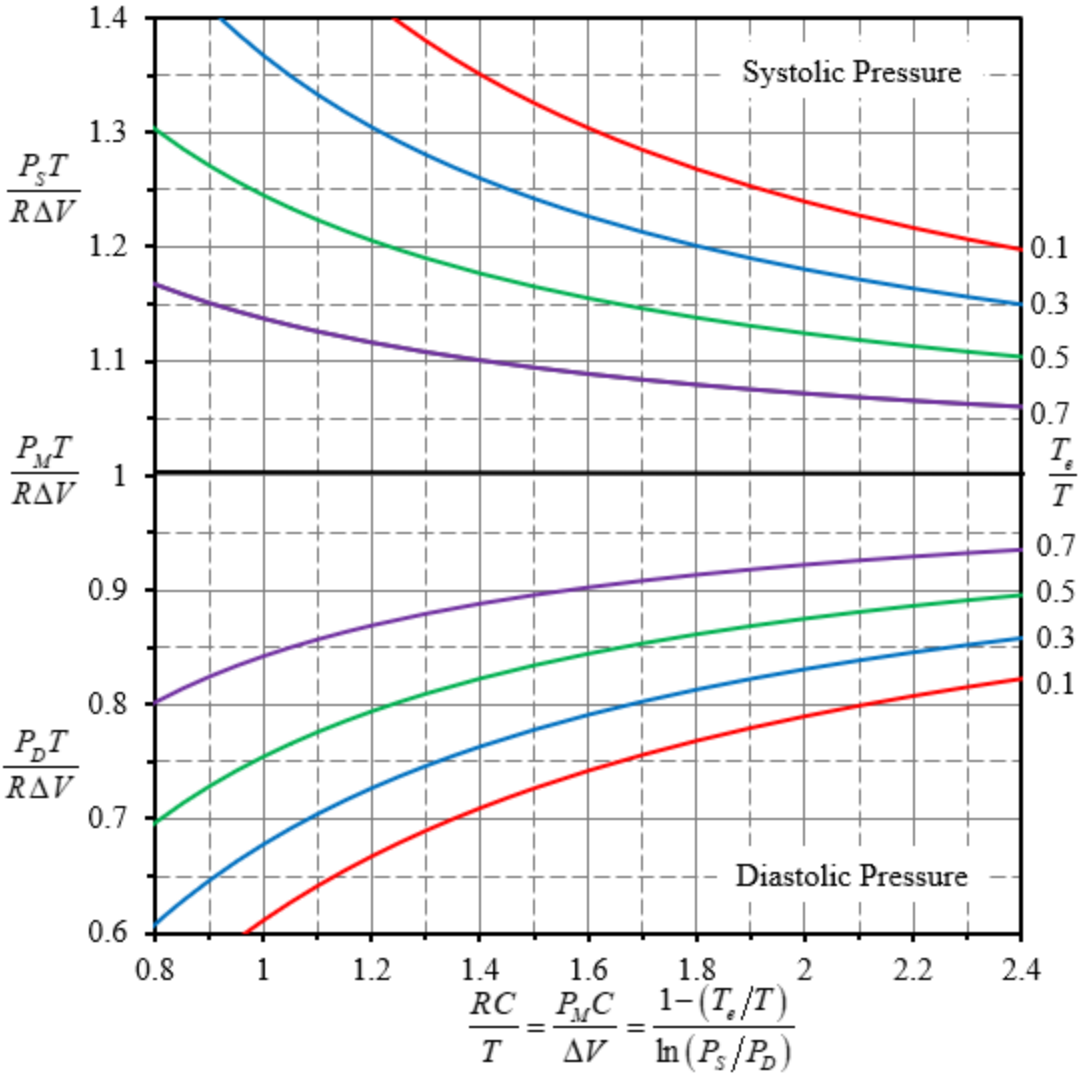

Figure 5-1. The blood-pressure diagram showing all blood-pressure characteristics as a function of stroke volume ΔV, heartbeat period T, peripheral resistance R, ejection period T_e, and capacitance C.

The lines that slop upward from the center are used to locate systolic-pressure state, while the lines that slope downward from the center are used to locate the diastolic-pressure state. The pulse pressure is simply the difference between the systolic and diastolic pressures. When the power of exponential in Eqs. (5.6) and (5.7) increases that means the pulse pressure will increase as the arteries become stiff and noncompliant, which is a well-known characteristic in patients with arteriosclerosis.

The capacitance defines how much blood a blood vessel can hold under pressure. Decreasing compliance at a constant ejection period, heartbeat, mean arterial pressure, and stroke volume causes an increase in systolic pressure and decrease in diastolic pressure meaning that the pulse pressure will increase because aortic stiffness increases. Figure 5-1 shows limitation for the graft aorta. Which is needed for design. The limitation is not much of benefit to increased graft compliance but instead causes an increase in diastolic pressure.

5.4 Experiment

The purpose of experimental tests is to explore a strong evidence of similarity in the blood pressure diagram between the present theoretical study and experimental data described by the experimental blood pressure for different mammals. In order to test real animals and simulated aortas machine is used to model the blood flow and pressure characteristics in the aorta using reciprocating piston pump that is derived by an electrical linear motor. This experimental way was employed because has software to allow variable control of stroke volume, heart rate and ejection period could be made somewhat like physiological. In real heart, there are two approaches to measure the stroke volume of the left ventricle, one of two methods is generally employed.

The first method is a thermodilution technique which injects a cold saline solution into the right atrium and uses temperature measurements to track the flow of saline through the right ventricle [21]. A computer algorithm is used to compute the stroke volume. Alternatively, and less invasively, an echocardiogram is used with radionuclide imaging techniques to estimate changes in the dimensions of the left

ventricle during systole, thus computing the stroke volume from the imagery [77, 80].

The left ventricle pump mechanism is controlled using software and the pressure test setup involved obtaining the pressure readings by using transducer pressures that connected to data acquisition then to PC where the reading is visualized on software. This testing approach provides the versatility of being able to measure left ventricle and aortic pressure as shown in Fig. 5-2 that mimics left ventricle pressure and aortic pressure in the ox#5. In general, the illustrative figure was created to understand how left ventricle and aortic pressure change.

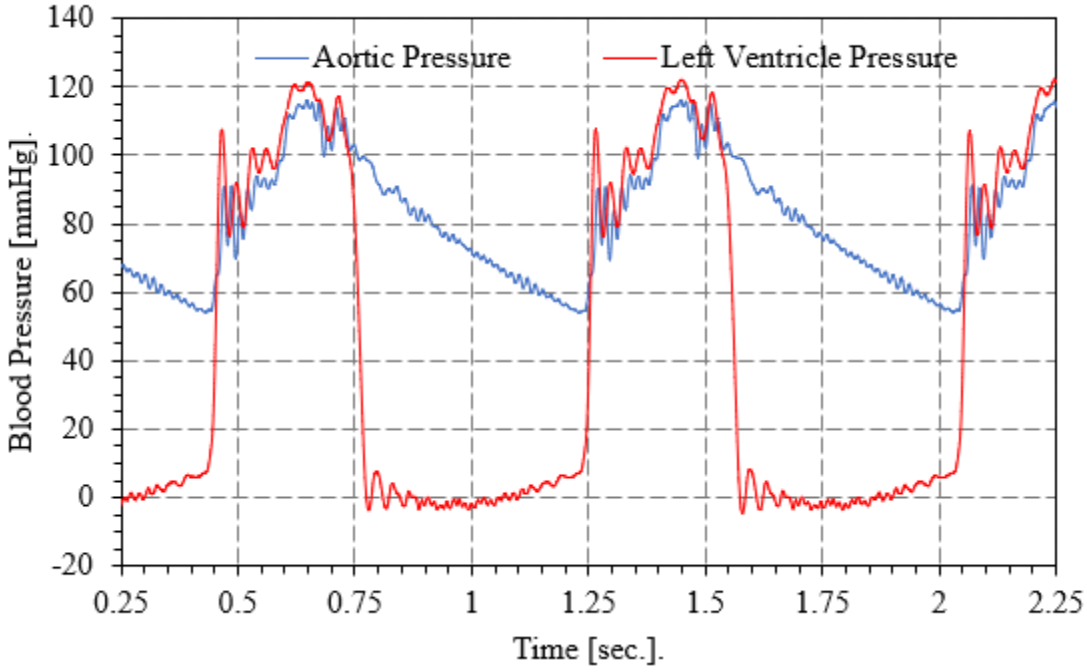

Figure 5-2. The left ventricle pressure and aortic pressure in the ox#5.

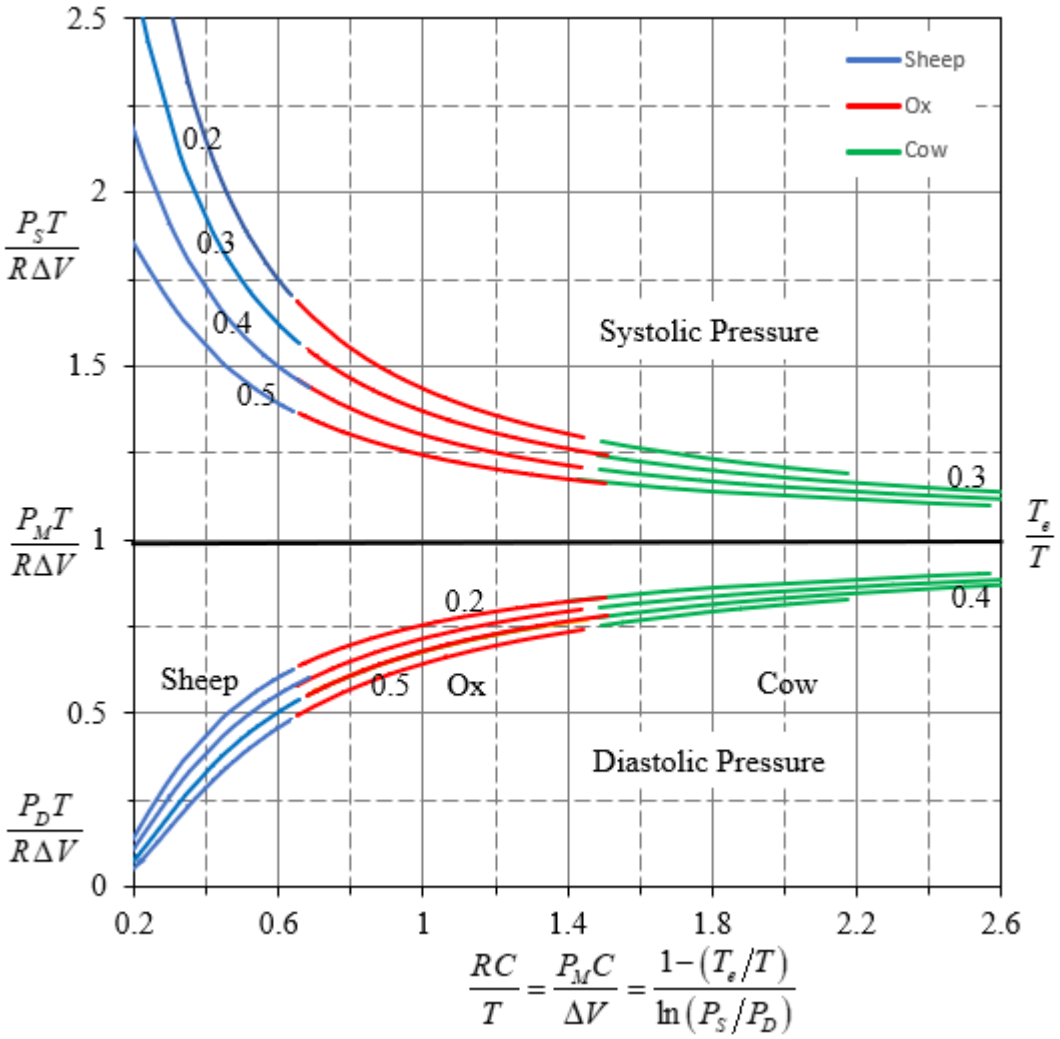

Figure 5-3. The blood-pressure diagram for sheep, ox and cow.

In Figure 5-3, results highlight that little is known about the blood pressure diagram. The new strategy enables to compare between the experimental data that collected from experiments for sheep ox and cow aortas. The blood pressure diagram provides a complete description of the pulse pressure and shows how a compliance of each them varies. clearly, the animal that has a big body size has large compliance and the have the continued path of curves.

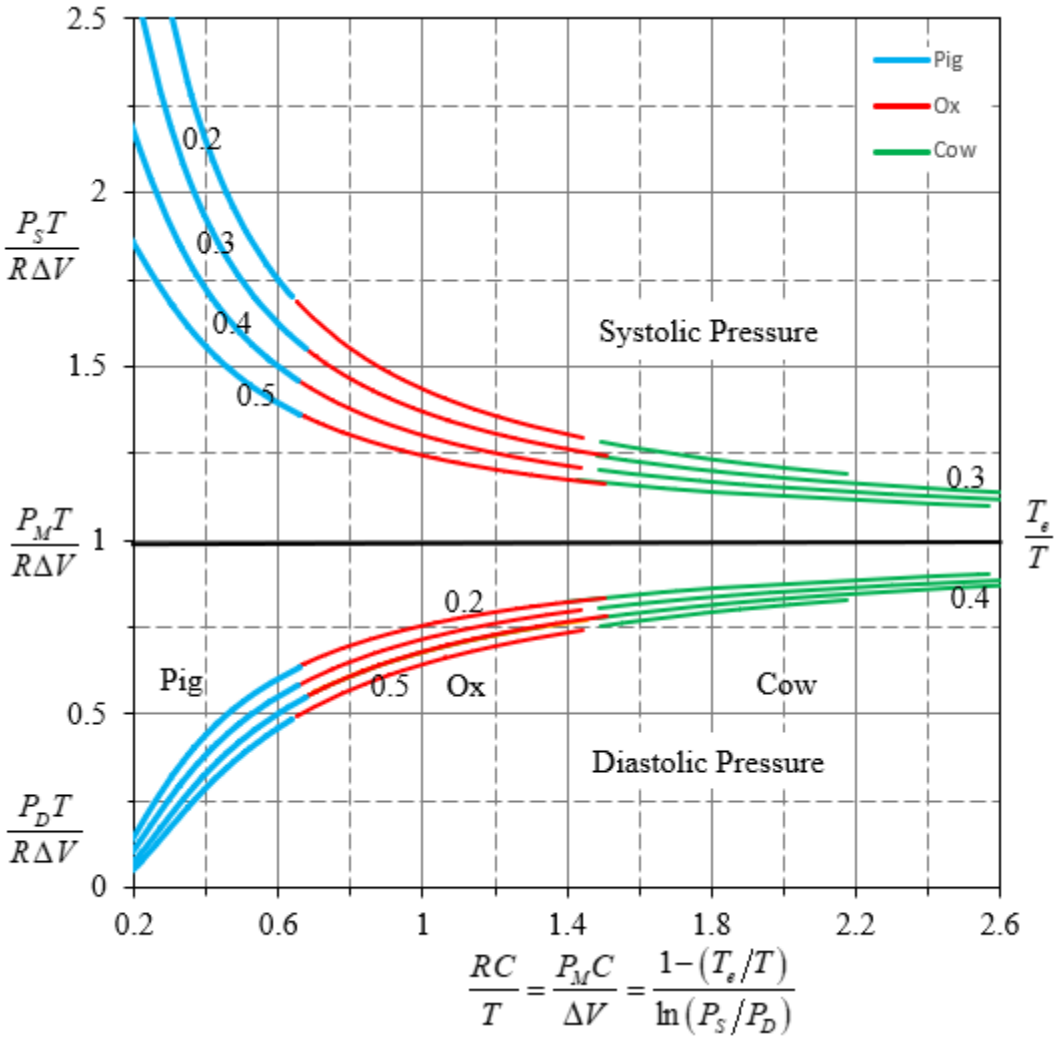

Figure 5-4. The blood-pressure diagram for pig, ox and cow.

The result, as seen in Fig. 5-4 elucidate that pig has higher pulse pressure than ox and cow, and less arterial compliance than ox and cow. That means pig has higher peripheral resistance than others. Generally speaking, an increase in the peripheral resistance will raise all pressures and will tend to raise the pulse pressure slightly will raise all pressures and will tend to raise the pulse pressure slightly.

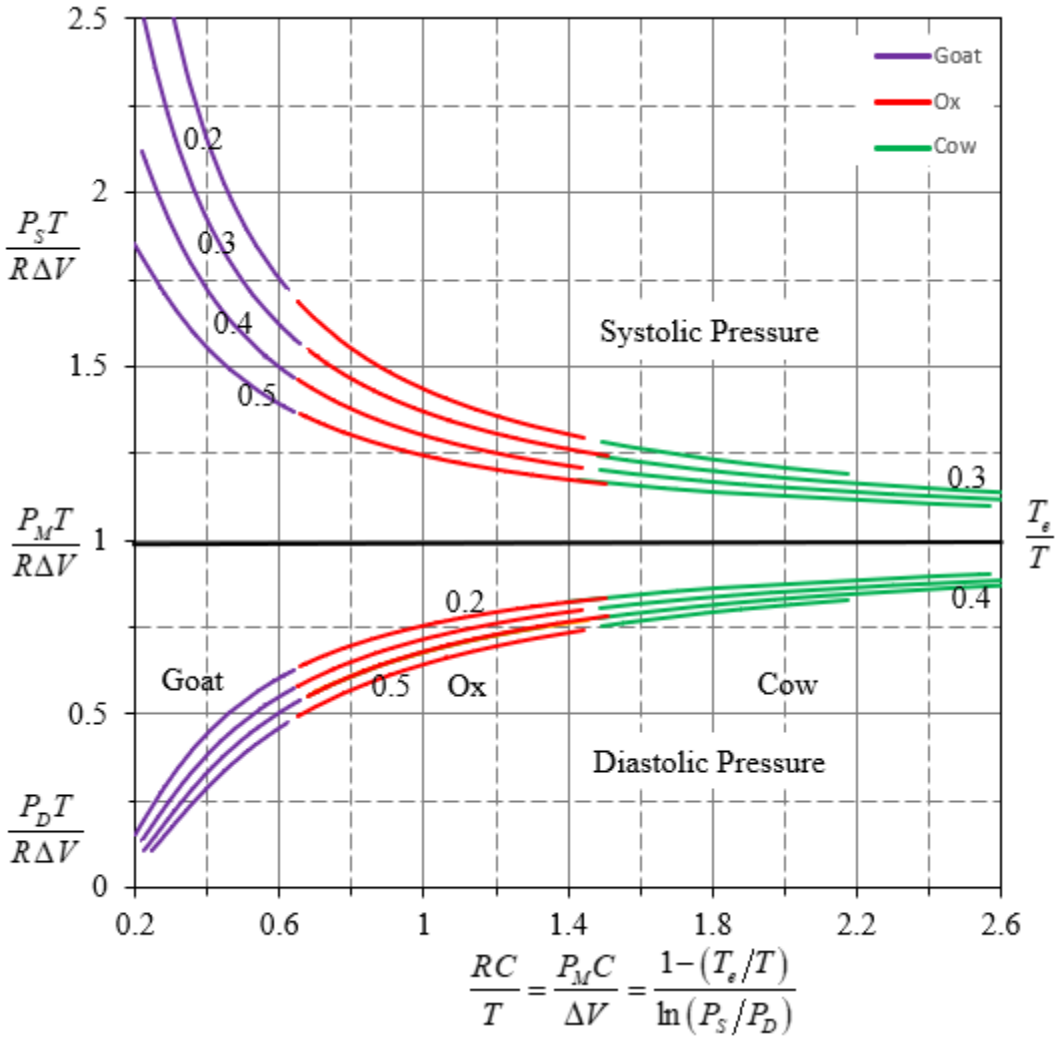

Figure 5-5. The blood-pressure diagram for goat, ox, cow.

For this study, the experimental data of the tests of goat, ox and cow aortas may be interpreted with Fig. 5-5. Further novel findings are that a good match between curves of goat, ox and cow. Figures from Fig. 5-3 to Fig. 5-5 reveal that sheep, pig and goat have close compliance value and peripheral resistance.

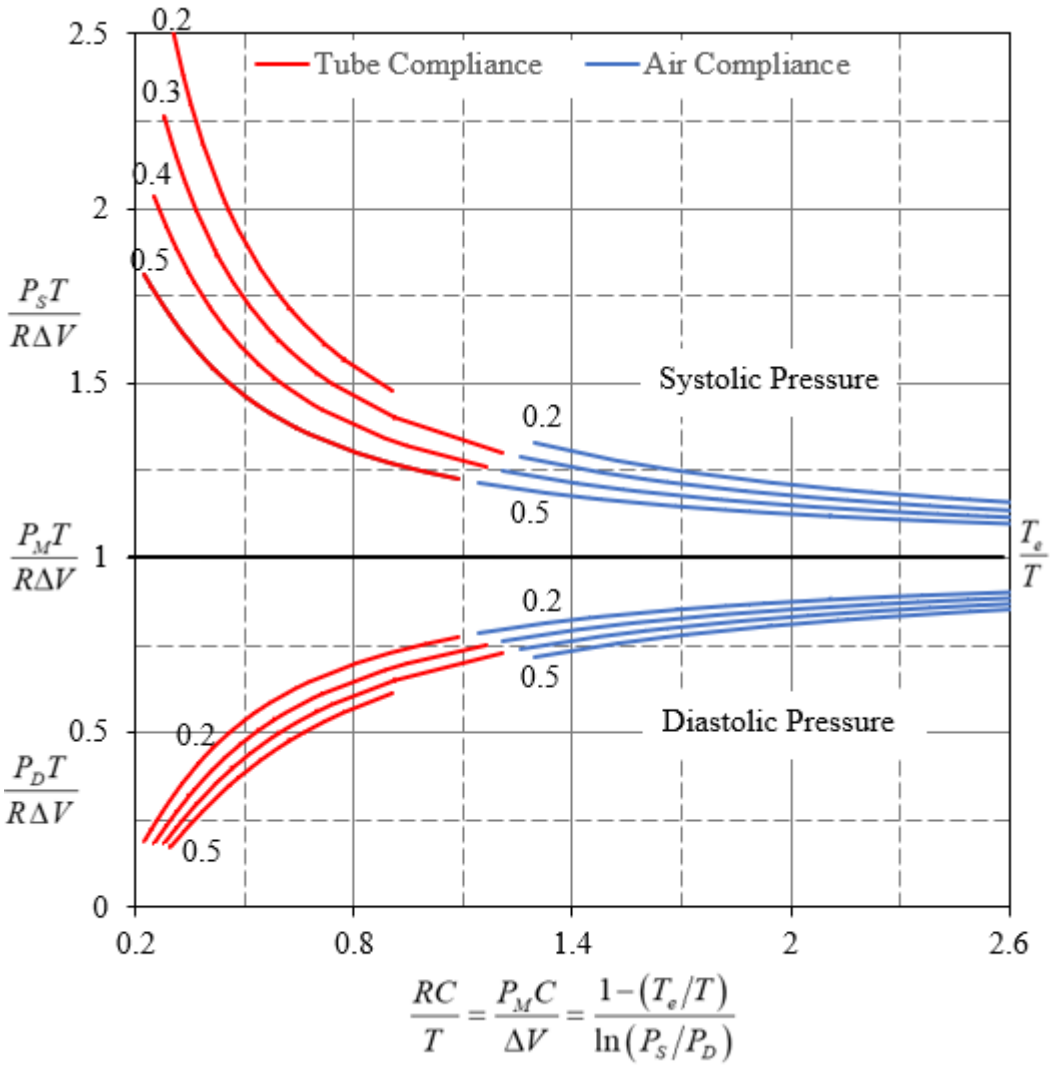

Figure 5-6. The blood-pressure diagram for silicon tube and air chamber.

The present findings might help to figure out correlations between elasticity of the silicon tube that mimics arterial compliance and the air chamber that mimics arterial compliance are shown in Fig. 5-6. The proposed concept of the blood pressure diagram was proved through theory, simulation and experimental results.

5.5 Conclusions

In this chapter, it is shown that clinical measurements of blood pressure and heartrate are insufficient and possibly misleading when used alone for diagnosing cardiovascular health. Indeed, without the additional measures of stroke volume and ejection period, a simple visit to the doctor's office may result in a failure to identify an abnormally high peripheral resistance, or an abnormally low capacitance of the aorta, or the incipient stages of a malfunctioning heart.

There are many cardiovascular medications that are widely used in the management of cardiovascular disease. Even though they decrease peripheral resistance, they can also affect the total arterial compliance. In other words, a simple visit to the doctor's office may result in a failure to identify 1) an abnormally high peripheral resistance, or 2) an abnormally low capacitance of the aorta, or 3) the incipient stages of a malfunctioning heart. Therefore, the estimation of the peripheral resistance and the arterial compliance becomes crucial to determine the right medication for treating hypertension. These parameters can be estimated using clinical measurements. For example, an echocardiogram measures the stroke volume and the ejection period of the heart. To make the physical phenomenon of blood pressure more predictive, we use the blood pressure diagram shown in Fig. 5-1, which depends upon the three nondimensional groups presented in Eq. (5.9).

The most important findings in this chapter reveal the following facts:

1. An increase in the aortic capacitance and / or an increase in the ejection period will decrease the pulse pressure.

2. An increase in the peripheral resistance will increase all pressure measurements in the aorta, while slightly increasing the pulse pressure.
3. An increase in the heartbeat period, corresponding to a slower heartrate, decreases the cardiac output thereby lowering all pressures, while slightly lowering the pulse pressure.
4. An increase in the stroke volume increases all pressure measurements proportionally, including the pulse pressure.
5. A full assessment of cardiovascular health depends upon the measurement of five cardiovascular parameters: stroke volume, heartbeat period, ejection period, systolic pressure, and diastolic pressure.
6. Increased peripheral resistance is stamp of establish hypertension, but altered compliance also probably contributes to the raised blood pressure.
7. An important result of this analysis is to understand that the compliance, and ejection period have no impact on the mean arterial pressure.

It is recommended that patient examinations should include an echocardiogram for measuring the stroke volume and the ejection period of the heart, in addition to measuring blood pressure and heartrate. From these measurements the peripheral resistance and aortic capacitance should be calculated using equations and compared to existing standards for cardiovascular health.

CHAPTER 6. SENSITIVITY ANALYSIS

6.1 Introduction

In the previous chapters, the governing equations of blood pressures, compliance, and peripheral resistance were presented in detail. In this chapter, we will use the Taylor series expansion to quantify the impact of perturbing the five hemodynamic parameters, which describe the blood pressure state of the cardiovascular system. Each parameter will be perturbed relative to a nominal value which describes a healthy blood pressure condition. All conclusions are based upon the mathematical model, which has not been compared to a real biological system in this chapter.

6.2 Sensitive Analysis

Sensitivity analysis utilizes tools designed to help us understand how model perturbing input parameters affect model outputs [82]. Based on the output of the sensitivity analysis we can identify the most important parameter adjustments that result in a hypertensive diagnosis. Sensitivity analysis can provide us with noteworthy insights on how fast responses are with respect to the chances of perturbing the five hemodynamic parameters that are 1) stroke volume ΔV , 2) heart rate T, 3) ejection period T_e, 4) peripheral resistance R, and 5) arterial compliance C. Additionally, Sensitivity analysis determines which are the key factors and the most sensitive parameters that affect hypertension.

Mathematically, sensitivity analysis is proposed based on the Taylor series expansion which allows us to determine the impact of altering each model input parameter based on the model output.

A nominal value is specified to provide a tolerance limit that makes it is possible to measure values between the norm, upper, and lower limits. Table 6-1 illustrates the nominal values used in the sensitivity coefficients.

Table 6-1. Nominal values used as input for the sensitivity analysis.

Symbol	Description	Unit	Nominal Value
P_S	Systolic Pressure	$mm\,Hg$	120
P_D	Diastolic Pressure	$mm\,Hg$	80
T	Heart Rate	s	0.923
T_e	Ejection Period	s	0.2769
R	Total Peripheral Resistance	$mm\,Hg.s\,/\,mL$	1.309
C	Arterial Compliance	$mL\,/\,mm\,Hg$	1.218

As previously noted, we derived a blood pressure equation, an arterial compliance equation, and a peripheral resistance equation to describe the physics of our problem. These equations give us the calculation needed to explain how system perturbing parameters in these equations affect systemic hypertension pressure. The objective of these equations to identify which one of the perturbing parameters has the greatest impact on hypertension.

6.2.1 Systolic Pressure Sensitive Analysis

Systolic pressure is a measure of the highest force that blood exerts on the walls of the large arteries during heart contractions. A mathematical expression for the systolic

pressure equation was derived in Chapter 3. This result is represented here for convenience:

$$P_S = \frac{\Delta V R}{T_e}\left(\frac{1-e^{\frac{-T_e}{RC}}}{1-e^{\frac{-T}{RC}}}\right) . \tag{6.1}$$

By using a first-order Taylor series expansion, this expression may be approximated as:

$$\begin{aligned} P_S = P_{S_o} + \left.\frac{\partial P_S}{\partial \Delta V}\right|_o (\Delta V - \Delta V_o) + \left.\frac{\partial P_S}{\partial T_e}\right|(T_e - T_{eo}) + \left.\frac{\partial P_S}{\partial R}\right|_o (R - R_o) + \\ \left.\frac{\partial P_S}{\partial C}\right|_o (C - C_o) + \left.\frac{\partial P_S}{\partial T}\right|_o (T - T_o) \ , \end{aligned} \tag{6.2}$$

where symbols with a subscript "*o*" are evaluated using the nominal parameters given in Table 6-1. This result can be rearranged and written as:

$$\begin{aligned} \left(\frac{P_S}{P_{S_o}} - 1\right) = \underbrace{\frac{\Delta V_o}{P_{S_o}}\left.\frac{\partial P_S}{\partial \Delta V}\right|_o}_{S_{\Delta V}}\left(\frac{\Delta V}{\Delta V_o} - 1\right) + \underbrace{\frac{T_{eo}}{P_{S_o}}\left.\frac{\partial P_S}{\partial T_e}\right|_o}_{S_{T_e}}\left(\frac{T_e}{T_{eo}} - 1\right) + \\ \underbrace{\frac{R_o}{P_{S_o}}\left.\frac{\partial P_S}{\partial R}\right|_o}_{S_R}\left(\frac{R}{R_o} - 1\right) + \underbrace{\frac{C_o}{P_{S_o}}\left.\frac{\partial P_S}{\partial C}\right|_o}_{S_C}\left(\frac{C}{C_o} - 1\right) + \underbrace{\frac{T_o}{P_{S_o}}\left.\frac{\partial P_S}{\partial T}\right|_o}_{S_T}\left(\frac{T}{T_o} - 1\right) . \end{aligned} \tag{6.3}$$

Where each of the leading coefficients in this equation is the sensitivity coefficient associated with a small perturbation of the associated parameter.

Using the definition shown in Eq. (6.3) the sensitivity coefficient for the stroke volume is given as:

$$S_{\Delta V} = +1 \ . \tag{6.4}$$

The sensitivity coefficient for the peripheral resistance can be expressed as:

$$S_R = \frac{\left(RC - T + T_e\right)e^{\frac{-(T+T_e)}{RC}} - \left(RC + T_e\right)e^{\frac{-T_e}{RC}} + \left(T - RC\right)e^{\frac{-T}{RC}} + RC}{RC\left(e^{\frac{-T_e}{RC}} - 1\right)\left(e^{\frac{-T}{RC}} - 1\right)} \quad . \quad (6.5)$$

The sensitivity coefficient for the arterial compliance is given as:

$$S_C = \frac{\left(T_e - T\right)e^{\frac{-(T+T_e)}{RC}} + T_e\left(e^{\frac{-T}{RC}} - e^{\frac{-T_e}{RC}}\right)}{RC\left(e^{\frac{-T_e}{RC}} - 1\right)\left(e^{\frac{-T}{RC}} - 1\right)} \quad . \quad (6.6)$$

The sensitivity coefficient for the heart rate is shown as:

$$S_T = \frac{-T}{RC}\frac{e^{\frac{-T}{RC}}}{\left(1 - e^{\frac{-T}{RC}}\right)} \quad . \quad (6.7)$$

The sensitivity coefficient for the ejection period is calculated as:

$$S_{Te} = \frac{1 - \left(1 + \frac{T_e}{RC}\right)e^{\frac{-T_e}{RC}}}{e^{\frac{-T_e}{RC}} - 1} \quad . \quad (6.8)$$

By evaluating each of these coefficients using the nominal conditions shown in Table 6-1, the results of Table 6-2 were generated to illustrate the relative sensitivity of the systolic pressure to small perturbations for each parameter. Figure 6-1 presents the same results using a graphical representation.

Table 6-2. Variation in sensitivity coefficients of the systolic pressure.

Sensitivity Coefficient	Systolic Pressure
Stroke Volume, $S_{\Delta V}$	+1.000
Ejection Period, S_{T_e}	– 0.084324
Heartbeat Period, S_T	– 0.73832
Peripheral Resistance, S_R	+0.82264
Compliance, S_C	– 0.1774

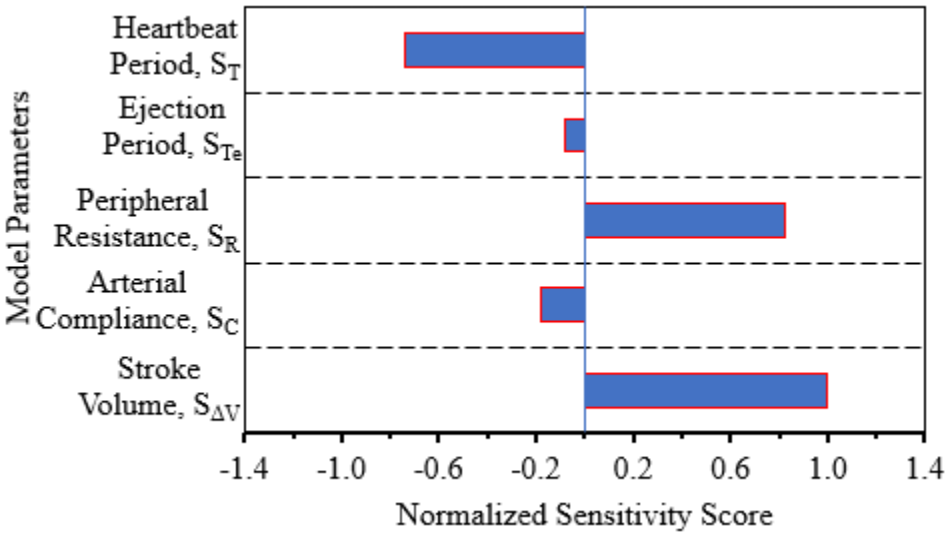

Figure 6-1. Variation in sensitivity coefficients of the systolic pressure.

Figure 6-1 clearly identifies the stroke volume of the left ventricle, total peripheral resistance, heart rate and arterial compliance to be the most important parameters that may be adjusted for altering systolic pressure from the standpoint of a healthy person. From this figure, it can be inferred that for a hypertension problem, these parameters should be given priority in treatments, because they would have the greatest influence on the systolic pressure.

The magnitude of the sensitivity coefficient reveals the amount of influence a parameter has on the objective function; its sign tells us the direction in which this influence acts. In other words, the sensitivity coefficient with the large absolute value will indicate that a plus or minus percent change in that parameter will create the largest impact on the blood pressure.

The results presented in Table 6-1 and Fig. 6-1 are useful for understanding the impact of adjusting one of the mechanical properties associated with the blood pressure problem. One of the great impacts on the systolic pressure is to adjust the stroke volume $\left(S_{\Delta V}\right)$. A small increase in stroke volume will increase the systolic pressure, while a small decrease in the stroke volume will have the opposite effect. This result suggests that the most important influence on the systolic pressure is the strength of the heart contraction. A large cardiac reserve provides the most flexibility for adjusting the systolic pressure.

As shown in Table 6-1, the reduction of the peripheral resistance $\left(R\right)$ coefficient will also have a significant impact on the systolic pressure, because the sensitivity coefficient associated with peripheral resistance has a large value. If the peripheral resistance decreases, then the systolic pressure will also decrease.

According to the sensitivity analysis, a slower heart rate (larger T) is shown to decrease the systolic pressure. Assuming that the stroke volume has not changed, a slower heartrate corresponds to a lower cardiac output. The impact of adjusting the compliance and ejection period is almost similar in magnitude and direction. By increasing the stiffness of the aorta, the systolic pressure and diastolic pressure decreases.

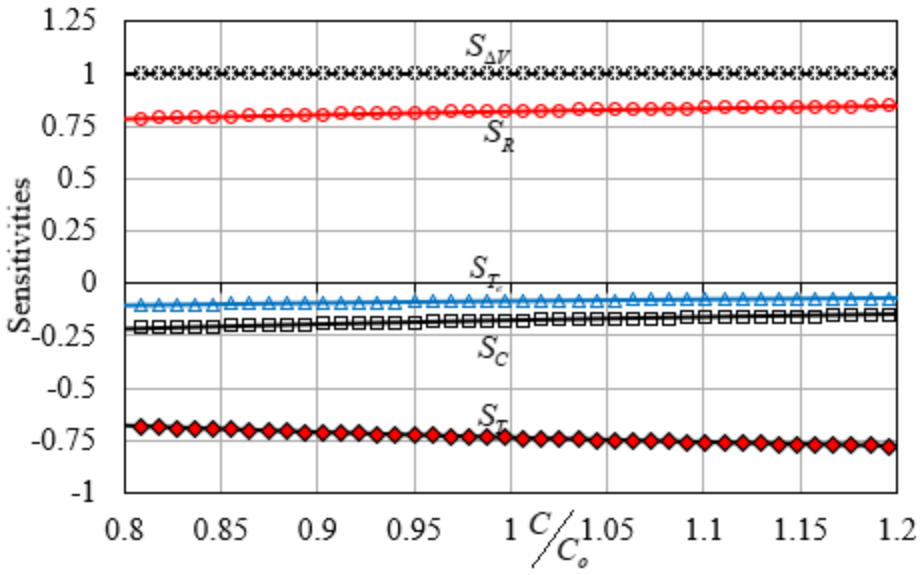

Figure 6-2. Variation in sensitivity coefficients for changes in peripheral resistance. These results have been generated for nominal values of R_o = 1.309 mm *Hg* s/*mL*, C_o = 1.218 *mL*/ *mm Hg*, T_o = 0.923 s, T_{e_o} = 0.2769 *s*, and ΔV_o = 70 *mL*.

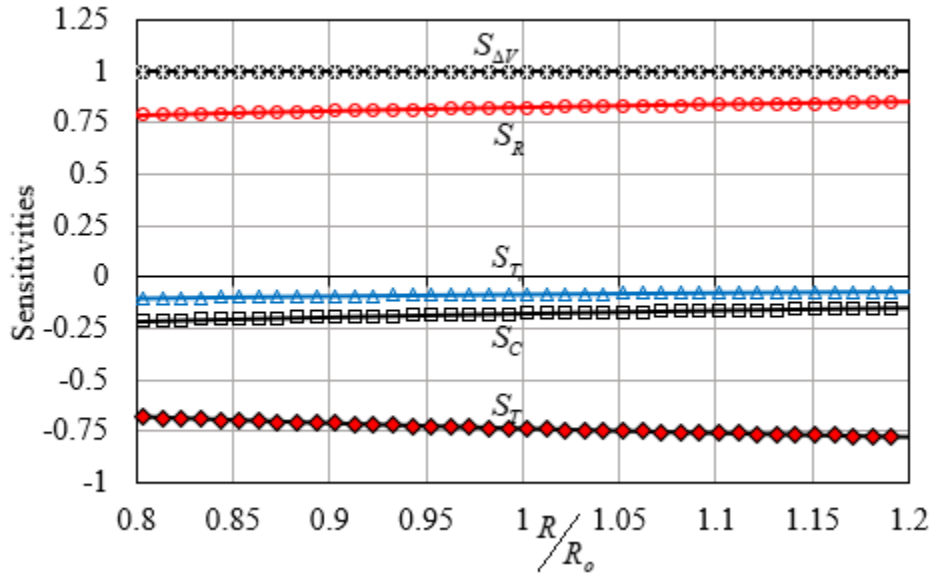

Figure 6-3. Variation in sensitivity coefficients for changes in peripheral resistance. These results have been generated for nominal values of R_o = 1.309 mm *Hg* s/*mL*, C_o = 1.218 *mL*/ *mm Hg*, T_o = 0.923 s, T_{e_o} = 0.2769 *s*, and ΔV_o = 70 *mL*.

Figures 6-2 and 6-3 have been created to show that sensitivity coefficients of stroke volume, arterial compliance, and ejection period remain almost constant with increasing C / C_o and R / R_o ,while sensitivities of peripheral resistance increases lightly while heart rate decreases lightly too.

For sake of showing, how sensitivity coefficients in Eq. (6.3) particularly change in C / C_o , R / R_o , T / T_o and T_e / T_{eo} . Figures 6-4 and 6-5 have been plotted to show that sensitivity coefficients of stroke volume, arterial compliance, and ejection period remain almost constant with increasing T / T_o and T_e / T_{eo} ,while sensitivities of peripheral resistance decreases proportionally with heart rate, and heart rate increases proportionally.

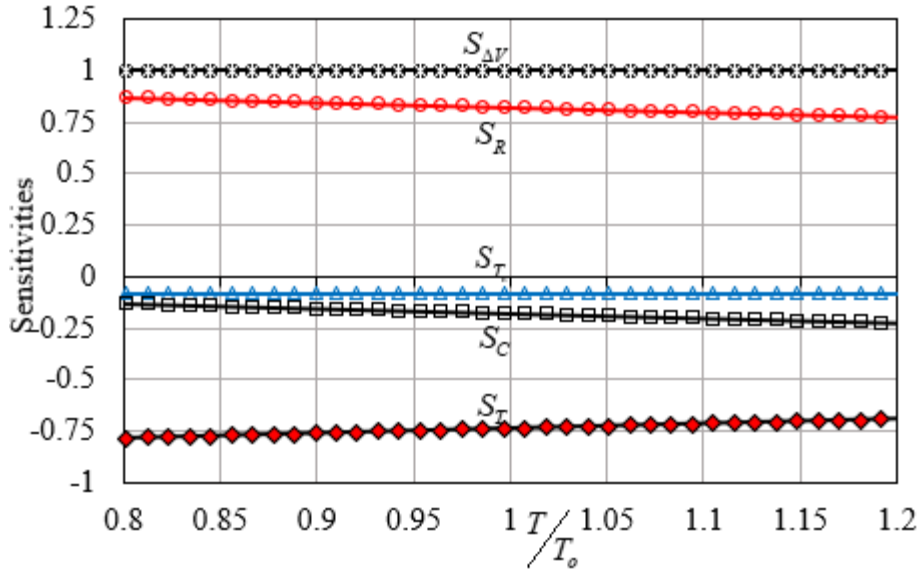

Figure 6-4. Variation in sensitivity coefficients for changes in heart rate. These results have been generated for nominal values of R_o = 1.309 mm *Hg.* s/*mL*, C_o = 1.218 *mL*/ *mm Hg*, T_o = 0.923 s, T_{e_o} = 0.2769 *s*, and ΔV_o = 70 *mL*.

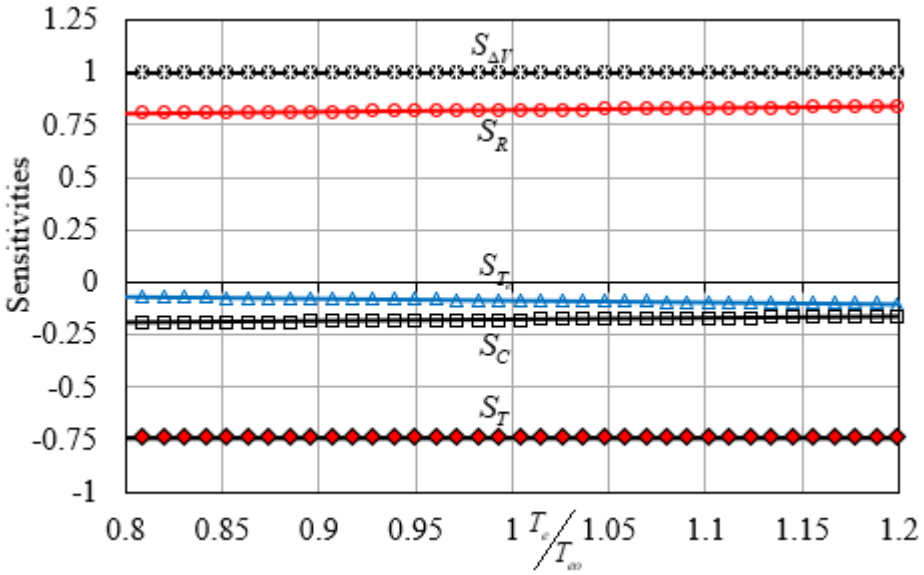

Figure 6-5. Variation in sensitivity coefficients for changes in ejection period. These results have been generated for nominal values of R_o = 1.309 mm *Hg.* s / *mL*, C_o = 1.218 *mL*/ *mm Hg*, T_o = 0.923 s, T_{e_o} = 0.2769 *s*, and ΔV_o = 70 *mL*.

6.2.2 Diastolic Pressure Sensitive Analysis

Diastolic pressure is a measure of the lowest force that blood exerts on the walls of the large arteries during the heart filling. The purpose of diastolic pressure equation in chapter three was to conduct a sensitivity analysis using sensitivity coefficients to reveal which perturbing parameters would have the greatest influence on the diastolic pressure. This result is reviewed here for convenience:

$$P_D = \frac{\Delta V R}{T_e}\left(\frac{1-e^{\frac{T_e}{RC}}}{1-e^{\frac{T}{RC}}}\right) \quad . \tag{6.9}$$

Applying the Taylor series expansion on Eq. (6.9) is given by:

$$\begin{aligned} P_D = P_{D_o} + \left.\frac{\partial P_D}{\partial \Delta V}\right|_o (\Delta V - \Delta V_o) + \left.\frac{\partial P_D}{\partial T_e}\right|(T_e - T_{eo}) + \left.\frac{\partial P_D}{\partial R}\right|_o (R - R_o) + \\ \left.\frac{\partial P_D}{\partial C}\right|_o (C - C_o) + \left.\frac{\partial P_D}{\partial T}\right|_o (T - T_o) \quad , \end{aligned} \tag{6.10}$$

which can be rearranged according to the following:

$$\begin{aligned} \left(\frac{P_D}{P_{D_o}} - 1\right) = \underbrace{\frac{\Delta V_o}{P_{D_o}}\left.\frac{\partial P_D}{\partial \Delta V}\right|_o}_{S_{\Delta V}}\left(\frac{\Delta V}{\Delta V_o} - 1\right) + \underbrace{\frac{T_{eo}}{P_{D_o}}\left.\frac{\partial P_D}{\partial T_e}\right|_o}_{S_{T_e}}\left(\frac{T_e}{T_{eo}} - 1\right) + \\ \underbrace{\frac{R_o}{P_{D_o}}\left.\frac{\partial P_D}{\partial R}\right|_o}_{S_R}\left(\frac{R}{R_o} - 1\right) + \underbrace{\frac{C_o}{P_{D_o}}\left.\frac{\partial P_D}{\partial C}\right|_o}_{S_C}\left(\frac{C}{C_o} - 1\right) + \underbrace{\frac{T_o}{P_{D_o}}\left.\frac{\partial P_D}{\partial T}\right|_o}_{S_T}\left(\frac{T}{T_o} - 1\right) \quad . \end{aligned} \tag{6.11}$$

The sensitivity coefficient is given for the stroke volume, which can be written as:

$$S_{\Delta V} = +1 \, . \tag{6.12}$$

The sensitivity coefficient for the peripheral resistance is expressed as:

$$S_R = \frac{\left(RC - T + T_e\right)e^{\frac{(T+T_e)}{RC}} + \left(T_e - RC\right)e^{\frac{T_e}{RC}} - \left(T + RC\right)e^{\frac{T}{RC}} + RC}{RC\left(e^{\frac{T_e}{RC}} - 1\right)\left(e^{\frac{T}{RC}} - 1\right)} \quad . \quad (6.13)$$

The sensitivity coefficient for the arterial compliance is given as:

$$S_C = \frac{\left(T - T_e\right)e^{\frac{(T+T_e)}{RC}} + T_e\left(e^{\frac{T_e}{RC}} - e^{\frac{T}{RC}}\right)}{RC\left(e^{\frac{T_e}{RC}} - 1\right)\left(e^{\frac{T}{RC}} - 1\right)} \quad . \quad (6.14)$$

The sensitivity coefficient for the heart rate is calculated as:

$$S_T = \frac{T}{RC}\frac{e^{\frac{T}{RC}}}{\left(1 - e^{\frac{T}{RC}}\right)} \quad . \quad (6.15)$$

The sensitivity coefficient for the ejection period is as:

$$S_{Te} = \frac{RC + \left(T_e - RC\right)e^{\frac{T_e}{RC}}}{RC\left(e^{\frac{T_e}{RC}} - 1\right)} \quad . \quad (6.16)$$

Table 6-3. Variation in sensitivity coefficients of the diastolic pressure.

Sensitivity Coefficient	Diastolic Pressure
Stroke Volume, $S_{\Delta V}$	+1.000
Ejection Period, S_{T_e}	+0.0893
Heartbeat Period, S_T	–1.3172
Peripheral Resistance, S_R	+1.22788
Compliance, S_C	+0.228

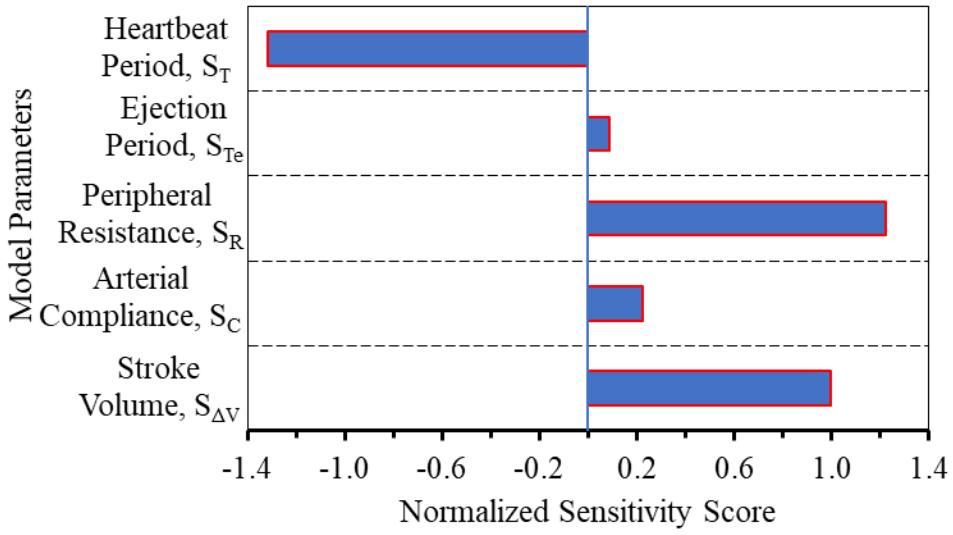

Figure 6-6. Variation in sensitivity coefficients of the diastolic pressure.

It is apparent from Table 6-3 and Figure 6-6 that stroke volume, peripheral resistance, and heart rate period have a significant impact on altering the diastolic pressure. Therefore, any increase in stroke volume peripheral resistance leads to an increase in diastolic pressure. In other words, a slower heartrate and reduced peripheral resistance will reduce diastolic pressure the most. The heart rate period has a greater impact on diastolic pressure mean arterial pressure than systolic pressure. Thus, the quickest way to reduce diastolic pressure from a physician's standpoint is to reduce

heartbeat or peripheral resistance because diastolic pressure is more likely to cause hypertension according to Table 6-3, While aorta compliance and ejection period have an almost equal impact on the diastolic pressure, these parameters have a greater impact on diastolic pressure than systolic pressure and there is no impact on mean arterial pressure.

Figure 6-7 to Figure 6-10 demonstrate how sensitivity coefficients in Eq.(6.11) particularly change in C/C_o, R/R_o, T/T_o and T_e/T_{eo}. Sensitivities of stroke volume, arterial compliance, and ejection period in Figs. 6-7 and 6-8 remain almost constant with an increasing C/C_o and R/R_o; hence, sensitivities of peripheral resistance decrease proportionally, while heart rate increases proportionally.

The relationship between (S_T), (S_R) and (S_C),and T/T_o were concluded in Fig. 5-9 that (S_R), and (S_C) linearly increase to T/T_o and the (S_T) shows linear decreasing proportionality to T/T_o while the remaining coefficients stay constant. Figure 5-10 illustrates that all sensitivity coefficients in Eq.(6-11) remain constant with an increase in C/C_o, R/R_o, T/T_o and T_e/T_{eo}.

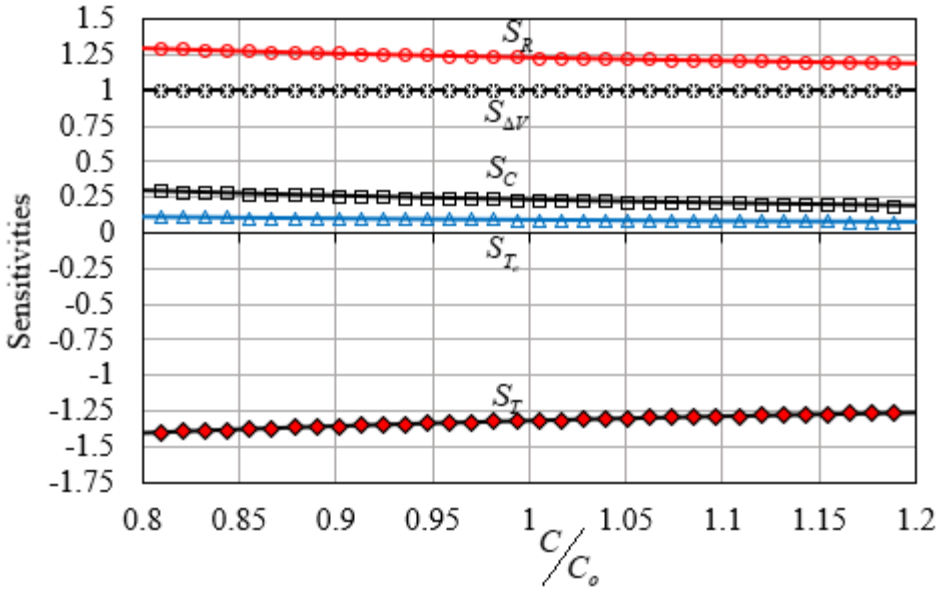

Figure 6-7. Variation in sensitivity coefficients for changes in arterial compliance. These results have been generated for nominal values of R_o = 1.309 mm *Hg.* s / *mL*, C_o = 1.218 *mL*/ *mm Hg*, T_o = 0.923 s, T_{e_o} = 0.2769 *s*, and ΔV_o = 70 *mL*.

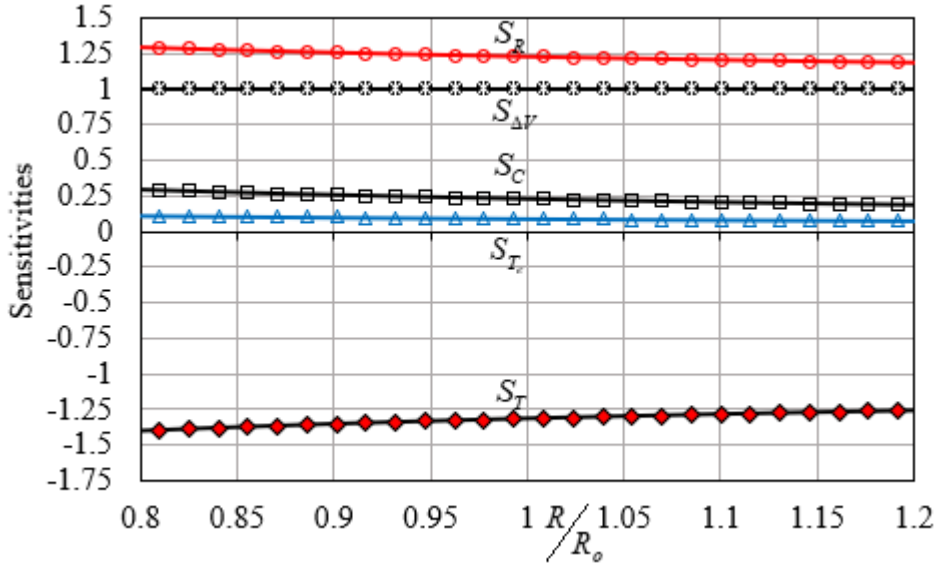

Figure 6-8. Variation in sensitivity coefficients for changes in peripheral resistance. These results have been generated for nominal values of R_o = 1.309 mm *Hg.* s / *mL*, C_o = 1.218 *mL*/ *mm Hg*, T_o = 0.923 s, T_{e_o} = 0.2769 *s*, and ΔV_o = 70 *mL*.

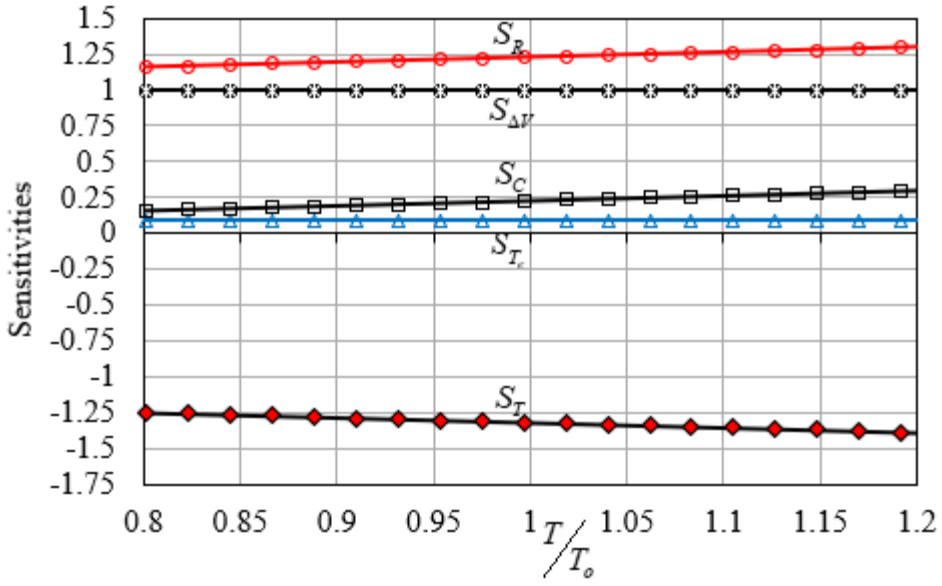

Figure 6-9. Variation in sensitivity coefficients for changes in heart rate. These results have been generated for nominal values of R_o = 1.309 mm *Hg* .s / *mL*, C_o = 1.218 *mL*/ *mm Hg*, T_o = 0.923 s, T_{e_o} = 0.2769 *s*, and ΔV_o = 70 *mL*.

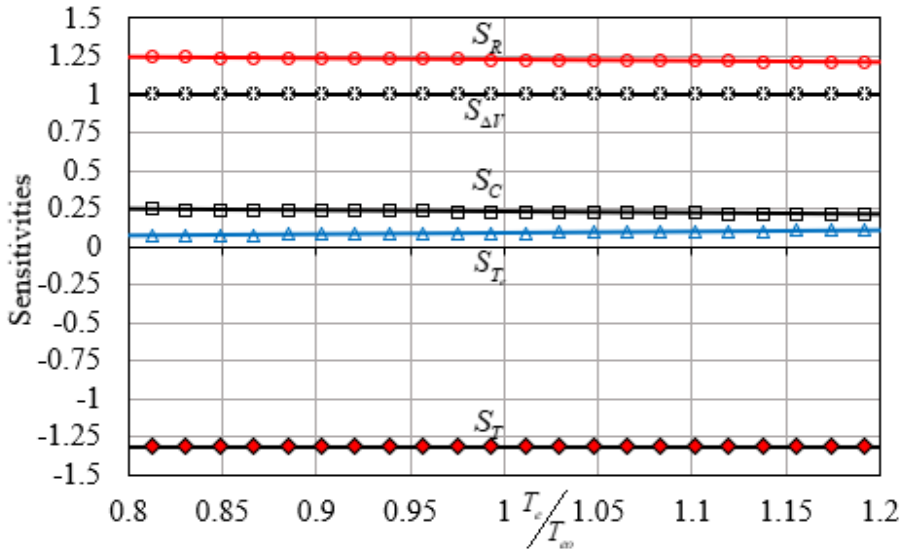

Figure 6-10. Variation in sensitivity coefficients for changes in heart rate. These results have been generated for nominal values of R_o = 1.309 mm *Hg*. s / *mL*, C_o = 1.218 *mL*/ *mm Hg*, T_o = 0.923 s, T_{e_o} = 0.2769 *s*, and ΔV_o = 70 *mL*.

6.2.3 Mean Arterial Pressure Sensitive Analysis

Mean arterial pressure is the average blood pressure throughout arteries. In Chapter three, the mean arterial pressure equation was derived that represents four perturbing parameters. These parameters can be measured, but then the question that must be answered is: What is the effect of undertrained parameters on the blood pressure? The sensitivity analysis provided a set of coefficients that can answer this question. The result is reviewed here for convenience:

$$P_M = P_D \frac{T_e}{T} \frac{1-(P_S/P_D)^{\frac{T}{T-T_e}}}{1-(P_S/P_D)^{\frac{T_e}{T-T_e}}} \quad . \tag{6.17}$$

Substituting Eqs. (6.1) and (6.9) into Eq. (6.17) we get

$$P_M = \frac{\Delta V R}{T} \tag{6.18}$$

Applying the Taylor series expansion for the mean arterial pressure in Eq. (6.17) is given by

$$\begin{aligned} P_M = P_{M_o} + \left.\frac{\partial P_M}{\partial \Delta V}\right|_o (\Delta V - \Delta V_o) + \left.\frac{\partial P_M}{\partial R}\right|_o (R - R_o) + \\ \left.\frac{\partial P_M}{\partial T}\right|_o (T - T_o), \end{aligned} \tag{6.19}$$

which can be rearranged according to the following

$$\begin{aligned} \left(\frac{P_M}{P_{M_o}} - 1\right) = \underbrace{\frac{\Delta V_o}{P_{M_o}} \left.\frac{\partial P_M}{\partial \Delta V}\right|_o}_{S_{\Delta V}} \left(\frac{\Delta V}{\Delta V_o} - 1\right) + \underbrace{\frac{R_o}{P_{M_o}} \left.\frac{\partial P_M}{\partial R}\right|_o}_{S_R} \left(\frac{R}{R_o} - 1\right) \\ + \underbrace{\frac{T_o}{P_{M_o}} \left.\frac{\partial P_M}{\partial T}\right|_o}_{S_T} \left(\frac{T}{T_o} - 1\right) \quad . \end{aligned} \tag{6.20}$$

In these equations, the subscript *o* is used to denote nominal values from which a parameter is slightly perturbed. The coefficient in front of the curve brackets are sensitivity coefficients $S_{\Delta V}$, S_R and S_T, and their relative magnitude describes how the sensitive the systolic pressure is to small changes in a respective parameter.

Table 6-4. Variation in sensitivity coefficients of the mean arterial pressure.

Sensitivity Coefficient	Mean Arterial Pressure
Stroke Volume, $S_{\Delta V}$	+1.000
Ejection Period, S_{T_e}	0.000
Heartbeat Period, S_T	– 1.000
Peripheral Resistance, S_R	+1.000
Compliance, S_C	0.000

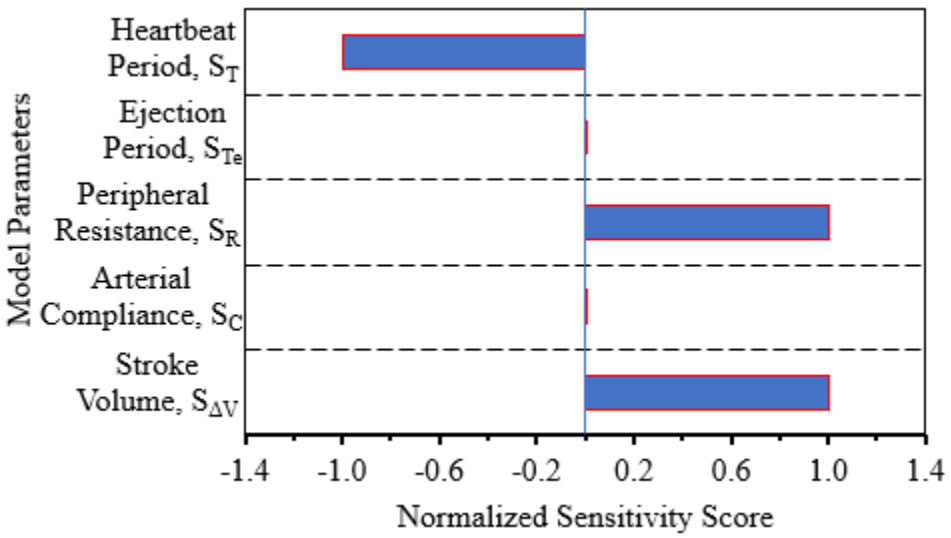

Figure 6-11. Variation in sensitivity coefficients of the mean arterial pressure.

Adjustments in all these parameters are equally important and an increase in each of them produces an increase in the mean arterial pressure. On the other hand, a decrease

in these parameters produces a decrease in the mean arterial pressure. An important result of this analysis is that the compliance and ejection periods have no impact on the mean arterial pressure as shown in Fig. 6-11 and Table 6-4. In other words, if a physician is trying to adjust the mean arterial pressure, then efforts should be made to modify these parameters.

6.2.4 Pulse Pressure Sensitive Analysis.

Pulse pressure is the difference between the systolic and diastolic pressure. Pulse pressure is the best measure of blood pressure when evaluating the health of people who have hypertension. Physicians consider a healthy pulse pressure as 40 and any number higher than that is considered a sign of risk for coronary artery disease. If the rate is higher than 40 mm Hg, it may be a sign of aortic valve regurgitation while a pulse rate lower than 40 mm Hg may be a sign of aortic stenosis [83]. Increasing pulse pressure is a strong predictor of cardiovascular mortality [70]. Elevations in pulse pressure strongly predict morbidity and mortality. To identify influential parameters the sensitivity analysis was applied to pulse pressure equation in chapter three to determine the effect of changes in parameters on the pulse pressure. This result is reviewed here for convenience:

$$\Delta P = \frac{R\Delta V}{T_e}\ \frac{1-e^{\left(\frac{T_e}{RC}\right)}}{1-e^{\left(\frac{T}{RC}\right)}}\left[e^{\left(\frac{T-T_e}{RC}\right)}-1\right]\ . \tag{6.21}$$

Appling the Taylor series expansion for the mean arterial pressure in Eq. (6.21) is given by:

$$\Delta P = \Delta P_o + \left.\frac{\partial \Delta P}{\partial \Delta V}\right|_o (\Delta V - \Delta V_o) + \left.\frac{\partial \Delta P}{\partial T_e}\right|_o (T_e - T_{eo}) + \left.\frac{\partial \Delta P}{\partial T}\right|_o (T - T_o) + \left.\frac{\partial \Delta P}{\partial R}\right|_o (R - R_o) + \left.\frac{\partial \Delta P}{\partial C}\right|_o (C - C_o) \quad , \tag{6.22}$$

which can be rearranged as follow:

$$\left(\frac{\Delta P}{\Delta P_o} - 1\right) = \underbrace{\frac{\Delta V_o}{\Delta P_o}\left.\frac{\partial \Delta P}{\partial \Delta V}\right|_o}_{S_{\Delta V}} \left(\frac{\Delta V}{\Delta V_o} - 1\right) + \underbrace{\frac{T_{eo}}{\Delta P_o}\left.\frac{\partial \Delta P}{\partial T_e}\right|_o}_{S_{T_e}} \left(\frac{T_e}{T_{eo}} - 1\right) + \underbrace{\frac{T_o}{\Delta P_o}\left.\frac{\partial \Delta P}{\partial T}\right|_o}_{S_T} \left(\frac{T}{T_o} - 1\right) + \underbrace{\frac{R_o}{\Delta P_o}\left.\frac{\partial \Delta P}{\partial R}\right|_o}_{S_R} \left(\frac{R}{R_o} - 1\right) + \underbrace{\frac{C_o}{\Delta P_o}\left.\frac{\partial \Delta P}{\partial C}\right|_o}_{S_C} \left(\frac{C}{C_o} - 1\right) \quad . \tag{6.23}$$

Table 6-5. Variation in sensitivity coefficients of the pulse pressure.

Sensitivity Coefficient	Pulse Pressure
Stroke Volume, $S_{\Delta V}$	+1.000
Ejection Period, S_{T_e}	– 0.43186
Heartbeat Period, S_T	+0.42025
Peripheral Resistance, S_R	+0.01161257
Compliance, S_C	– 0.98828

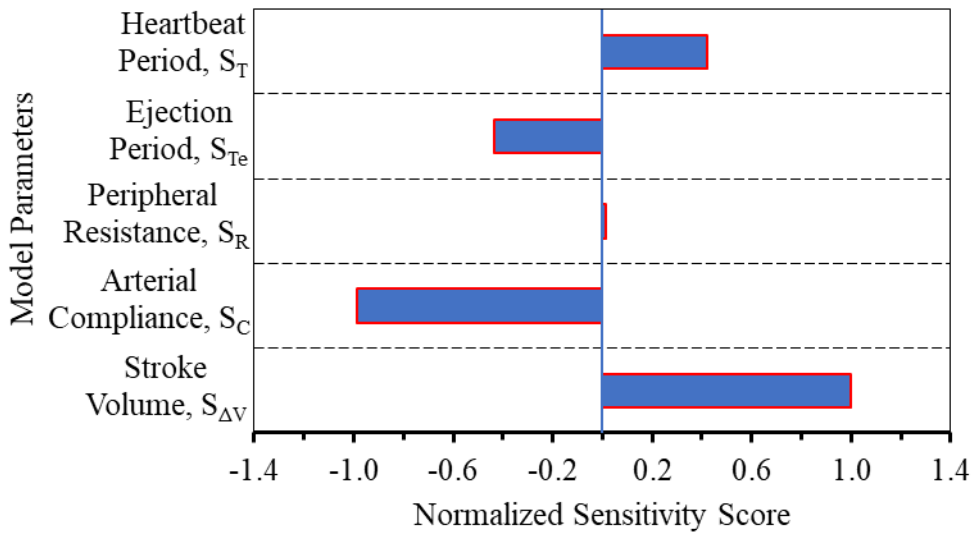

Figure 6-12. Variation in sensitivity coefficients of the pulse pressure.

The arterial compliance and stroke volume have the greatest impact on pulse pressure, while the sensitivity analysis also reveals that the peripheral resistance has no impact on pulse pressure. Arterial stiffness and stroke volume cannot be reduced by drugs, but the sensitivity analysis gives another choice to treat the high pulse pressure by increasing heart rate (T) and decreasing ejection period (T_e). Therefore, pulse pressure must be dealt with care in the guidance of a hypertension therapy [82].

The preceding figures show the effect of increasing the ejection period of both the mean arterial pressure and the pulse pressure. The effect of increasing the ejection period on the mean arterial pressure has less than it has on the impact of pulse pressure. These findings agree with the sensitivity analysis results, which show us the values of these impacts $S_{T_e} = -0.43186$ (for pulse pressure) and $S_{T_e} = 0.008323$ (for mean arterial pressure) as shown in Fig. 6-12 and Table 6-5.

Figures 6-13 and 6-14 have been created to illustrate that sensitivity coefficients of Eq. (6.20) have a little or no effect can be seen that means remain constant with an increase in C/C_o or R/R_o, and the analysis performed of Eq. (6.20) indicate that the sensitivity coefficients of pulse pressure can be illustrated (in Figs. 6-15 and 6-16) as follows: Sensitivity coefficients of arterial compliance and peripheral resistance as well as $\left(S_{\Delta V}\right)$ remain constant. The $\left(S_{T_e}\right)$ in Fig. 6-15 shows increasing proportionality to T/T_o. It is apparent from Fig. 6-13 that the $\left(S_T\right)$ shows decreasing proportionality to T/T_o, while the $\left(S_{T_e}\right)$ shows increasing and other sensitivity coefficients have no effect can be seen. In contrast to earlier Figure, the $\left(S_T\right)$ in Fig. 6-16 shows increasing proportionality to T/T_o while the $\left(S_{T_e}\right)$ shows increasing. In Fig. 6-16 the $\left(S_T\right)$ shows decreasing, and other sensitivity coefficients remain constant.

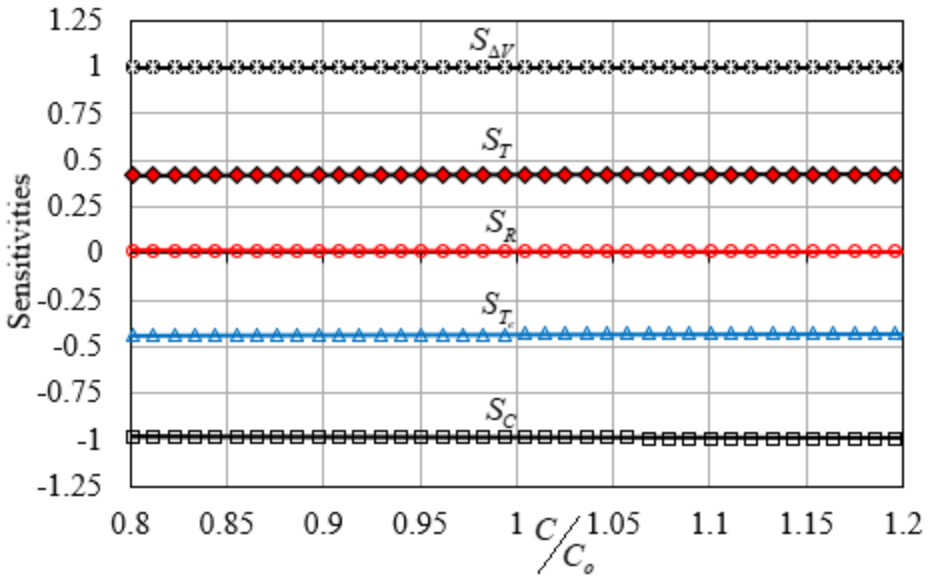

Figure 6-13. Variation in sensitivity coefficients for changes in arterial compliance. These results have been generated for nominal values of R_o = 1.309 mm *Hg.* s / *mL*, C_o = 1.218 *mL*/ *mm Hg*, T_o = 0.923 s, T_{e_o} = 0.2769 *s*, and ΔV_o = 70 *mL*.

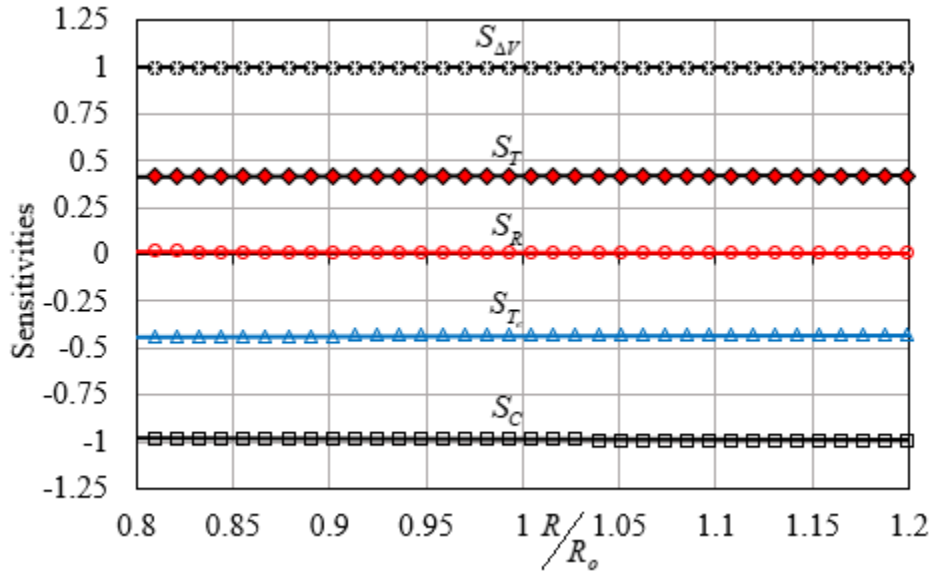

Figure 6-14. Variation in sensitivity coefficients for changes in peripheral resistance. These results have been generated for nominal values of R_o = 1.309 mm *Hg.* s/*mL*, C_o = 1.218 *mL*/ *mm Hg*, T_o = 0.923 s, T_{e_o} = 0.2769 *s*, and ΔV_o = 70 *mL*.

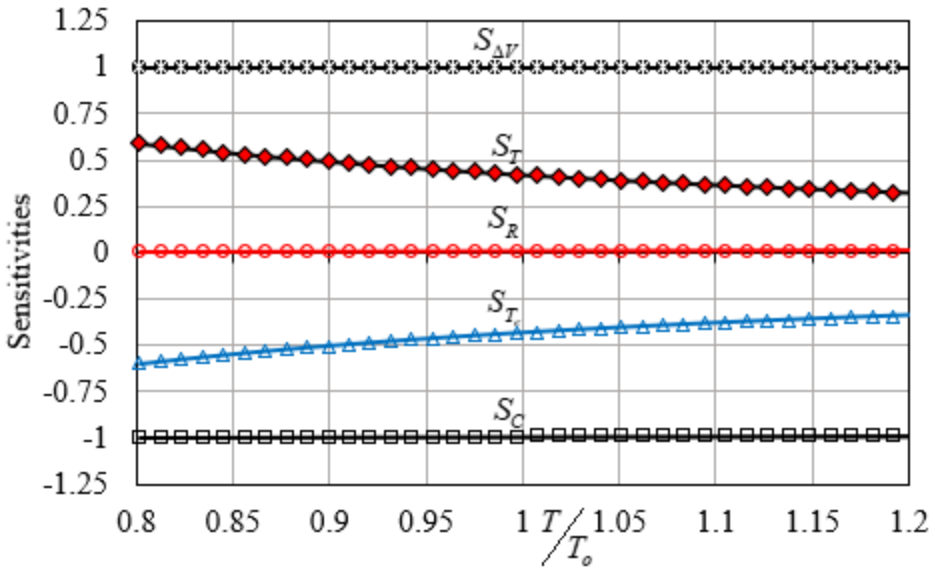

Figure 6-15. Variation in sensitivity coefficients for changes in ejection period. These results have been generated for nominal values of R_o = 1.309 mm *Hg.* s/*mL*, C_o = 1.218 *mL*/ *mm Hg*, T_o = 0.923 s, T_{e_o} = 0.2769 *s*, and ΔV_o = 70 *mL*.

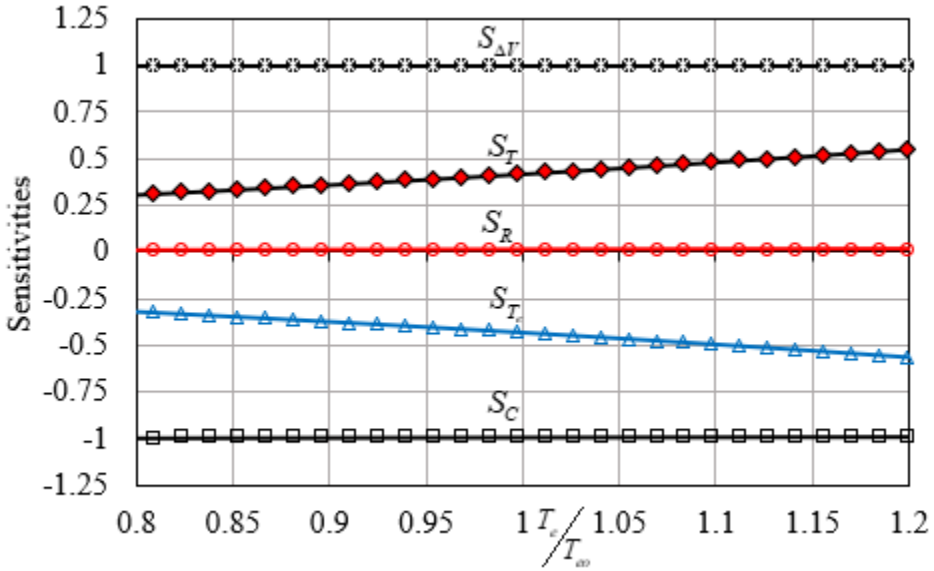

Figure 6-16. Variation in sensitivity coefficients for changes in ejection period. These results have been generated for nominal values of R_o = 1.309 mm *Hg.* s/*mL*, C_o = 1.218 *mL*/ *mm Hg*, T_o = 0.923 s, T_{e_o} = 0.2769 *s*, and ΔV_o = 70 *mL*.

6.2.5 Independent Perturbing Parameters

In the present research, we have tried to present the simplest interpretation for reasons that cause a hypertension. Stroke volume, heart rate, and ejection period are three independent perturbing parameters that belong to heart parameters.

Figure 6-17 shows heart rate (T) has the greatest impact on diastolic pressure while, we see no effect on mean arterial pressure; thus, the mean arterial pressure relies on four parameters: systolic and diastolic pressures, heart rate, and ejection period. Therefore, the effect of heart rate on arterial pressure appears through systolic and diastolic pressures. The effect of weight on the heart rate under diastolic pressure is twice that of the systolic pressure and in the same direction.

To understand the impact of altering the ejection period on various hemodynamic properties, Figure 6-18 has been created to show the sensitivity coefficient of the ejection period has the greatest impacts on pulse pressure, while the ejection period has same impact on systolic pressure and diastolic pressure, but opposite effect, and has no impact on mean arterial pressure.

Physically speaking, to assess the impact of stroke volume variation we find an equal effect on systolic, diastolic and pulse pressure as shown in Fig. 6-19. The stroke volume obviously has no effect on a mean arterial pressure; thus, based on Eq. (6.17), we can determine that the mean arterial pressure relies on four parameters: systolic and diastolic pressures, heart rate, and ejection period. Therefore, the effect of stroke volume on the arterial pressure appears through systolic and diastolic pressures.

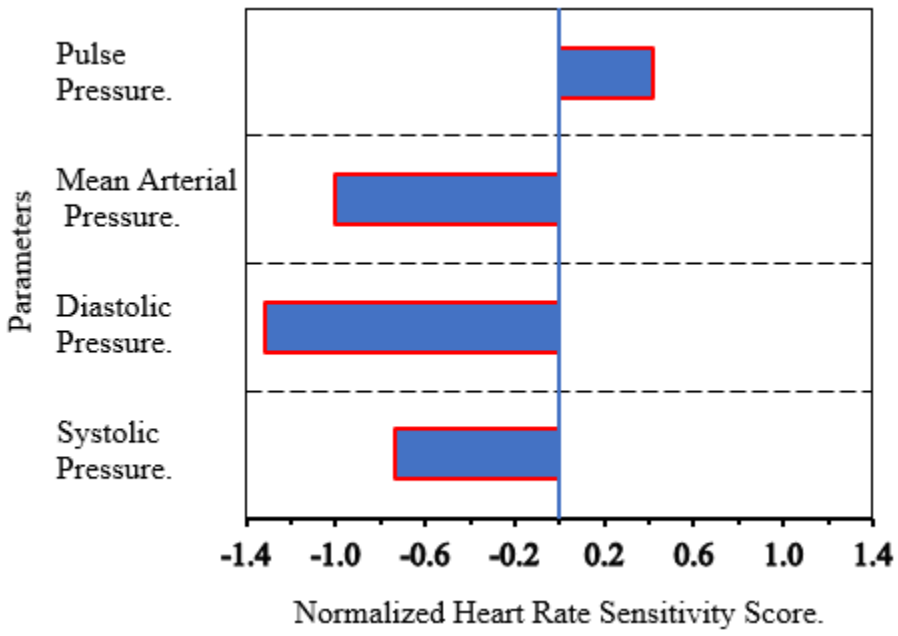

Figure 6-17. The effect of altering the heart rate on various hemodynamic properties.

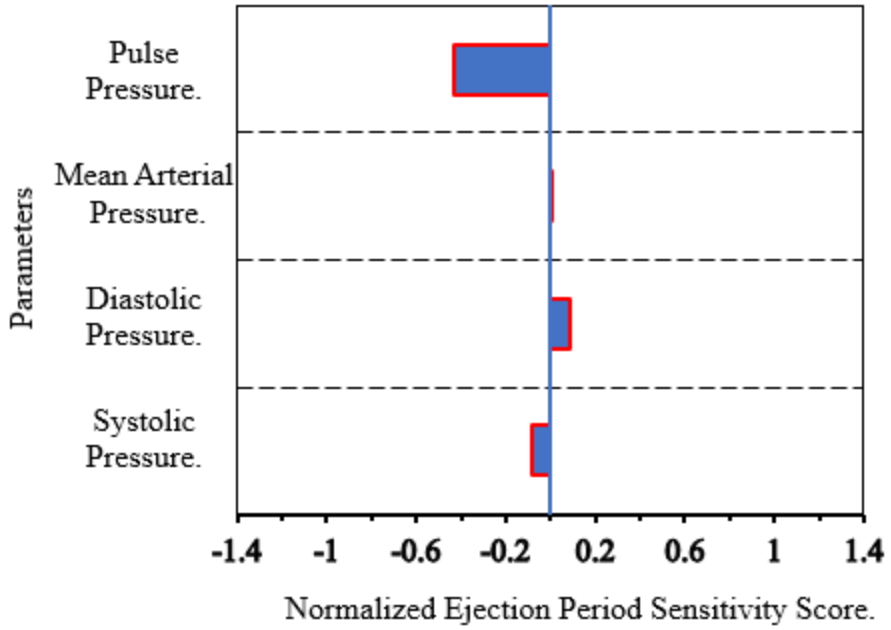

Figure 6-18. The effect of altering the ejection period on various hemodynamic properties.

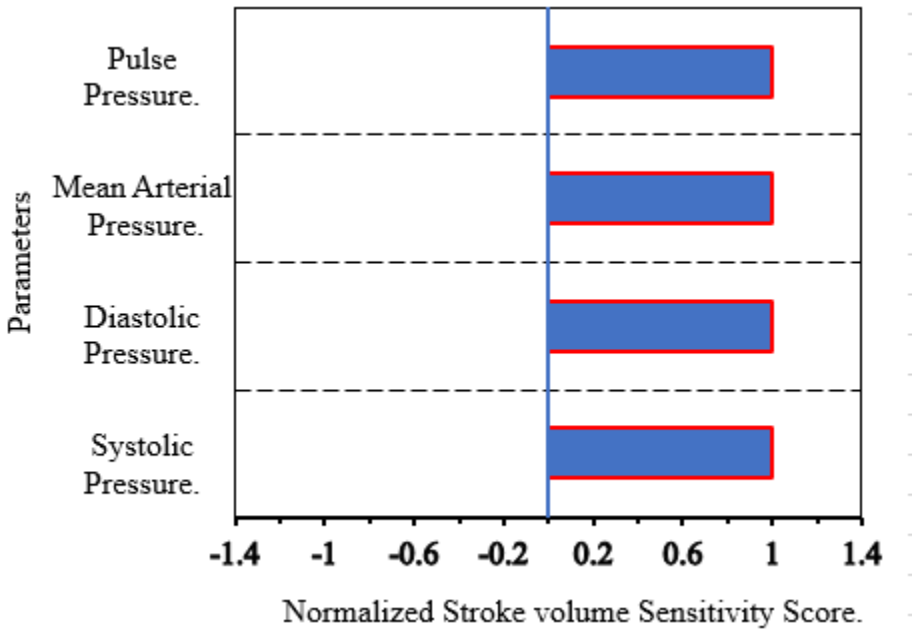

Figure 6-19. The effect of altering the stroke volume on various hemodynamic properties.

6.2.6 Comparison Between Sensitivity Coefficient for Blood Pressure

The controlling key to hypertension is to prevent high blood pressure, which is a result of the parameters listed in Table 6-6.

Table 6-6. Comparison between sensitivity coefficients for blood pressure.

Sensitivity Coefficient	Systolic Pressure	Diastolic Pressure	Mean Arterial Pressure	Pulse Pressure
Stroke Volume, $S_{\Delta V}$	+1.000	+1.000	+1.000	+1.000
Ejection Period, S_{Te}	– 0.0843	+0.0893	0.000	-0.4318
Heartbeat Period, S_T	– 0.7383	– 1.3172	–1.000	+0.42025
Peripheral Resistance, S_R	+0.82264	+1.2278	+1.000	+0.0116
Compliance, S_C	– 0.1774	+0.228	0.000	– 0.988

The findings in Table 6-6. have a number of implications for revealing how each parameter affects blood pressure:

- Adjusting the stroke volume (ΔV) has an almost equal impact on the systolic, diastolic, and pulse pressure, and also shows that a small increase in stroke volume will increase the systolic pressure, diastolic pressure, and pulse pressure, while a small decrease in the stroke volume will have the opposite effect.
- Increasing ejection period (T_e) has an almost negative impact on pulse pressure.
- Increasing heart rate (T) has a more negative impact on diastolic pressure than systolic pressure and a positive impact on pulse pressure. The heart rate and ejection period almost have the same amount of impact, but the ejection period has an opposite impact on the pulse pressure.
- Reduction of peripheral resistance (R) will have a significant impact on both the systolic and diastolic pressures because the sensitivity coefficient associated with

peripheral resistance has a large value. If the peripheral resistance is decreased, then the systolic and diastolic pressures will also decrease.

- Decreasing arterial compliance (C) has a more negative impact on pulse pressure than systolic and diastolic pressures.

6.3 Mechanical Analysis for Arterial Capacitance

Cardiovascular disease is still one of the major causes of death in the United States today [84]. Arterial stiffness is the number one of cardiovascular diseases. Treatment of arterial stiffness problem depends on severity of the disease; artificial graft may be used to replace arteries. Arterial stiffness problem has motivated many researchers to figure out different ways to design and manager different kind of arteries.

The equation of the arterial capacitance that was developed in Chapter 3 helps to predict computing of an arterial graft capacitance. This result is reviewed here for convenience:

$$C = \frac{\pi L d^2}{2E}\left(\frac{D^2 + d^2}{D^2 - d^2} + \nu\right). \tag{6.24}$$

The mechanical properties of an artery are of interest from pathophysiologic point of view. Young's modulus is the ratio of tensile stress to strain. In other words, Young's modulus is a measure of the ability of an artery to withstand changes in artery diameter when under high blood pressure.

Appling the Taylor series expansion for the arterial capacitance in Eq.(6.24) is given by:

$$C = C_o + \left.\frac{\partial C}{\partial E}\right|_o (E - E_o) + \left.\frac{\partial C}{\partial d}\right|_o (d - d_o) + \left.\frac{\partial C}{\partial D}\right|_o (D - D_o) + \left.\frac{\partial C}{\partial L}\right|_o (L - L_o) + \left.\frac{\partial C}{\partial \nu}\right|_o (\nu - \nu_o) \quad , \tag{6.25}$$

which can be rearranged according to the following

$$\left(\frac{C}{C_0} - 1\right) = \underbrace{\frac{E_o}{C_o}\left.\frac{\partial C}{\partial \Delta V}\right|_o}_{S_E}\left(\frac{E}{E_o} - 1\right) + \underbrace{\frac{d_o}{C_o}\left.\frac{\partial C}{\partial d}\right|_o}_{S_d}\left(\frac{d}{d_o} - 1\right) + \underbrace{\frac{D_o}{C_o}\left.\frac{\partial C}{\partial D}\right|_o}_{S_D}\left(\frac{D}{D_o} - 1\right) + \underbrace{\frac{L_o}{C_o}\left.\frac{\partial C}{\partial L}\right|_o}_{S_L}\left(\frac{L}{L_o} - 1\right) + \underbrace{\frac{\nu}{C_o}\left.\frac{\partial C}{\partial \nu}\right|_o}_{S\nu}\left(\frac{\nu}{\nu_o} - 1\right) \quad . \tag{6.26}$$

Table 6-7. Nominal values are input for the sensitivity analysis of arterial capacitance.

Symbol	Description	Unit	Nominal Values
d	Inside Diameter	*cm*	1.94
D	Outside Diameter	*cm*	2.54
ν	Poisson's Ratio	-	0.47

The sensitivity coefficient for Young's modulus is $S_E = -1,$

The sensitivity coefficient for the arterial inside diameter is expressed as:

$$S_d = 2 + \frac{2d^2\left(\frac{1}{\left(D^2 - d^2\right)} + \frac{\left(D^2 + d^2\right)}{\left(D^2 - d^2\right)^2}\right)}{\nu + \frac{D^2 + d^2}{D^2 - d^2}} \quad . \tag{6.27}$$

The sensitivity coefficient for the outside diameter is given as:

$$S_D = \frac{2D^2\left(\frac{1}{\left(D^2 - d^2\right)} - \frac{\left(D^2 + d^2\right)}{\left(D^2 - d^2\right)^2}\right)}{\nu + \frac{D^2 + d^2}{D^2 - d^2}} \quad . \tag{6.28}$$

The sensitivity coefficient for the length is $S_L = +1$,

The sensitivity coefficient for the Poisson's ratio is calculated as:

$$S_v = \frac{v}{v + \frac{D_o^2 + d_o^2}{D_o^2 - d_o^2}} \quad . \tag{6.29}$$

Table 6-8. Variation in sensitivity coefficients of the arterial capacitance.

Sensitivity Coefficient	Arterial Capacitance
Young's Modulus S_E	–1.000
Inside Diameter, S_d	+5.147
Outside Diameter, S_D	–3.147
Length, S_L	+1.000
Poisson's Ratio, S_υ	+0.110

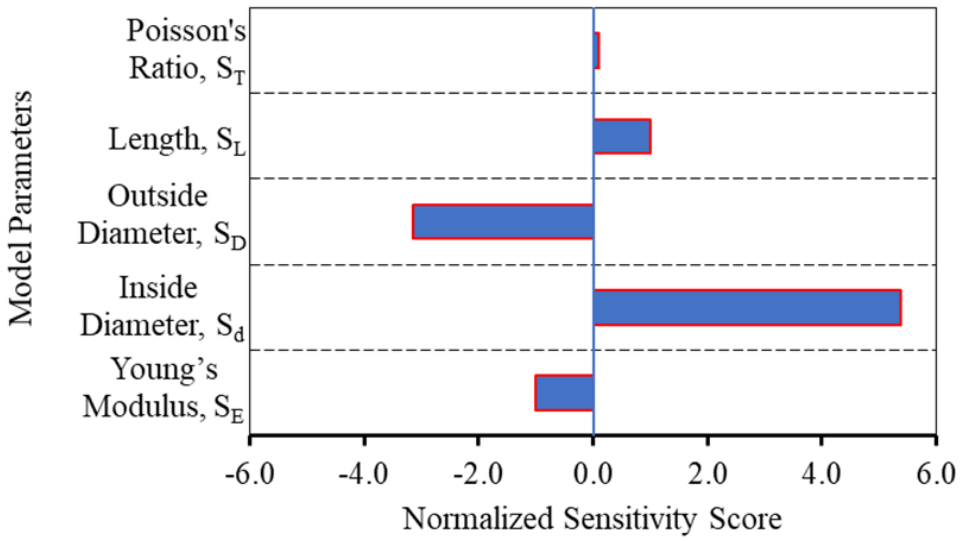

Figure 6-20. Variation in sensitivity coefficients of the arterial capacitance.

In this study, the results presented in Table 6-8 and Figure 6-20 clearly show that effects of the inner and outer arterial diameter are much more pronounced than the effects of artery length. All of these mechanical parameters should be considered when

determining the need for medical surgery. We used Young's modulus to determine artery health. This is because Young's modulus can measure an organ's tensile elasticity. Therefore, it can be used to determine the potential of different effects on the heart, especially when considering arterial diameter and length. A smaller arterial diameter from wall to wall is associated with high blood pressure. A larger outer diameter is also associated with high blood pressure. When comparing inner and outer arterial diameters to arterial stiffness the diameters are more strongly related to increased systolic blood pressure; however, an increase in arterial stiffness is associated with a decrease in diastolic blood pressure. On the other hand, a decrease in the inner arterial diameter is associated with both high diastolic and systolic blood pressures. An increase in systolic pressure combined with a decrease in diastolic blood pressure is associated with an increased risk of death [77, 80].

The results in Figs 6-21 to 6-23 provide evidence that no change in S_E, S_L and S_υ with d/d_o, D/D_o or υ/υ_o. Poisson's ratio has light impact on the arterial capacitance as shown in Table 6-8 and Figure 6-21 to Figure 6-23. Sensitivity coefficients of the arterial capacitance can be illustrated in Fig. 6-23 as follows: inside and outside diameters, Young's modulus, length, and Poisson's ratio sensitivity analysis remain constant with change in υ / υ_o.

Another interesting finding in Figs 6-21 and 6-22, that it is relatively to predict the effect of decreasing or increasing of inside and outside diameters as well as the wall thickness on the arterial capacitance.

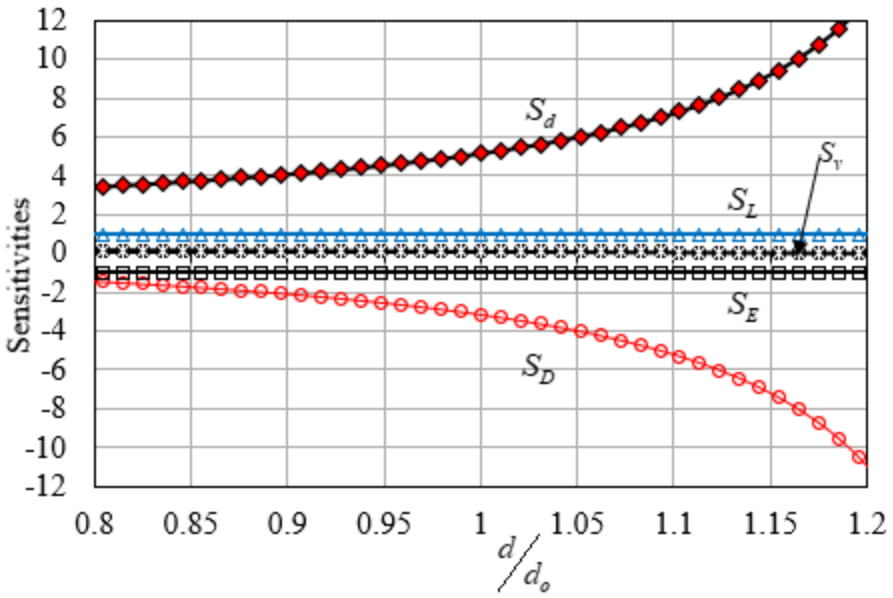

Figure 6-21. Variation in sensitivity coefficients for changes in inside diameter. These results have been generated for nominal values of d_o =1.94 *cm*, D_o =2.54 *cm*, E_o =751.88 *mm Hg*, and ν_o = 0.47.

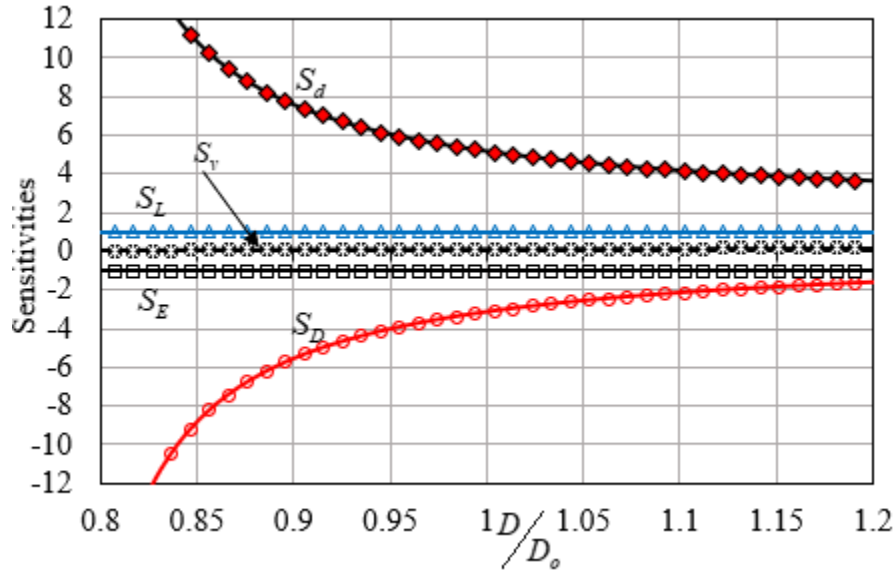

Figure 6-22. Variation in sensitivity coefficients for changes in outside diameter. These results have been generated for nominal values of d_o =1.94 *cm*, D_o =2.54 *cm*, E_o =751.88 *mm Hg*, and ν_o = 0.47.

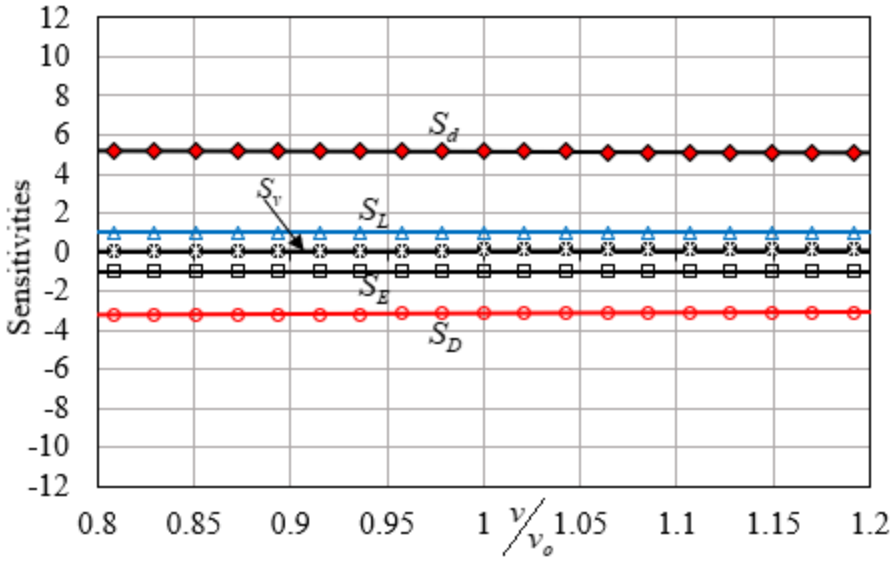

Figure 6-23. Variation in sensitivity coefficients for changes in poison's ratio. These results have been generated for nominal values of d_o =1.94 *cm*, D_o =2.54 *cm*, and v_o = 0.47.

6.4 Summary

Often in engineering analysis, we are concerned with sensitivity of the predicted hypertension to changes in perturbing the five hemodynamic parameters, which describe different types of blood pressure effects (e.g., systolic vs. diastolic), arterial compliance, and peripheral resistance states. The quantification of the sensitivity of these perturbing parameters is called sensitivity analysis. In other words, the goal of this chapter was to elucidate how blood pressures, arterial compliance, and peripheral resistance respond to perturbation in the input parameters, based on sensitivity analyses. A sensitivity analysis investigates the stability of constitutive equations by examining the extent to which results are affected by changes in the parameters. This can lead us to a more structured study on the influence of the parameters on hypertension. The sensitivity coefficient with

a large absolute value will indicate a plus or minus percent change in that parameter, which helps us determine which change has the largest impact.

In this chapter, we introduced the novel idea of interpretation roles for each parameter in blood pressures, peripheral resistance and arterial compliance. This interpretation helps us determine and how they these parameters relate to hypertension by using sensitivity analysis. We hope that this intuitive idea will serve a successful candidate for treating hypertension. The sensitivity analysis that has been used to figure out sensitivity coefficients with the largest magnitude is based on the most sensitive parameter that can be adjusted if we want to alter a pressure. The five governing parameters for the sensitivities related to hypertension are 1) stroke volume, 2) heart rate, 3) ejection period, 4) peripheral resistance, and 5) arterial compliance.

This study reveals a correlation that shows the reduction in systolic pressure as being associated with an increase in diastolic pressure. We investigated the correlation between systolic and diastolic pressures as the pulse pressure that relies on five governing parameters, but the biggest role in the pulse pressure is arterial compliance while the peripheral resistance approximately has no impact on this correlation. The heart rate and ejection period almost have the same amount of impact, but the ejection period has an opposite impact on the pulse pressure. In other words, increasing in the ejection period causes a decrease in the pulse pressure. The trend of increasing and decreasing the arterial compliance with heart rate and ejection period is linear because their sensitivities have a unity magnitude. This means that by increasing the heart rate and decreasing the ejection period, the arterial compliance increases, while the corresponding systolic pressure decreases, and the diastolic pressure increases [85].

Physically speaking, increasing P_D and keeping the pulse pressure at the same value has the effect of decreasing arterial compliance. When making an arterial compliance adjustment, the physician must keep in mind that the diastolic pressure cannot exceed the limit; otherwise the diastolic will cause the hypertension.

All conclusions are based upon the mathematical model, which has not been compared to a real biological system in this chapter.

CHAPTER 7. VASCULAR STIFFNESS

7.1 Introduction

What is the relationship between high blood pressure (hypertension) and arterial stiffness? This chapter answers and presents methods and indicates how to estimate vascular stiffness. Vascular stiffness is reciprocal of compliance and explicitly defined as a fundamental property of the relationship of pulsatile pressure and wave propagation.

The function of the arterial compliance is the ability to store a portion of cardiac output per one beat in the aorta and the remaining is directly pumped to the rest body during systole without excessive pressure rise. In the diastole, the stored portion in the aorta is pushed to peripheral circulation by the elastic forces of the aortic walls [86, 87] as shown in Fig. 7-1. Any reduction of arterial compliance leads to an increase in pulse wave velocity (PWV).

Recently, many studies have revealed a strong link between arterial compliance and hypertension and coronary artery disease [88].

Vascular stiffness is recognized increasingly as one powerful predictor that can point to future cardiovascular risks. It is an independent marker of cardiovascular mortality in the United States [89] and globally represents 31% of all deaths worldwide according to the World Health Organization estimation in 2016 [84].

Researchers have been focusing on aortic stiffness for these reasons: 1- The aorta has the most compliance of the other arteries in the human body. It contains no muscular layers or very small muscular layers mostly containing elastic fibers and elastic parts, thus the aorta is the typical artery of the elastic type artery while other arteries are more

muscular containing muscular layers [90]. 2- A large artery has less arterial stiffness because systolic pressure has an inverse correlation with aortic diameter while diastolic pressure has a proportional correlation with aortic diameter. 3- The heart only gets its blood during diastole when the heart rests. When the heart is pumping the whole body gets blood except the heart because of the contracting of the heart's muscles. For a good heart function, the heart needs a maximum of possible time resting and minimal possible aortic stiffness.

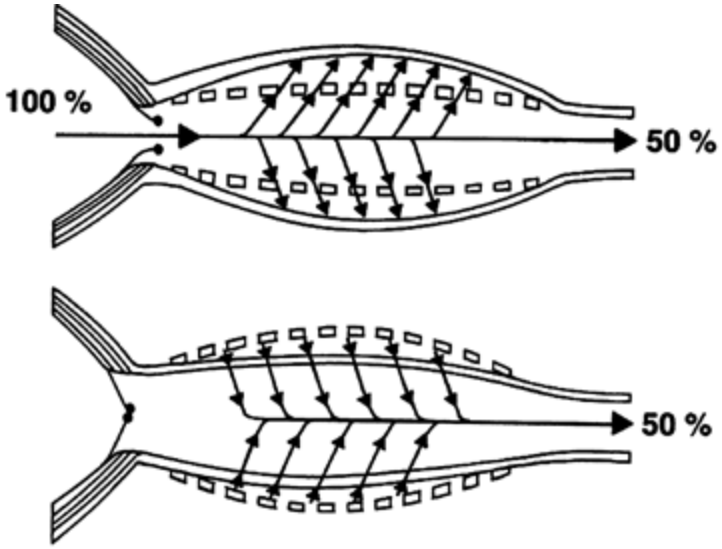

Figure 7-1. Scheme shows how aorta works [87].

7.2 Measurements of Total Arterial Stiffness.

Measuring total arterial stiffness is still feasible and complex in every day clinical practice, because of some limitation for instance requiring simultaneous recordings of the arterial pressures and cardiac output [91].

The posed problem in this chapter deals with measuring total arterial stiffness; therefore, the fundamental element of hemodynamics, hydraulic theories and the elastic mechanical theories have been used to derive several approaches of measuring arterial

stiffness. The aorta is not easily accessible to measure its stiffness; thus, techniques are helpful to estimate arterial stiffness. In terms of methods for calculation of arterial compliance, we present three ways of measuring arterial compliance: mechanical properties, PWV, and blood pressures. Elastic tubes and ox aortas were used to verify these three ways.

7.2.1 Measurement of Mechanical Capacitance

This part of work focuses on a technique that uses elastic theory to describe arterial stiffness, because the aorta is consisted of tissues that are very extensible. Young's Modulus expresses a constant proportional relationship between applied force per unit area (stress) and relative change in dimension (strain). Young's Modulus is an important determinant of arterial wall mechanical properties that give a better understanding for physiology of the arteries. Many researches explain that a distensibility of arteries and flexible tubes is happened in two dimensions and circumferential compliance plays a fundamental role more than longitudinal [92].

A simple correlation has been used for compliance calculation in hemodynamics research depending on the Young's Modulus. The Young's Modulus was considered constant with the limited range of pressure, and that leads to the compliance being constant. So, blood flow and blood pressure are causing stresses in the vessels and then these mechanical stresses can result in strain in the radial direction of the vessels. This result is re-presented here for convenience:

$$C = \frac{\pi L d_o^2}{2E}\alpha \quad . \tag{6.30}$$

Where α is a nondimensional geometry and material factor given by

$$\alpha = \frac{D_o^2 + d_o^2}{D_o^2 - d_o^2} + \nu \quad . \tag{6.31}$$

This equation computes mechanical capacitance using the tensile modulus of elasticity for the vessel (E) , Poisson's ratio (*v)*, the original outside diameter of the vessel (D_o), and the original inside diameter of the vessel (*d*).

In our equation, we propose a simple calculating arterial compliance with a constant value, so it assumes no significant changes in inner and outer diameter and the Young's Modulus. This equation has been simply used to predict the compliance of the simulated aorta before manufacturing.

Table 7-1. Physical properties of the silicon-rubber aorta model used in this research.

L	D_o	d_o	*E*	*υ*
550 mm	31.4 mm	28 mm	1,501 mm-Hg	0.499

Equation (6.32) re-presented here for convenience:

$$C = 2\alpha \frac{V_o}{E}\left(1 + \alpha \frac{P}{E}\right) \quad . \tag{6.32}$$

This applied pressure to the fluid is dimensionally significant, especially for an aorta with a high capacitance, and increases the PWV as shown in the equation.

7.2.2 Calculation of Aortic Pulse Wave Velocity and Total Arterial Compliance

Increased PWV has been considered to be an important parameter of cardiovascular diseases, and cardiovascular diseases are the number one cause of death.

Pulse wave velocity is a very interesting phenomena and currently considered as the gold standard method which can be utilized for the estimation of the arterial stiffness, because it reflects the elastic nature of arterial walls. Here, there is a need of understanding the nature of a PWV, and how the body generates it. At each heartbeat, a forward pressure wave is generated in the left ventricle by its contraction and travels along the arterial system. Bifurcation points and peripheral resistance generate a reflected pressure wave back to the heart. The velocity of the reflected pressure wave depends upon the arterial compliance, peripheral resistance, and mean arterial pressure. The compliant arterial system slows the reflected wave to reach the heart during diastole and increases the diastolic pressure. While the stiff arterial system. PWV is the transmission of energy through the arterial wall, and it is directly related to elasticity of the aortic wall. A decrease in the elasticity of the aorta causes an increase in PWV. This will result in an increase in systolic pressure, a decrease in diastolic pressure, and an increase in pulse pressure. When the elasticity of aortic wall decreases, time delay decreases. We can notice, in rigid wall, the value of time delay is zero that means PWV be infinity. In other words, changes in compliance affect systolic and diastolic pressure, but it does not affect mean pressure. Systolic, diastolic and mean arterial pressures are increased when the peripheral resistance is increased.

Pulse wave velocity continues to increase from about 6 m/s in a healthy child to 10 m/s in an older person [13]. The 1 m/s increase in PWV is corresponded to a 15% increase in cardiovascular risk [93].

The in-vitro hemodynamic simulator was used to accomplish the comparison between C from pressure and C from PWV. The simulator consists of a pulsatile flow

generator, water as artificial blood, artificial aorta, and two pressure transducers. The artificial aorta has linear elastic properties within the range of working pressures. Two pressure transducers detect the pulses at two different position along the aortic simulator.

According to the Eq. 1.3 the time difference (Δt) between the pressure wave arrival at each pressure transducer position [94, 95]. The distance between the two pressure transducers at upstream and downstream of the simulated aorta recording sites.

The tangent intersection method has been used to calculate the wave speed [96], and it is common way to measure pulse wave velocity. The identification of the start points of the sharp upstroke of the systolic ascending waveforms are very important. Human eyes are used to identify these starting points, because of the lack of using EKG signal in our research. Sequence of pulse waves are recorded from inlet and outlet for the same pressure wave the simulated aorta as shown in Fig 7-2.

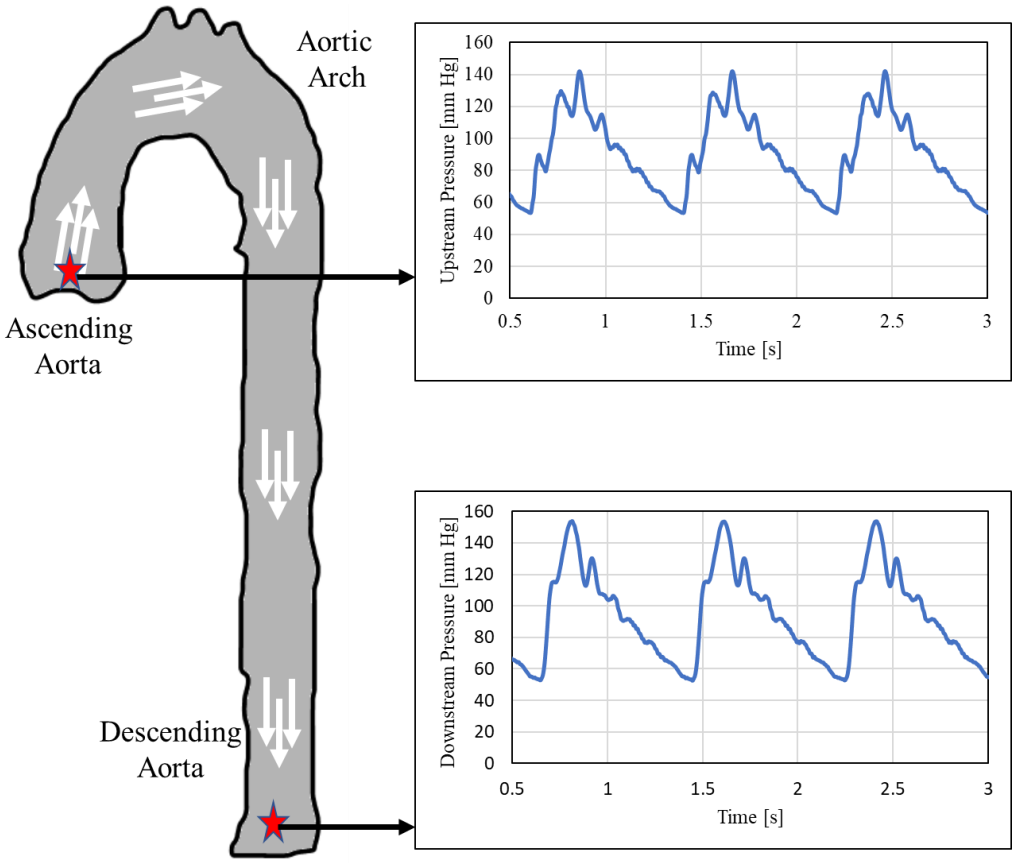

Figure 7-2. Modified figure of the pressure experimentally measured for the ascending and descending simulated aorta [97].

Foot is that point of intercept of the systolic ascending waveform with diastolic descending waveform. Identification of a foot point depends on personal judgement.

The most well-known dependence describing the pulse wave velocity is the time delay which is between two waves on simultaneous recording. The feet of waveforms divided by the distance of wave travel between two aperture of pressure transducer is represented the pulse wave velocity.

$$PWV = \frac{L}{\Delta t} \quad . \tag{6.33}$$

Where is L= the distance between two pressure transducers at upstream and downstream of the simulated aorta recording sites simultaneously.

Where is Δt= the time difference between the pressure wave arrival at each pressure transducer position.

This way characterizes the average PWV over a given arterial length, and the average PWV provides an average equivalent value of arterial compliance. By using the Moens - Koretewg- equation gives the Young modulus of artery wall.

There are different ways to determine the foot of pulse wave for example using an intercept point between a parallel line to time axis passes through the minimum diastolic descending portion and tangent drawn half the height of the systolic ascending portion [95].

$$C = \frac{V_o}{\rho \mathrm{PWV}^2 - 2P_m} \quad . \tag{6.34}$$

Where V is aortic volume and ρ denotes the fluid density.

This denotes a fractional change in arterial volume per change in arterial pressure. The increase in heart rate was associated with an increase in PWV measured using foot to foot.

Propagation time is measured from the foot carotid waveform to that femoral waveform. The time difference between the two waves, correspond to the pulse transit time. The ratio value of the distance between the two sensors, allows us to obtain the PWV.

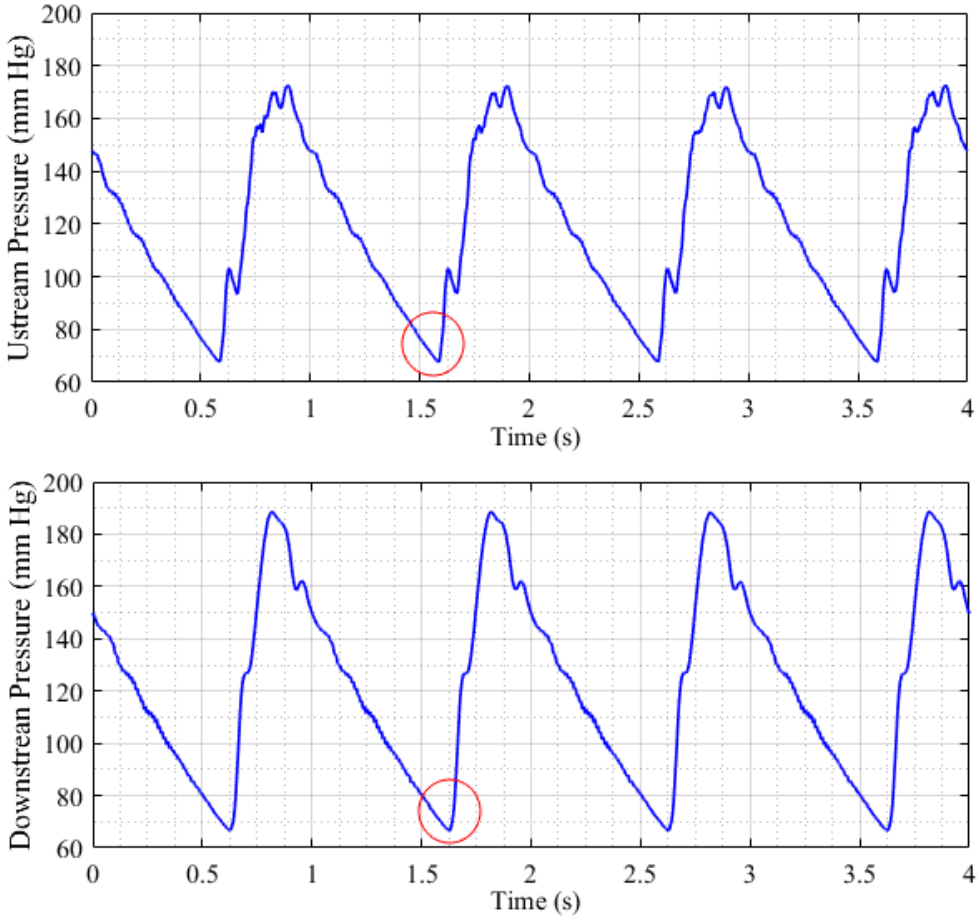

Figure 7-3. Continuous blood pressure recording measured in the upstream simulated aorta through pressure transducer.

The heart rhythm causes the cycle movement, and contraction of the left ventricle cause the steep rise in the pressure that depends on ejection period.

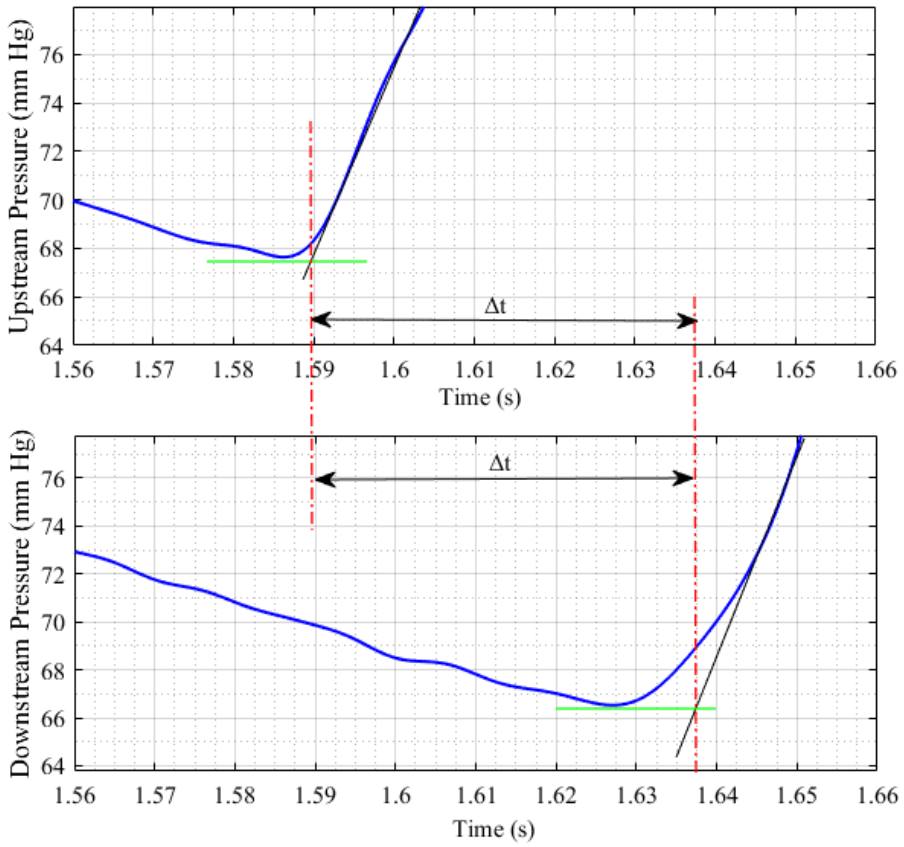

Figure 7-4. Measuring of upstream to downstream propagation time using the intersecting tangent foot to foot.

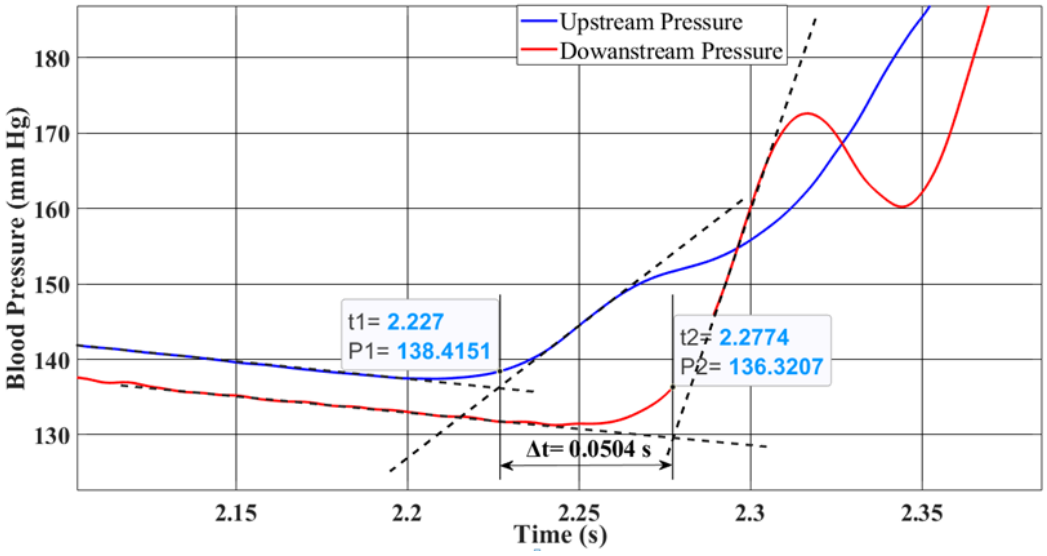

Figure 7-5. Another way of measuring of upstream to downstream propagation time using the intersecting tangent foot to foot.

Different ways to determine the foot of pulse wave were used: the point of intercept of a tangent drawn to the systolic ascending and a parallel line to the time axis passing through the end of end-diastolic contour as shown in Fig.7-4 [96, 98]. Choosing the foot way is continuing to be the subject of ongoing debate by researchers for years to come because the identification of this way has been dependent on personal judgement.

Figure 7-5 illustrates another extrapolation from the end-diastolic portion with a line drawn through the initial steep upstroke and using the intersection of these lines to define the foot [80].

The limitation of this technique generally centers around the variability which occurs in the late diastolic portion of the pressure waveform and the initial upstroke. There is no automated method was used to find delay time, but we performed the measurement manually. From the graphic display, and using a hand-controlled “mouse” selected points on the end-diastolic portion of the curve and on ascending curve. The measurement site when be close to reflection site that affects measuring wave.

Figures 7-6 and 7-7 show that an effect of closing and opening of the aortic valve systolic pressure profile that creating a secondary wave hump that happens immediately after the closure of aortic valve and before dropping down during diastolic phase. This wave hump is known as a dicrotic notch. This dicrotic notch is frequently considered as a marker for the end of the ejection period. Occurring of dicrotic notch happens when the pressure in the aorta is greater than in the left ventricle, elasticity of the aortic wall attempts to equalize the pressure by pushing blood backwards. Rebounding aortic elasticity closes the aortic valve. Closing aortic valve marks the end of the systolic phase and the onset of the diastolic phase.

From the observation it becomes possible to determine the onset and end of the systolic and diastolic phase. Changes in the dicrotic diastole appear to correlate with ejection period, heartrate, peripheral resistance or arterial compliance.

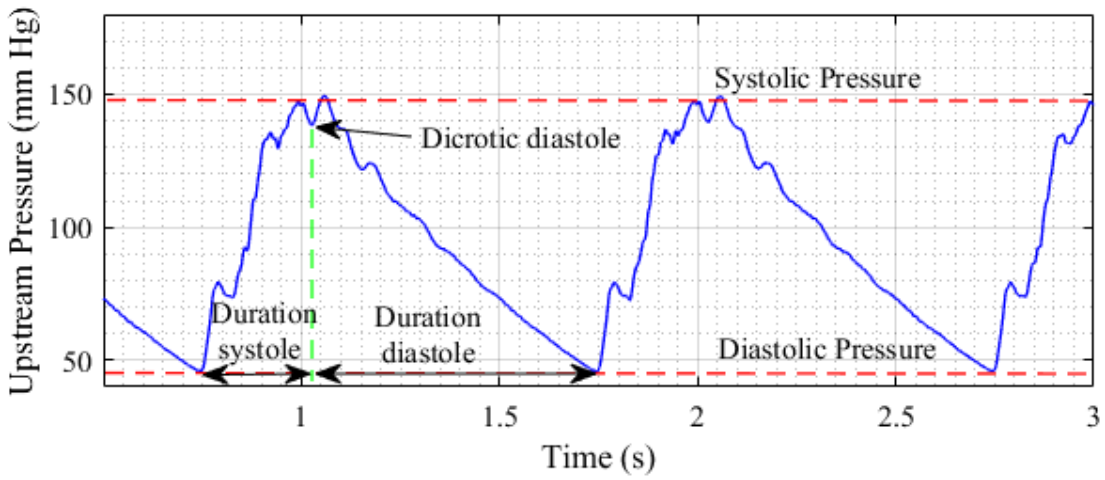

Figure 7-6. Upstream blood pressure waveform.

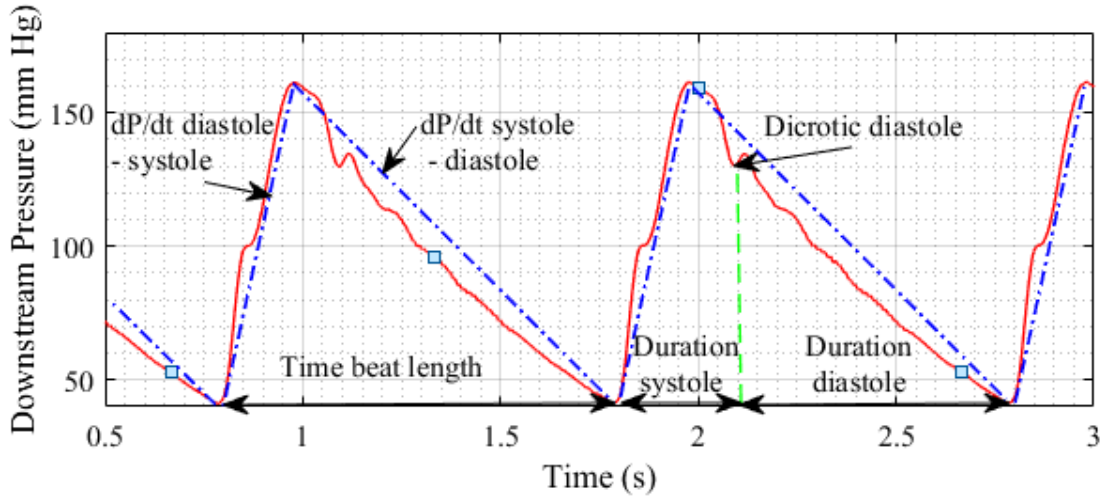

Figure 7-7. Downstream blood pressure waveform.

7.2.3 Measurement of Compliance that Computed from Blood Pressures

The arterial compliance function is the ability to store a portion of cardiac output per one beat in the aorta during diastole without excessive pressure rise, and then the aorta recoils the stored blood into the rest of the body. The elasticity of the aorta determines the storage capacity of the aorta. When the aorta becomes stiffer the amount of the blood ejected that is store in the aorta during the systolic phase decreases. While the most of stroke volume is pushes during the systolic phase. So many researchers have been focusing on this topic in order to present better understanding for this link that may help treating hypertension.

This result is re-presented here for convenience:

$$C = \frac{\Delta V}{P_D}\ \frac{T - T_e}{T_e}\ \frac{1}{\ln(\frac{P_S}{P_D})}\ \frac{1-(P_S / P_D)^{\frac{T_e}{T-T_e}}}{1-(P_S / P_D)^{\frac{T}{T-T_e}}} \tag{6.35}$$

This equation describes the mechanical properties of resistance and capacitance in terms of five cardiovascular parameters: stroke volume ΔV, heartbeat period T, ejection period T_e, systolic pressure P_S, and diastolic pressure P_D. In other words, if these five cardiovascular parameters are known the aortic capacitance may be calculated using this equation. Three of these five parameters are routinely measured in the clinic (heartbeat period, systolic and diastolic pressure). The other two parameters (stroke volume ΔV and ejection period T_e) must either be estimated or measured using an echocardiogram.

7.3 Experiment Comparison of Methods for the Determination of Pulse Wave Velocity and Arterial Compliance

Different kind of silicone, urethane and latex materials were used to manufacture tubes which used in the experimental work to verify PWV and arterial compliance models. PWV and arterial compliance have utilized to describe elastic properties of arterial wall, which depict the correlation between change in pressure and change in arterial volume. Particularly, the aorta has ability to store blood almost half of the cardiac output during systole, and the stored blood is pushed again to periphery during systole. This ability depends upon elastic properties of the aorta walls. The arterial compliance is inversely related to pulse wave velocity PWV. The PWV is the speed of pressure pulse traveling through blood.

The summation of the forward and reflected back waves creates the final shape of aortic pressure waveform. Several methods have been used the non-invasive assessment to estimate average pulse wave velocity and arterial compliance. Most them depend upon pulse transit time of pressure wave and distance traveled between two arterial sites.

7.3.1 Experimental results of Silicone Tube Aortas

Graft replacement of a portion of the aorta is used to replace the diseased portion. Different kind of silicone, urethane and latex materials were used to manufacture tubes which used in the experimental work to verify PWV and arterial compliance models. These used were set up on the simulator that has a capability to produce the arterial flows and pressures. PWV defined as the speed of the pulse wave that travels in along the aorta. PWV is directly related to the mechanical properties of the aortic wall. In the association

tests, all PWV measurement showed significant correlation with mean arterial pressure. The test protocol was designed to capture date for three different settings of the needle valve, and we simulated many different hemodynamic cases shown in Fig. These settings correspond roughly to a peripheral resistance R of 1, 1.3, and 1.6 mm-Hg-s / Ml. For each of the peripheral-resistance settings, a stroke volume ΔV of 50, 60, and 70 Ml was exercised. Each stroke-volume setting was performed three different heart rates (60, 70, 80 BPM), and for six different systolic percent (a ratio of the ejection period to the heartbeat period T_e / T of 0.25, 0.3, 0.35, 0.4, 0.45, and 0.5). Due to the limitations of the pressure transducers some of the data points could not be measured for this test protocol. However, 101 different lines of data we able to be captured with reliability and these data were used to generate the results of the research.

Pressure waveforms were captured for 15 seconds using pressure transducer, and using the experimental data capture to plot Fig. 7-8 that shows a plot of dimensional calculations for peripheral resistance R, arterial capacitance from pressure arterial capacitance from PWV. Since the experiments were conducted by altering the resistance of the needle valve, the resistance R, as shown by the purple line in Fig. 7-8, varies widely with respect to the Test Number. This was intentional. The significant thing to notice in Fig. 7-9 is that the capacitance of the aorta C remains fairly constant and near the predicted value of 0.395 ml / mm-Hg for all Test Numbers. Over the entire range of experiments, the root-mean-square-error was calculated to be 0.029 ml / mm-Hg and $P < 0.0001$, which corresponds to a percent error from the expected value of 14.4%.

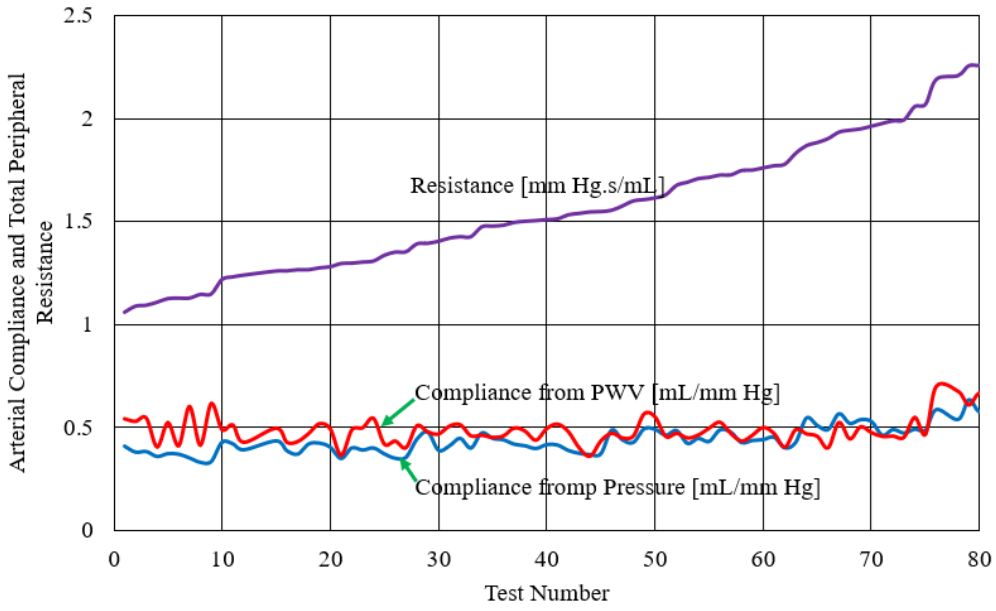

Figure 7-8. Plotting arterial compliance and peripheral resistance against test number for the tube manufactured from PMC-770 urethane material.

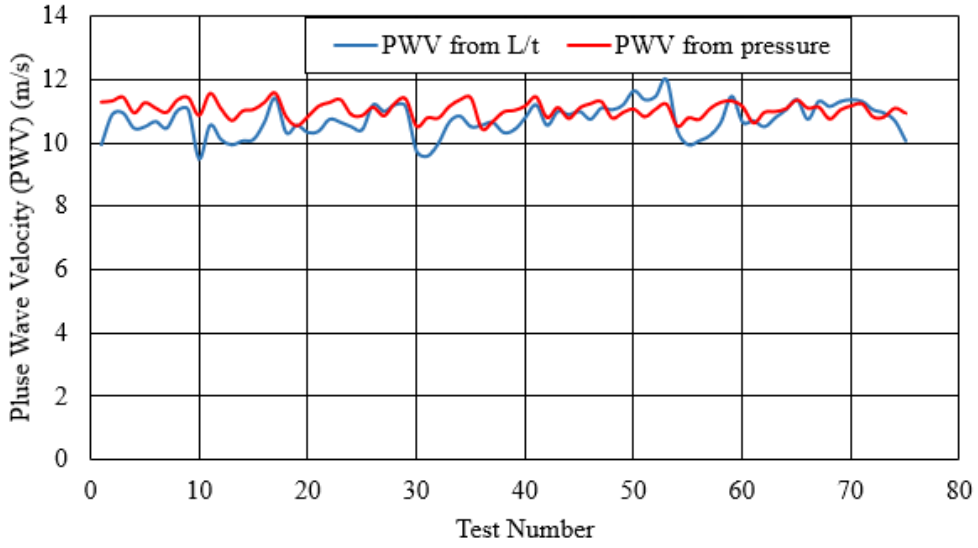

Figure 7-9. Plotting arterial compliance against test number for the tube manufactured from PMC-770 urethane material and a good agreement can be seen in this graph.

The results in Figs. 7-8 and 7-9 show a good agreement and the small differences between the results of them come from different sources of error for instant human error and machine error.

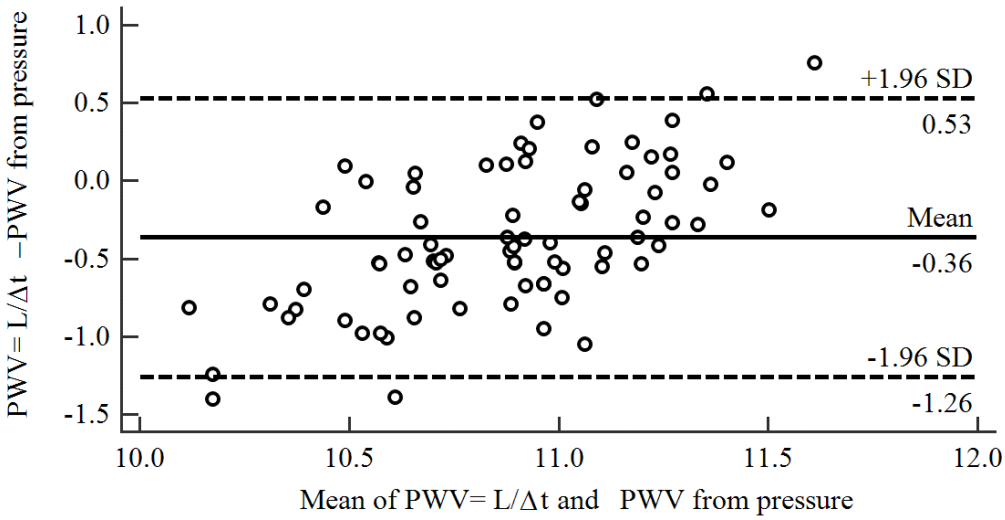

Figure 7-10.Shows agreement between PWV determined pressure and PWV determined from distance. The middle horizontal solid line indicates to the mean of difference of PWV determined by both methods. The upper and lower horizontal dashed lines indicate to 1.96 of the standard deviation.

Bland Altman plot as shown in Fig. 7-10 is a popular graphical technique for showing the levels of agreement between the two measurements that would be acceptable. A scatterplot is used to plot the difference and average between the two measurements that would be fallen evenly on the bias line and between a limit of agreement is ±1.96 standard deviation of the mean difference. Figure 7-10 shows further agreement between PWV estimated from the different methods.

Coefficient of correlation determine the strength of a correlation between two variables, while coefficient of determines shows percentage variation in a one variable which is explained by the other variable.

In this research work, also a clear silicone length tube of 0.375 m was used to estimate PWV from transit time measures, and then estimate a capacitance of the tube. Pressure transducers are used to draw pressure waves.

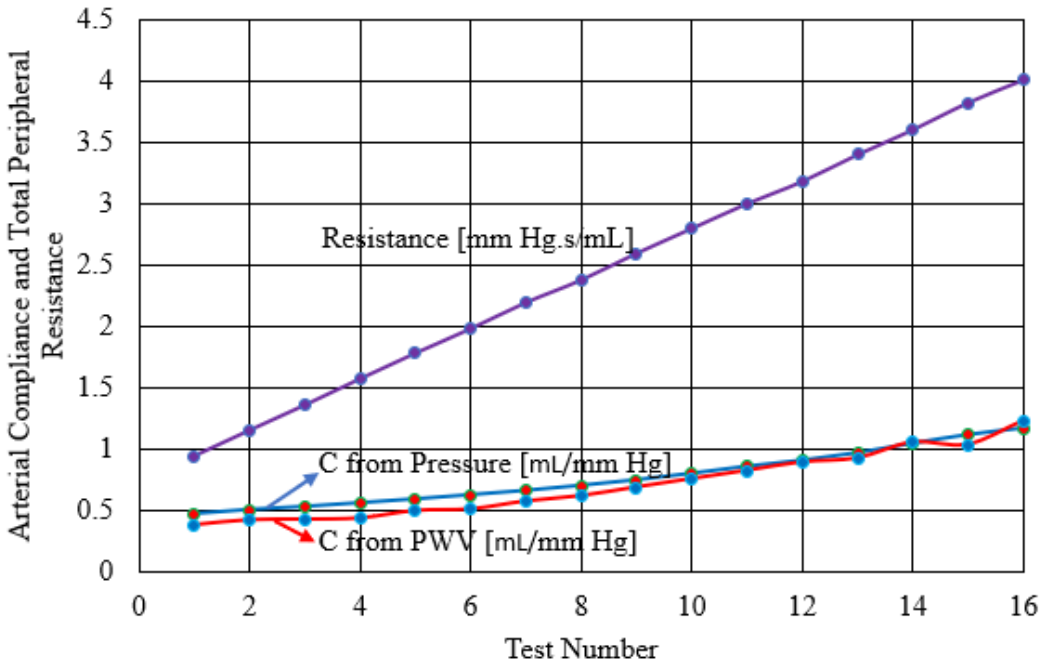

Figure 7-11. Plotting arterial compliance and peripheral resistance against test number for the clear tube manufactured from sorta clear 40 material.

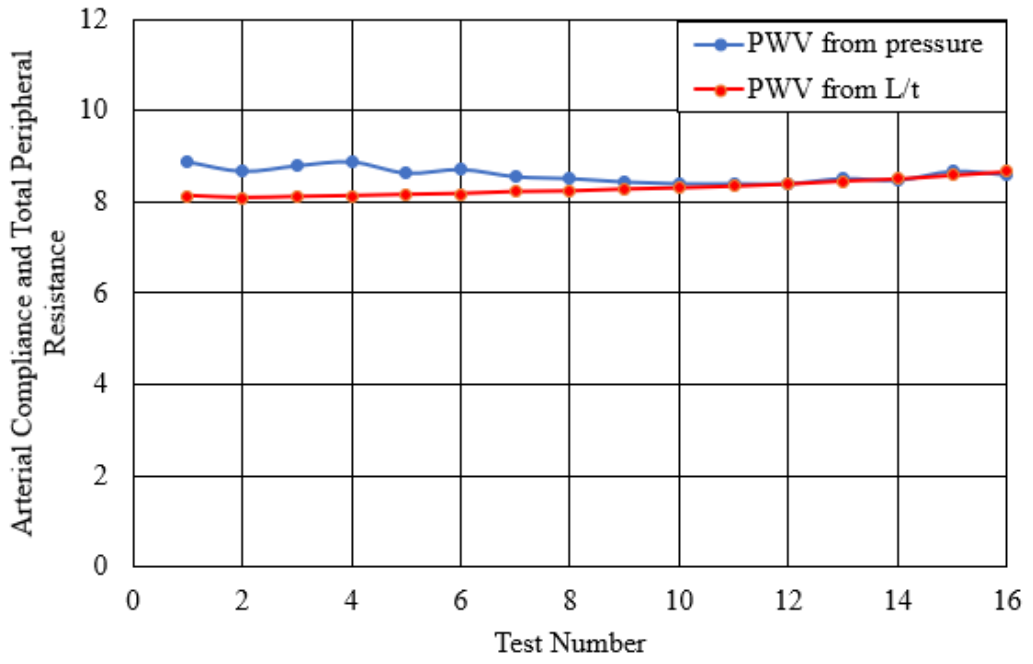

Figure 7-12. shows the results of the arterial compliance determined from pressures way and foot-to- foot way in the clear tube manufactured from sorta clear 40 material and a good agreement can be seen in this graph.

.

Figures 7-11 and 7-12 were plotted to compare the model to the extracted experimental data. The model demonstrates a good agreement with the experiment results that represents one main novelties of our research work.

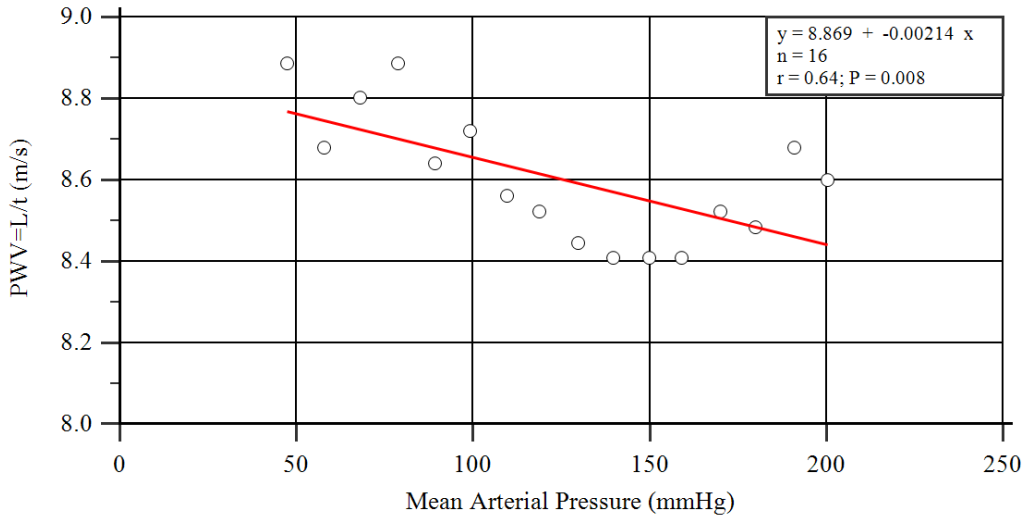

Figure 7-13. shows the results of the arterial compliance determined from pressures way and foot-to- foot way in the clear tube manufactured from sorta clear 40 material.

Figure 7-13 shows that the PWV decreases with the increase in the main arterial pressure. This correlation between PWV and mean arterial pressure opposite of what in blood vessel [15]. The reason for this is the Young Modulus of the elastic tube increases with the mean arterial pressure.

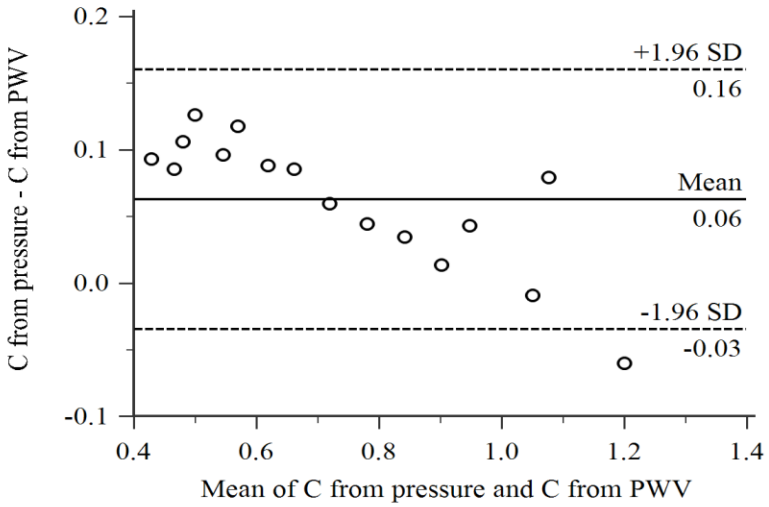

Figure 7-14. Agreement between capacitance determined pressure and capacitance determined from distance. The middle horizontal solid line indicates to the mean of difference of capacitance determined by both methods. The upper and lower horizontal dashed lines indicate to 1.96 of the standard deviation.

The agreement between the compliance (m/s) from pressure and compliance (m/s) from PWV is assessed using Bland-Altman method. The findings reveal that mean of difference between these two ways to compute arterial compliance is 0.06 m/s with acceptable range of mean ±2SD as shown in Fig 7-14.

7.3.2 Experimental result of Ox Aortas

To evaluate PWV and arterial compliance and verify their models, ox aortas were set up on the simulator machine. Before the setup the excess adipose tissue was removed from ox aortas, and all their branches were tied to close at their roots.

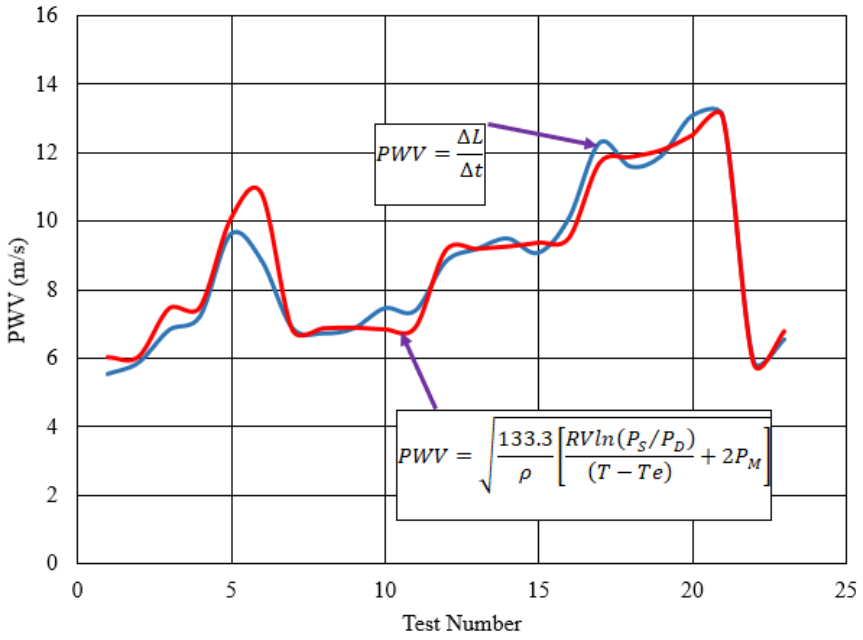

Figure 7-15 Plotting arterial compliance against test number in the OX 6 aorta and a good agreement can be seen in this graph.

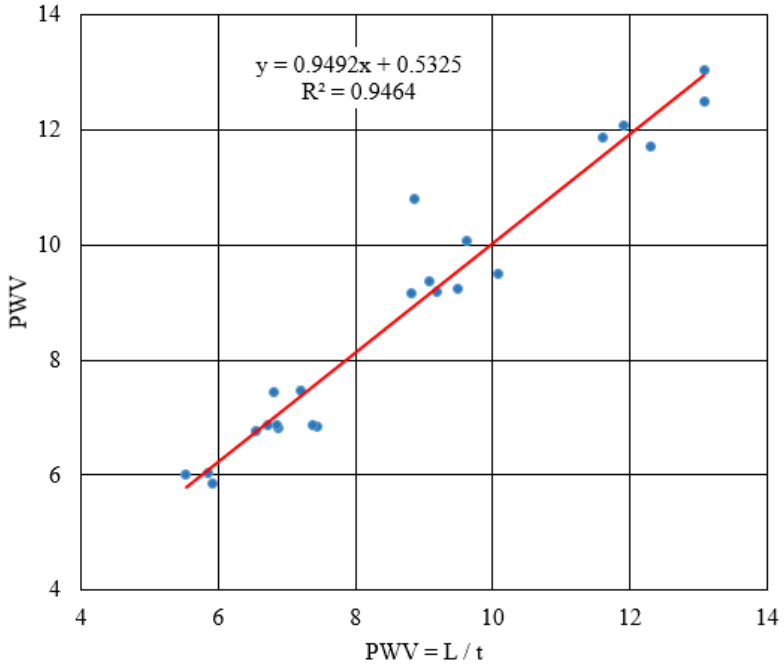

Figure 7-16 Scatter plot between the values of PWV from pressure and PWV from distance in the OX 6 aorta. Red solid line represent equality.

In Figs. 7-15 and 7-16, the results of the two ways of estimating PWV are in a good agreement and the small differences between the results of them come from different sources of error for instant human error and machine error.

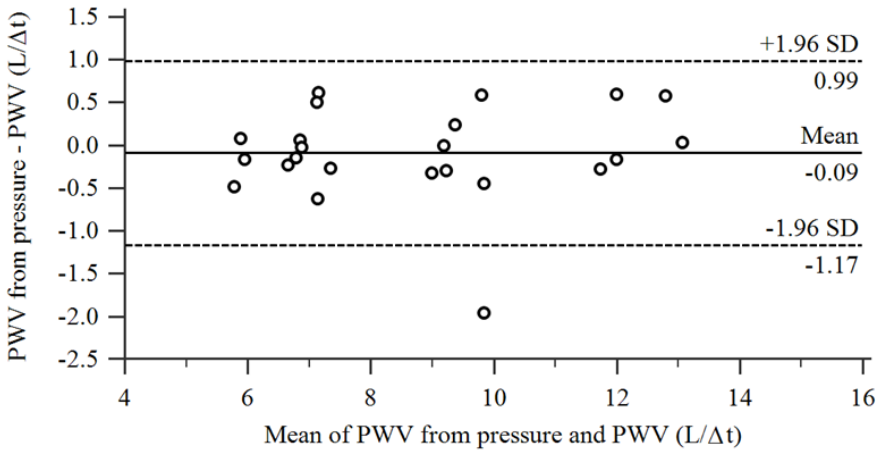

Figure 7-17. Agreement between PWV determined pressure and PWV determined from distance. The middle horizontal solid line indicates to the mean of difference of PWV determined by both methods. The upper and lower horizontal dashed lines indicate to 1.96 of the standard deviation.

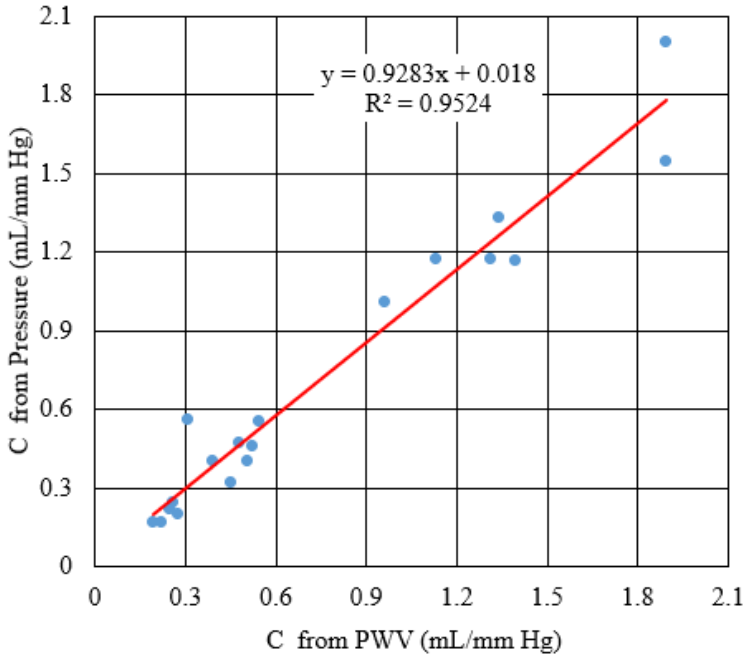

Figure 7-18. Scatter plot between the values of PWV from pressure and PWV from distance in the OX 6 aorta. Red solid line represent equality.

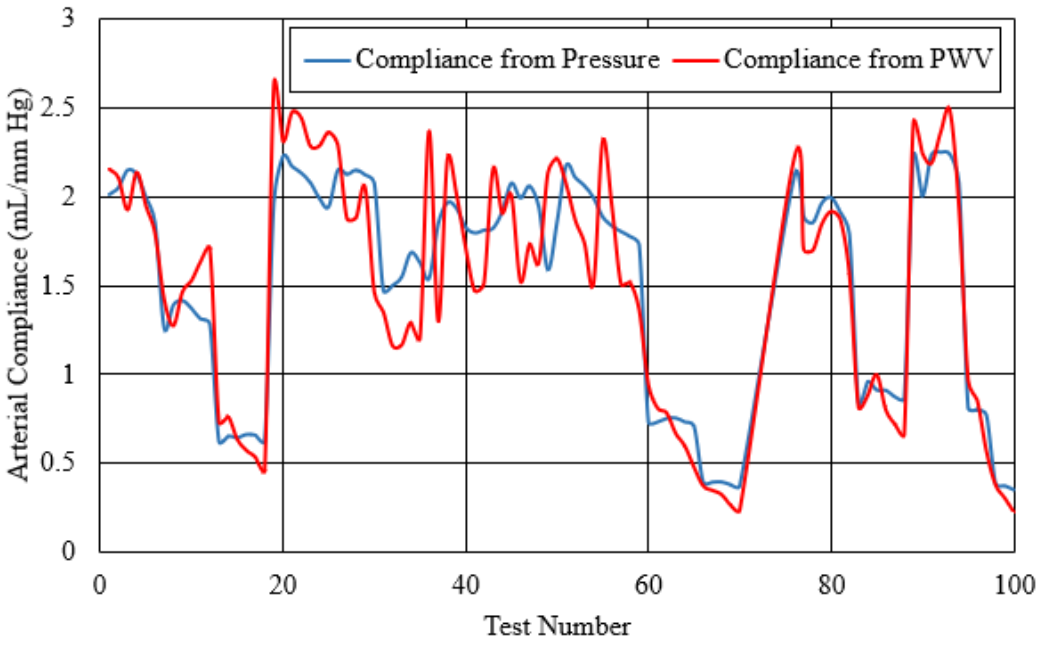

Figure 7-19.The regression line and t-test show that capacitance from pressure and capacitance from PWV is significantly correlated (R^2=0.8806) in the OX 7 aorta and a good agreement can be seen in this graph.

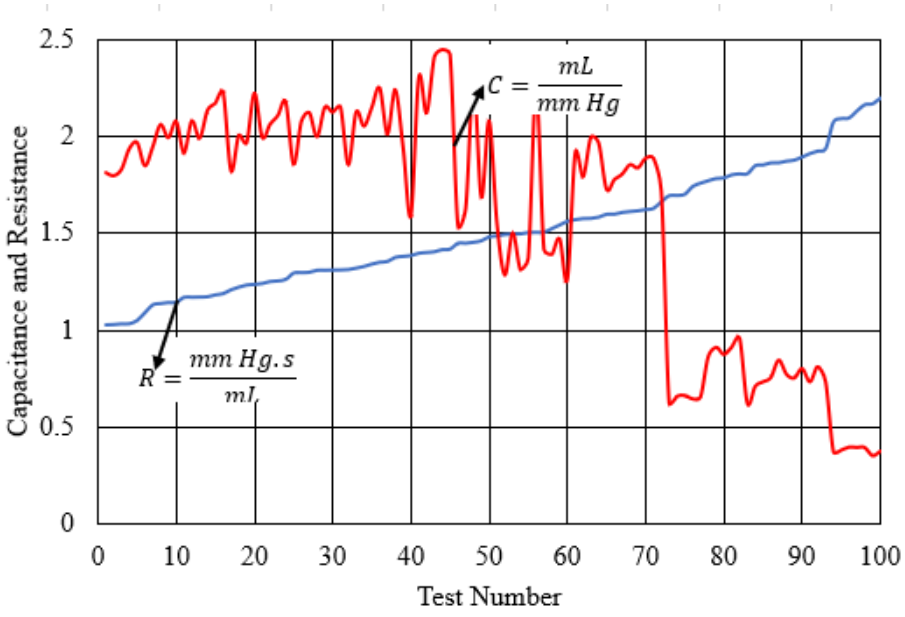

Figure 7-20. Experimental results for capacitance and resistance in the OX 7 aorta.

Figure 7-19 shows the arterial compliance from PWV close to the arterial compliance predicted by the model from pressure. The capacity storage of the aorta is reduced by increasing the peripheral resistance as shown in Fig. 7-20. That means the peripheral resistance causes an increase in mean arterial pressure which leads to an increase in the aorta diameter and a decrease in thickness of the aortic wall.

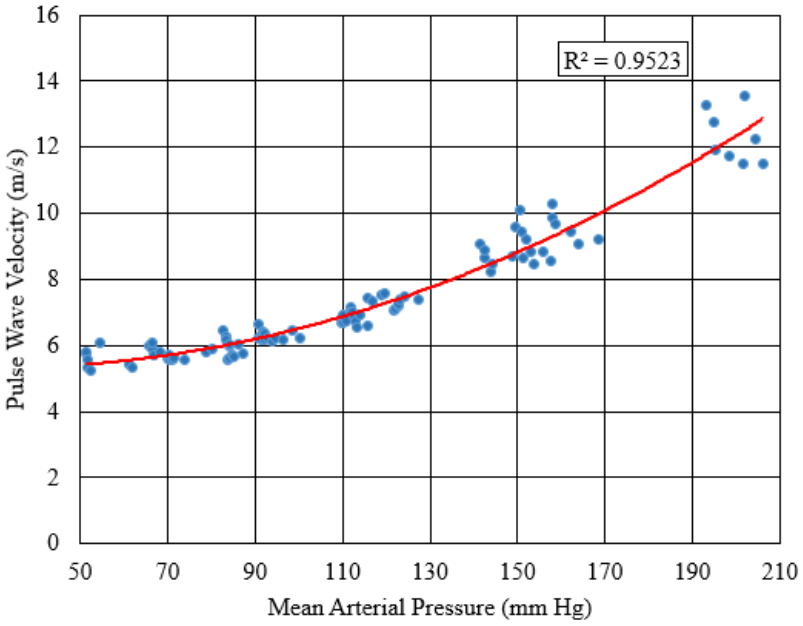

Figure 7-21. Power relationship between PWV and the main arterial pressure in OX 7 aorta.

Figure 7-21 displays a proportional correlation between the mean arterial pressure and pulse wave velocity PWV showing $R^2 = 0.95$ representing an excellent correlation between them. During the experiments, the increasing arterial mean pressure above 100 mm Hg seemed to lead to an increase of PWV and decrease in arterial compliance. That means with 100 mmHg the diameter of the aorta more increasing.

The results obtained from testing show that the pulse wave simulation created by the machine was useful way to understand how wave prorogation can change the pressure wave form.

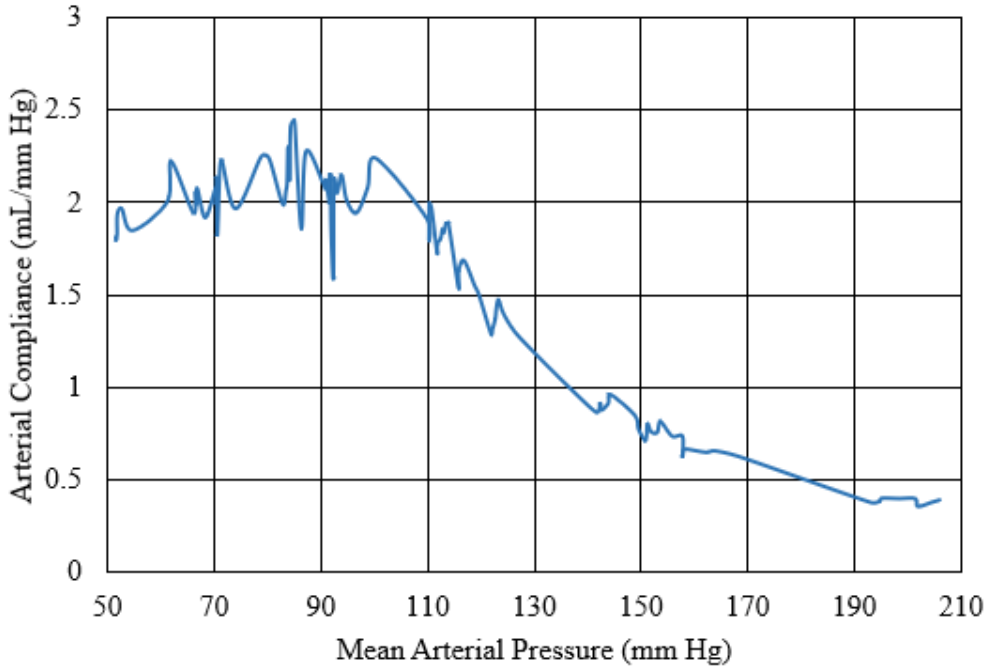

Figure 7-22. Experimental results for capacitance and mean arterial pressure in OX 7 aorta.

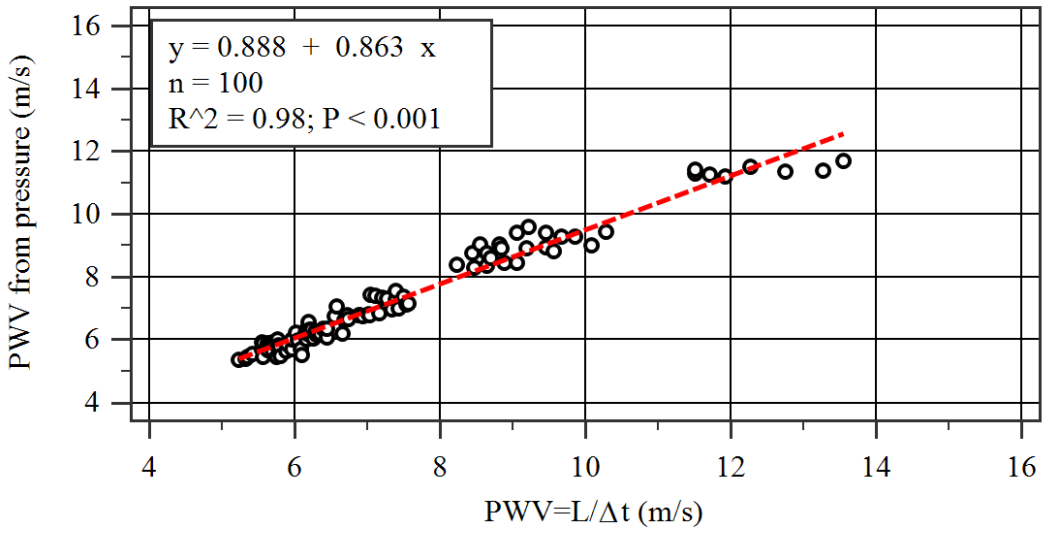

Figure 7-23. Scatter plot between the values of PWV from pressure and PWV from distance in the OX 6 aorta. Red solid line represent equality.

Figure 7-22 shows that the arterial compliance decreases with the increase in the main arterial pressure because increasing in diameter and decreasing in thickness of the wall of the aorta. That means an increase of mean arterial pressure will increase arterial stiffness and PWV. The steep decreasing starts after reaching mean arterial pressure 100 mm Hg.

In Figure 7-23, the results of the two ways of estimating PWV are in a good agreement and the small differences between the results of them come from different sources of error for instant human error and machine error.

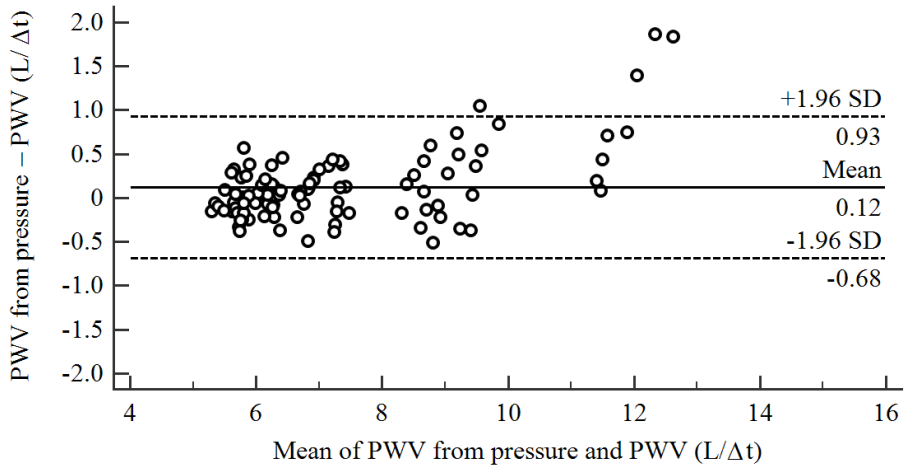

Figure 7-24. Agreement between PWV determined pressure and PWV determined from distance. The middle horizontal solid line indicates to the mean of difference of PWV determined by both methods. The upper and lower horizontal dashed lines indicate to 1.96 of the standard deviation.

In Figures 7-25 and 7-26, There are a significant inverse relationship between arterial compliance PWV. There is no significant difference between the two approaches to find arterial compliance.

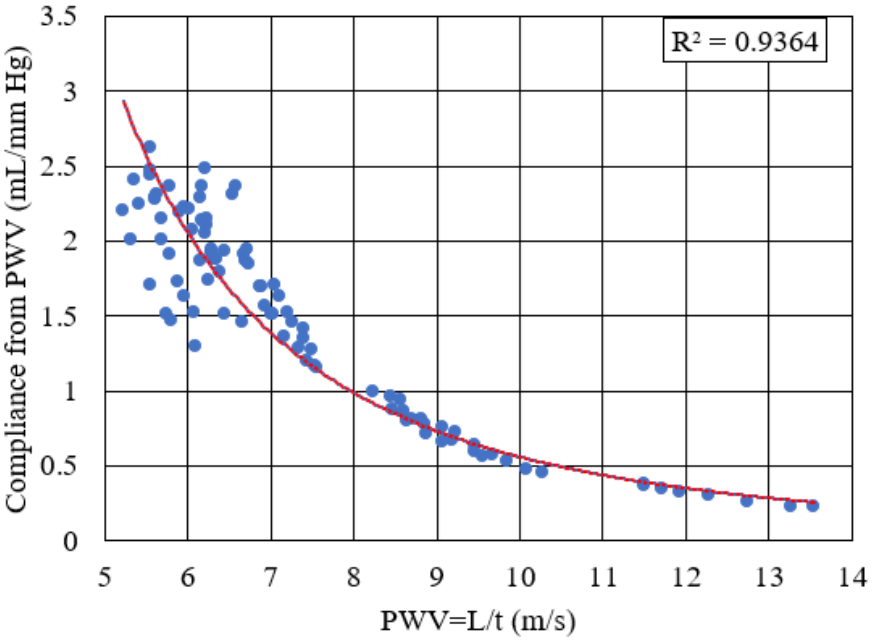

Figure 7-25. Power relationship between total arterial compliance from PWV equation and pulse wave velocity (PWV) OX 7.

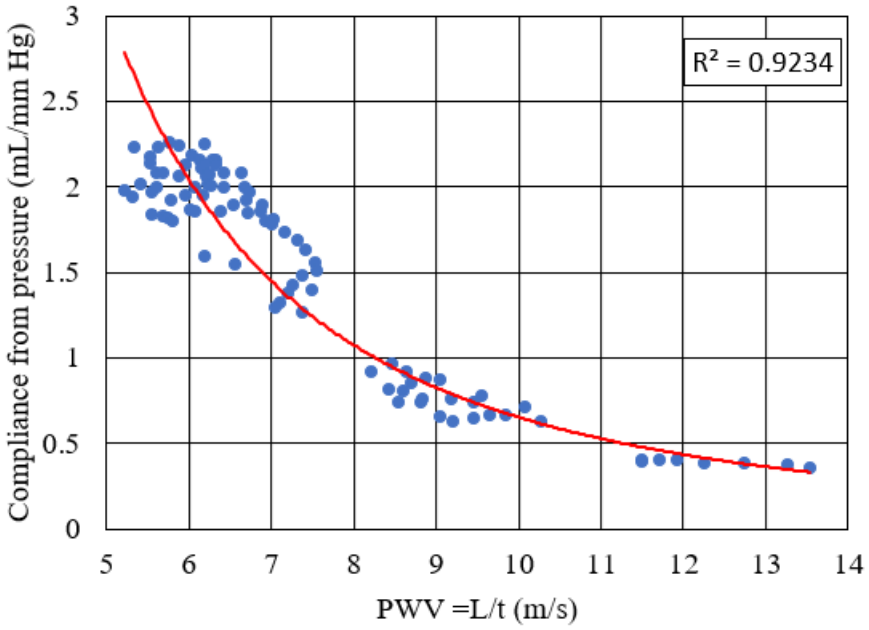

Figure 7-26. Power relationship between total arterial compliance from pressure and pulse wave velocity (PWV) OX 7.

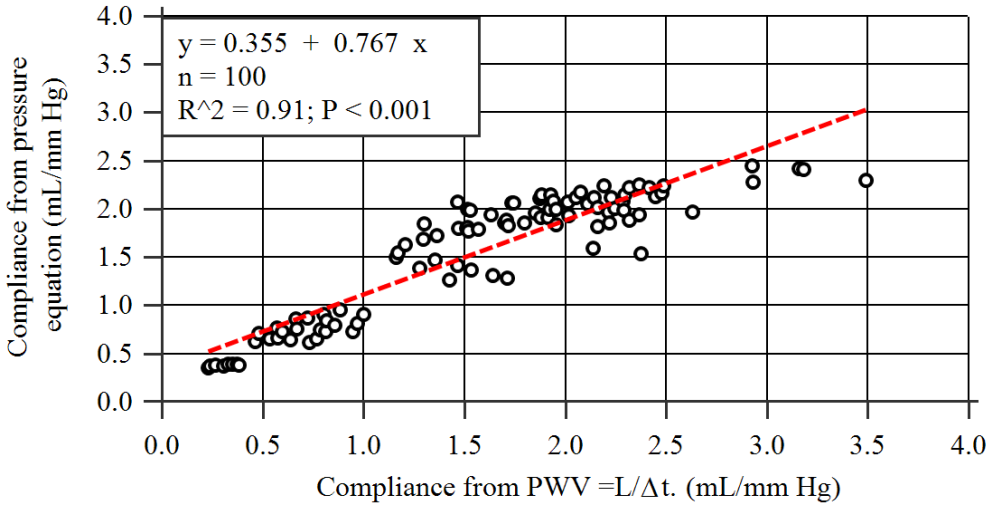

Figure 7-27. Scatter plot between the values of total arterial derived from PWV and total arterial compliance derived from pressure. Red solid line represents equality and a good agreement can be seen in this graph.

The results are summarized by Table 7-2. That shows a variety of different hemodynamic and vascular mechanical properties were simulated for the ox 7.

Table 7-2 Descriptive characteristics of the 101 tests for aorta of ox 7.

	Min	Max	Mean	SD
Aortic diastolic Pressure (mmHg)	43.5	130.1	84.72	24.85
Aortic systolic Pressure (mmHg)	58.2	212.5	110.29	38.11
Aortic pulse pressure (mmHg)	12.5	83.6	35.82	15.66
Mean arterial Pressure (mmHg)	51.35	168.96	97.39	31.2
Arterial compliance (mL/mmHg)	0.41	2.22	1.58	0.47
Peripheral Resistance (mmHg s/mL)	1.027	1.81	1.35	0.20
PWV (m/s)	5.22	10.27	6.65	1.17

Figure 7-27 displays the correlation between the mean arterial pressure and pulse wave velocity PWV showing $R^2 = 0.95$ representing an excellent correlation between them. During the experiments, the increasing arterial mean pressure above 100 mm Hg seemed to lead to an increase of PWV and decrease in arterial compliance. That means with 100 mmHg the tube diameter increasing.

The results obtained from testing show that the pulse wave simulation created by the machine was useful way to understand how wave prorogation can change the pressure wave form.

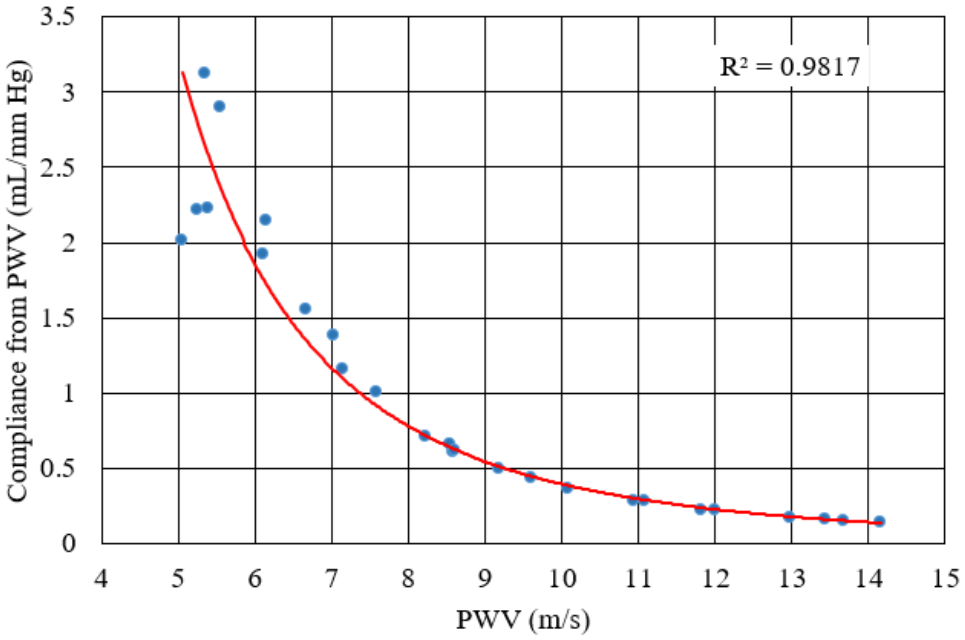

Figure 7-28. Experimental results for capacitance from PWV and PWV.

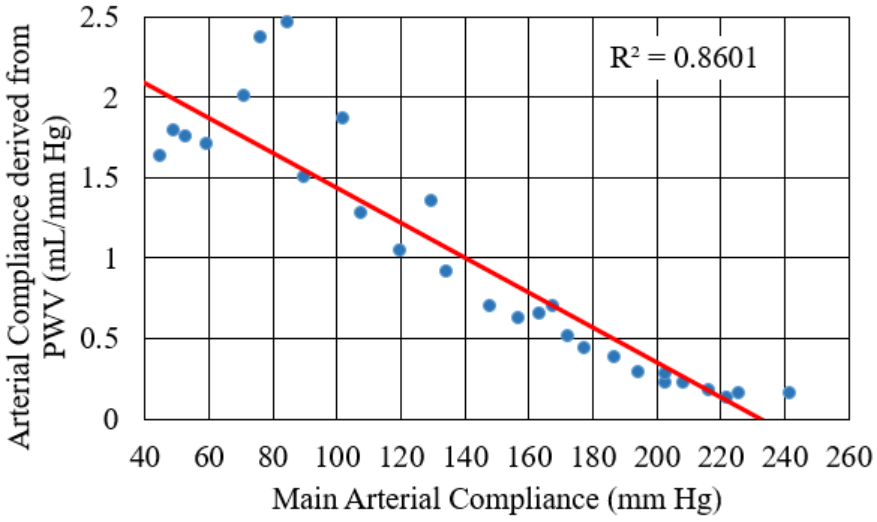

Figure 7-29. in the OX 7 aorta.

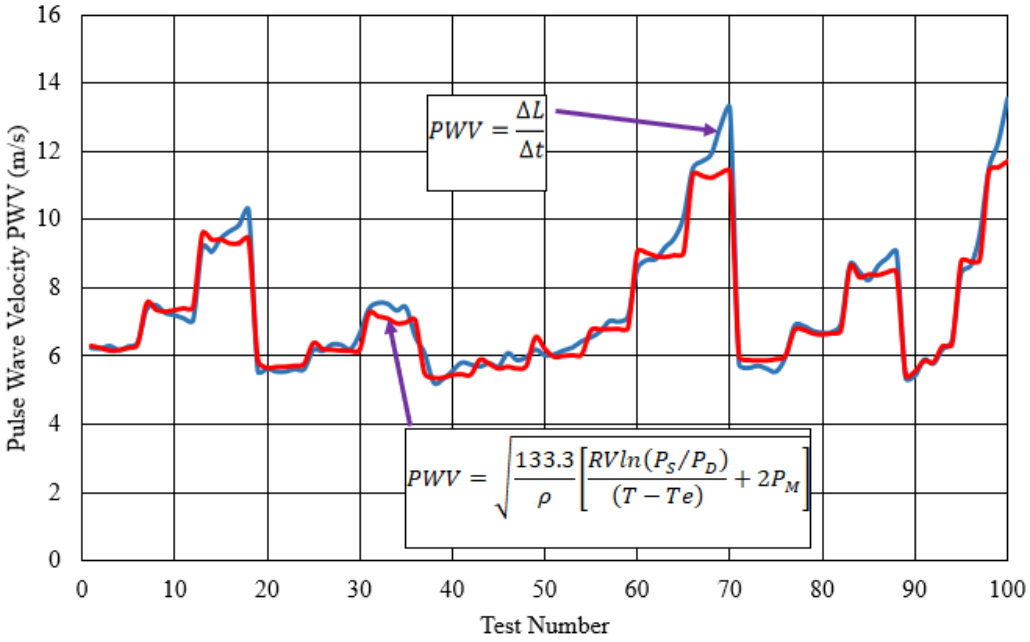

Figure 7-30. Plotting arterial compliance against test number in the OX 7 aorta and a good agreement can be seen in this graph.

Figure 7-28 clearly shows a relationship was established between pulse wave velocity (PWV) and the predicted values of the total arterial compliance via the fitted curve. PWV is considered as the gold standred method to estimate arterial stiffness [31], while aterial compliance is physiologically more relevant than aortic siffness. Compliance is an expression of the ability of the arterial system to store blood during systole without excessive pressure rise.

The complexity of the methods to estimate arterial compliance has limited these assessment, while PWV methods have been used more often [31].

There is a need for figuring out the coleration between PWV and the arterial compliance. More importantly, PWV is considered an independent predictor of hypertension and CV mortality [99].

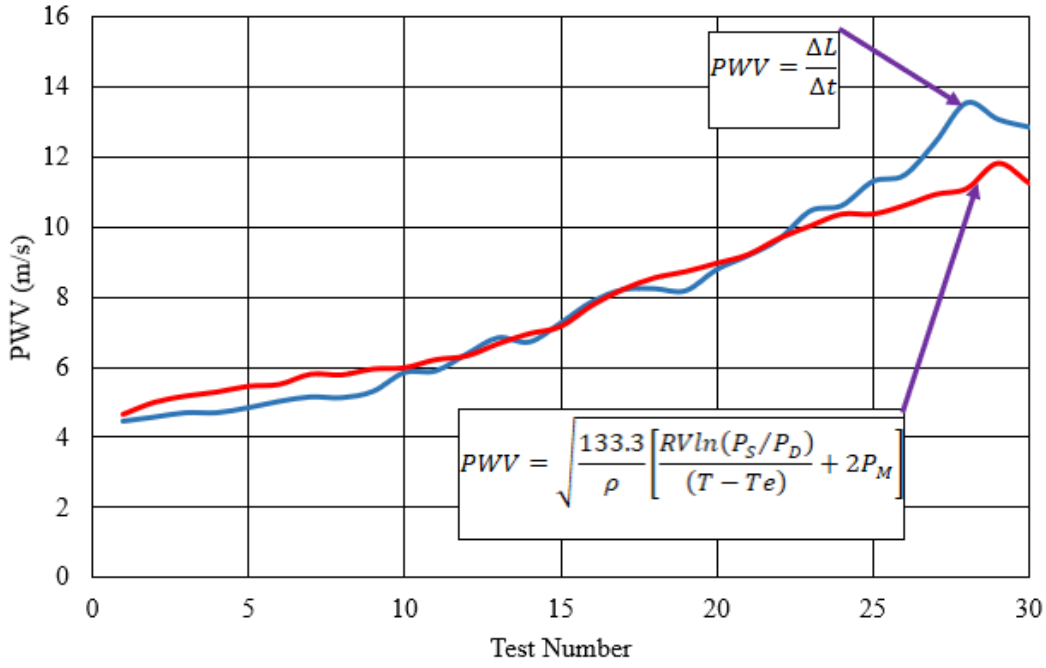

Figure 7-31. Plotting arterial compliance against test number in the cow 2 aorta and a good agreement can be seen in this graph.

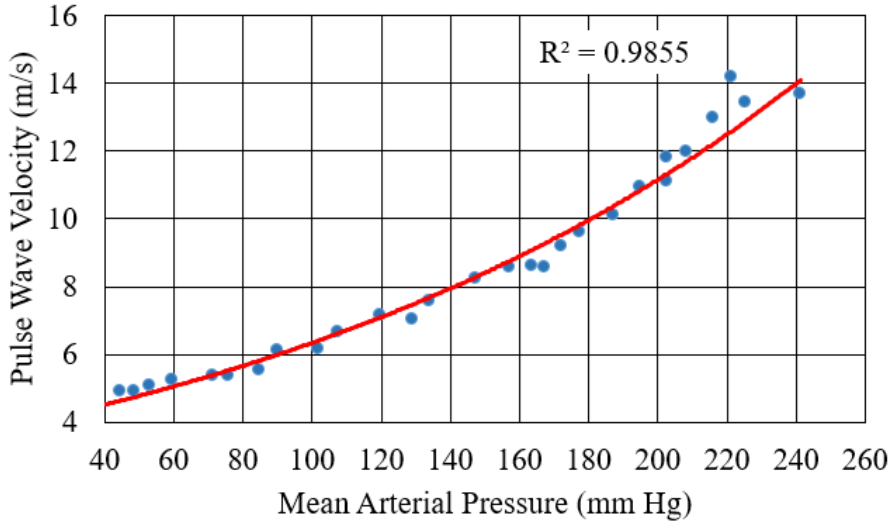

Figure 7-32.Shows the results of the PWV determined from foot-to- foot way and mean arterial pressure in the cow 2 aorta and a good agreement can be seen in this graph.

Figure shows that the PWV increases with the increase in the main arterial pressure because increasing in diameter and decreasing in thickness of the wall of the aorta. That means an increase of mean arterial pressure will increase arterial stiffness and PWV. Figure displays the correlation between the mean arterial pressure and pulse wave velocity PWV showing $R^2 = 0.98$ representing an excellent correlation between them. During the experiments, the increasing arterial mean pressure above 100 mm Hg seemed to lead to an increase of PWV and decrease in arterial compliance. That means with 100 mmHg the diameter of the aorta more increasing.

The results obtained from testing show that the pulse wave simulation created by the machine was useful way to understand how wave prorogation can change the pressure wave form.

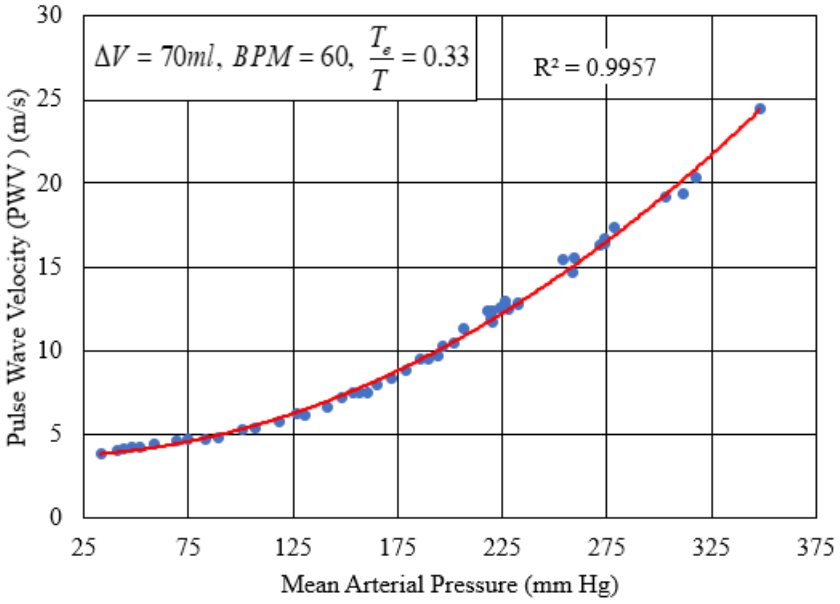

Figure 7-33. Shows the results of the PWV determined from foot-to- foot way and mean arterial pressure in the cow 2 aorta. The PWV is largely dependent on the mean arterial pressure.

Figure displays the correlation between the mean arterial pressure and pulse wave velocity PWV showing $R^2 = 0.99$ representing an excellent correlation between them. During the experiments, the increasing arterial mean pressure above 100 mm Hg seemed to lead to an increase of PWV and decrease in arterial compliance. That means with 100 mmHg the tube diameter increasing.

The results obtained from testing show that the pulse wave simulation created by the machine was useful way to understand how wave prorogation can change the pressure wave form.

7.4 Clinical Implications

During a normal visit to the doctor's office, a patient will have his or her blood pressure and heartrate measured by a nurse. As the previous analysis shows, these measurements describe three of the five cardiovascular parameters that must be measured in order to have a complete picture of the cardiovascular health of the patient. During an ordinary doctor's visit, the stroke volume and ejection period are not measured as these generally require an echocardiogram. However, without these two measurements from an echocardiogram a visit to the doctor's office may either mask a health problem or fail to reveal the root cause of high blood pressure. This fact is illustrated in the paragraphs that follow.

Table 7-3 is presented to illustrate a visit to the doctor's office that results in a "clean bill of health". In this table, three patients are described and each of them leaves the doctor's office with an assessment of good health based upon a measured systolic and diastolic pressure of 120 and 80 mm-Hg respectively, and a heartrate of 65 beats per

minute (BPM). As shown in Table 7-3, the Healthy Patient has a stroke volume and ejection period that are considered to be normal and healthy for an adult.

A healthy peripheral resistance is calculated to be 1.309 mm-Hg-s/mL and a healthy aortic capacitance is calculated as 1.218 mL/mm-Hg. These parameters are recorded in Table 7-3 for a healthy patient and will be used as the baseline for considering health deviations for other patients.

Table 7-3. Three combinations of cardiovascular parameters that will produce a blood pressure state of 120/80 for a heartrate of 65 BPM. Parentheses indicate a percent change from a healthy patient. Note: All table data is hypothetical for the purposes of illustration.

Parameter	Healthy Patient	Patient #1	Patient #2
Peripheral resistance, R [mm-Hg-s/mL]	1.309	1.832 (+40%)	1.313 (+1%)
Aortic capacitance, C [mL/mm-Hg]	1.218	0.870 (-29%)	1.041 (-15%)
Stroke volume, ΔV [mL]	70	50 (-29%)	70
Non-dimensional ejection period, T_e / T [no units]	0.300	0.300	0.400 (+33%)

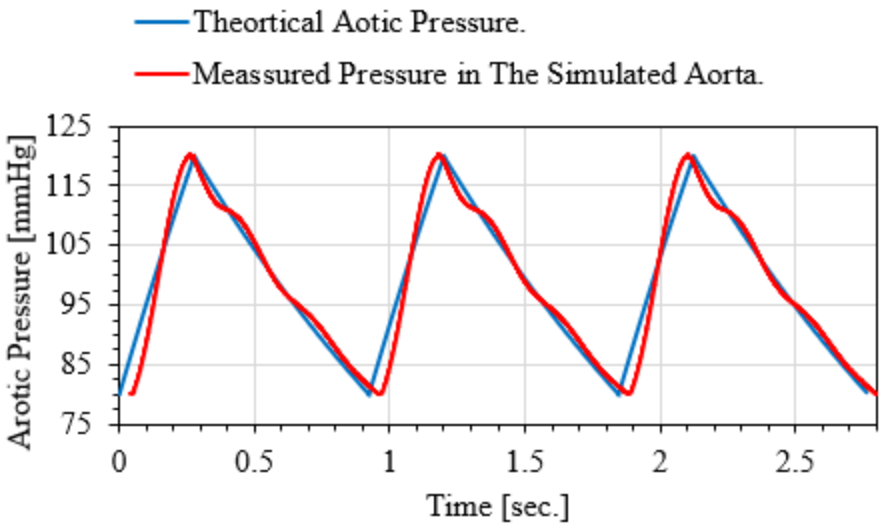

Figure 7-34. Comparison between theoretical aortic pressure and experimental aortic pressure for healthy patient.

The simulated aortic pressures for patients were plotted to demonstrate the difference between simulated and theoretical aortic pressure by using the variable compliance and resistance. The variable compliance was gotten by changing the air volume and the value of peripheral resistance was gotten by changing the needle valve. The theoretical aortic pressure was compared with experimental aortic pressure for healthy patient as shown in Fig.7-34 the characteristic differences on the pressure waveform are minimal.

As shown in Fig. 35 Patient #1 comes into the doctor's office and receives a clean bill of health from the examining nurse because the blood pressure measurements and the heartrate appear to be within a healthy range. However, this patient's heart is exhibiting a shallow stroke volume which produces a 29% reduction in cardiac output. In order for this patient to exhibit "healthy" blood pressure measurements, the peripheral resistance must be 40% higher than that of a healthy patient, and the aortic capacitance must be 29% lower. If the clinical visit had revealed this case, a doctor may not have considered

this patient to be healthy.

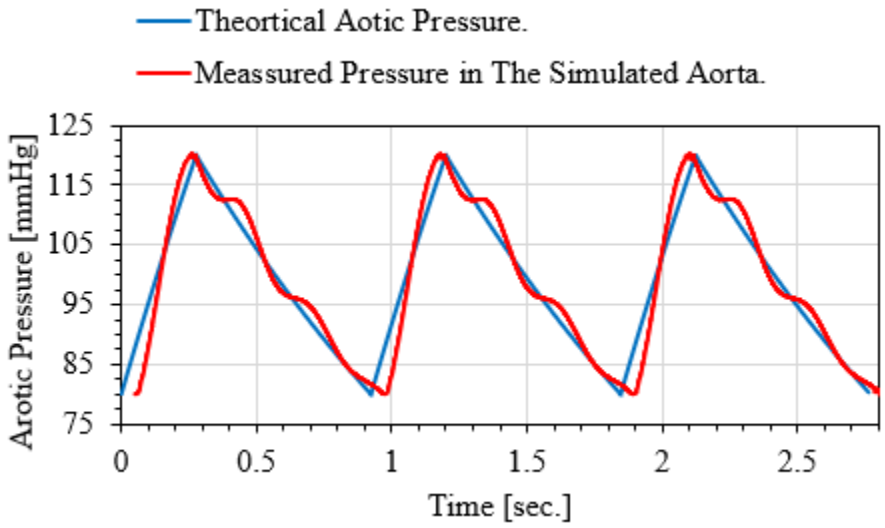

Figure 7-35. Comparison between theoretical aortic pressure and experimental aortic pressure for the patient #1.

Figure 7-35 has been created to show the aortic pressure of each theoretical aortic pressure and experimental aortic pressure patient#1. The difference between two pressure appear more clear than healthy patient but two pressure still close each other.

Figure 7-36 shows another case, where Patient #2 is examined and exhibits a healthy blood pressure and heartrate. In this case, the diastolic period of the heart has been reduced by an ejection period which has been extended 33%. Note: a reduced diastolic period may have a negative impact on coronary blood flow to the heart [10]. In order for this patient to exhibit "healthy" blood pressure measurements, the peripheral resistance remains essentially unchanged from that of a healthy patient, but the aortic capacitance has decreased by 15%. Again, if the clinical visit had revealed this condition, a doctor may not have considered this patient to be healthy.

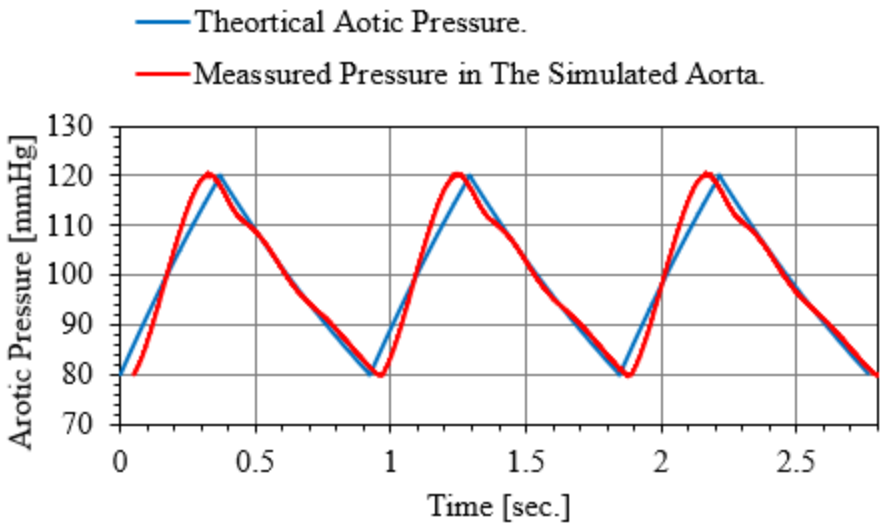

Figure 7-36. Comparison between theoretical aortic pressure and experimental aortic pressure for the patient #2.

The data in Fig. 7-36 shows the aortic theoretical and experimental aortic pressures for patient# 2. Apparently. the diastolic phase for each two pressures is almost same, but the systolic phase lightly differs for both pressures.

Table 7-4 is presented to illustrate a visit to the doctor's office that results in a clinical assessment where the systolic and diastolic pressures are 150 and 90 mm-Hg respectively, and the heart rate is 65 BPM. Based on this assessment, all three patients in Table 7-4 are diagnosed with high blood pressure with identical symptoms; however, the root cause for each diagnosis is significantly different. For instance, Patient #3 has a peripheral resistance and an aortic compliance that are typical of a healthy patient. The root cause for this patient's diagnosis is an overactive heart that has a 19% increase in stroke volume and a 61% decrease in the ejection period. If the doctor knew this by way of examination, perhaps the treatment plan would include a beta-blocker as opposed to a diuretic.

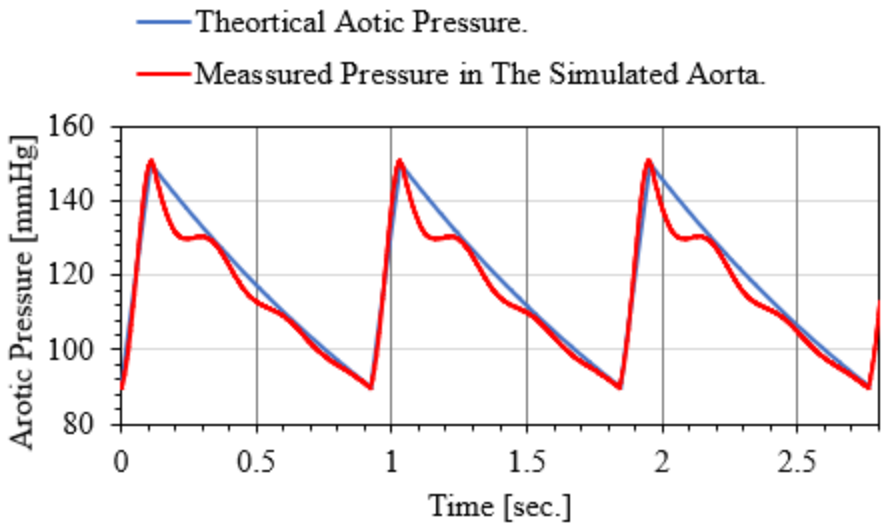

Figure 7-37. Comparison between theoretical aortic pressure and experimental aortic pressure for the patient #3.

The results, as seen in Fig. 7-37 for the patient#3 indicate that the systolic phase for both theoretical and experimental aortic pressure is exactly at the same, but there is clear difference between these pressure in the diastolic phase.

On the other hand, Patient #4 shows a normal heart function but the peripheral resistance has increased 19% while the aortic capacitance has decreased by 34%. A treatment for this patient may include a diuretic as opposed to a beta-blocker.

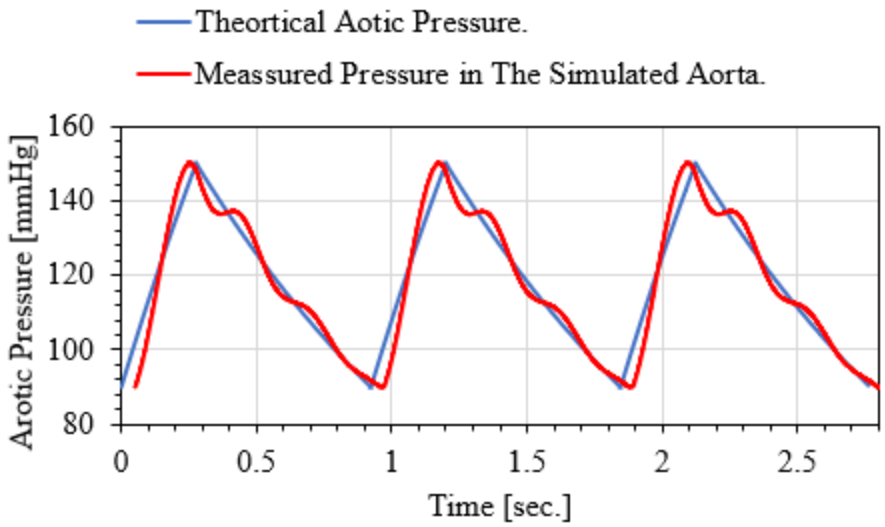

Figure 7-38. Comparison between theoretical aortic pressure and experimental aortic pressure for the patient #4.

The shape of pressure plotting for each theoretical and experimental aortic pressures the same at the patient #1 but different systolic and diastolic pressure as shown in Fig. 7-38.

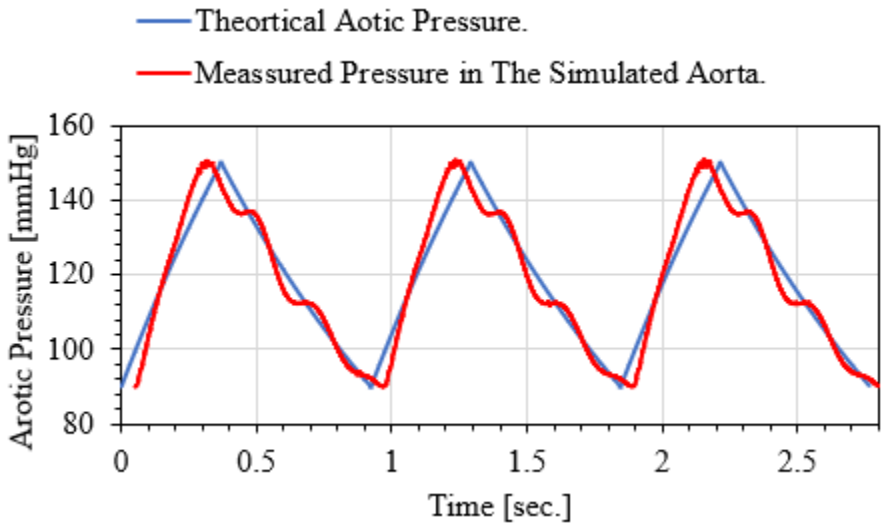

Figure 7-39. Comparison between theoretical aortic pressure and experimental aortic pressure for patient #5.

Patient #5 is presented to illustrate a combination of abnormalities that have produced the high blood pressure diagnosis. The treatment for this patient may be more

complicated.

Comparison was made between the measured pressure in the simulated aorta for patient #5 and the theoretical aortic pressure as shown in Fig. 7-39. The simulated aortic pressure is close to that on a body.

Table 7-4. Three combinations of cardiovascular parameters that will produce a high blood pressure state of 150/90 for a heartrate of 65 BPM. Parentheses indicate a percent change from a healthy patient shown in Table 7-4. Note: All table data is hypothetical for the purposes of illustration.

Parameter	Patient #3	Patient #4	Patient #5
Peripheral resistance, R [mm-Hg-s/mL]	1.309	1.563 (+19%)	2.2 (+68%)
Aortic capacitance, C [mL/mm-Hg]	1.218	0.809 (-34%)	0.493 (-60%)
Stroke volume, ΔV [mL]	83 (+19%)	70	50 (-29%)
Non-dimensional ejection period, T_e / T [no units]	0.118 (-61%)	0.3	0.4 (+33%)

As shown in Fig. 7-39. the cardiovascular health of a patient cannot be truly assessed by using the clinical measures of blood pressure and heartrate alone. In order to make a full assessment of cardiovascular health, doctors need to know the stroke volume and ejection period of the heart in addition to the traditional measures of blood pressure and heartrate.

7.5 Conclusions

An extensively increasing interest in the understanding of arterial compliance plays a crucial role in proper medical diagnosis and prognosis. The experiments that have been done have the goal of calculating the arterial compliance in three ways mechanical capacitance, pulse wave velocity, and compliance computed from blood pressure. Comparing their results shows a good agreement.

In our study, we found the arterial compliance that was computed from blood pressure is very close to these computed from pulse wave velocity. The arterial compliance computed from blood pressure is more reliability than these computed from pulse wave velocity. Because the identification of the onset points of the sharp upstroke of the systolic ascending waveforms were determined by human eyes because of the lack of using EKG signal in our research.

The difference in computing the arterial compliance between mechanical capacitance and the way from blood pressure is within an acceptable range. The way from blood pressure explain that arterial compliance depends on blood pressure, heartrate, stroke volume and ejection period. That means the arterial compliance is not constant and it limitedly varies with changing in those parameters.

This research opens the possibility to estimate pulse wave velocity mean arterial pressure, stroke volume, heart rate, ejection period and initial volume of the artery.

Our findings provide possible mechanistic insight that PWV is associated with mean arterial pressure. We noticed the compliance at low heart rate is higher than at high heart rate, but the peripheral resistance at low heart rate is lower than at high heart rate.

The heart is a positive displacement pump that pushes blood in cardiovascular vessels. Resistance against blood flow is as a load. This load consists of the peripheral resistance, and also the arterial compliance, so decreased compliance increases this load. When the total peripheral resistance increases, or the arterial compliance decreases this load becomes greater.

CHAPTER 8. CONCLUSIONS AND RECOMMENDATIONS

8.1 Conclusions

We assessed cardiovascular properties by developing new novel methods for estimating the major arterial parameters which are arterial stiffness, peripheral resistance, and PWV. Research questions and main findings drawn from this research work are

- An increase in the peripheral resistance will increase all pressure measurements in the aorta, while slightly increasing the pulse pressure.
- Increased peripheral resistance is stamp of establish high blood pressure, but altered compliance also probably contributes to the raised blood pressure.
- The mean arterial pressure depends on three parameters; stroke volume, heartrate and peripheral resistance while pulse pressure depends on forward wave and reflected wave.
- Increasing in peripheral resistance leads to increase systolic and diastolic pressures while increasing in arterial stiffness leads to increase systolic pressure and decrease diastolic pressure.
- The compliance, and ejection period have no impact on the mean arterial pressure.
- The blood pressure diagram gives us a visualization about a body size and its peripheral resistance and arterial compliance.
- An increase in the stroke volume increases all pressure measurements proportionally, including the pulse pressure.

- An increase in the heartbeat period, corresponding to a slower heartrate, decreases the cardiac output thereby lowering all pressures, while slightly lowering the pulse pressure.
- Increasing ejection period (T_e) has an almost negative impact on pulse pressure.
- Increasing heart rate (T) has a more negative impact on diastolic pressure than systolic pressure and a positive impact on pulse pressure.
- Decreasing arterial compliance (C) has a more negative impact on pulse pressure than systolic and diastolic pressures.
- There is a non-relationship between PWV and mean arterial pressure. A small variation in low PWV cause wide variation in mean arterial pressure, but this variation in the pressure be less with variation at high PWV.

8.2 Recommendation for Future Work

Several recommendations for further work can be summarized in the following points:

- It could be informative to study the effect of the blood viscosity on the pulse wave velocity by using distilled water and solution of ethyl alcohol at deferent concentration.
- The mechanical properties such as Young modulus of arterial system changes with various conditions such as hypertension, ageing.
- PWV Measuring is affected by reflecting site which is the needle valve. It would be useful to improve that by making the needle valve relatively far away from measurement sites.

- Using MRI to measure PWV avoids the error that induced between two transducer pressure sites.
- Studying effect of the gravity force on PWV by setting up the simulated aorta in vertical position instead of horizontal.

REFERENCES

[1] A. C. Guyton and J. Hall, "Text book of medical physiology 8th ed," *VVB Saunders, Philadelphia*, pp. 159-169, 1991.

[2] N. M. Kaplan, *Kaplan's clinical hypertension*. Lippincott Williams & Wilkins, 2010.

[3] R. Hajar, "Risk factors for coronary artery disease: historical perspectives," *Heart views: the official journal of the Gulf Heart Association*, vol. 18, no. 3, p. 109, 2017.

[4] A. H. Association, "Heart disease and stroke statistics 2017 at-a-glance," *Geraadpleegd van: https://healthmetrics. heart. org/wp-content/uploads/2017/06/Heart-Disease-and-Stroke-Statistics-2017-ucm_491265. pdf*, 2017.

[5] M. R. Alfonso, R. L. Armentano, L. J. Cymberknop, A. R. Ghigo, F. M. Pessana, and W. E. Legnani, "A novel interpretation for arterial pulse pressure amplification in health and disease," *Journal of healthcare engineering*, vol. 2018, 2018.

[6] H. A. J. AL-Ziarjawey and I. Çankaya, "Heart rate monitoring and PQRST detection based on graphical user interface with Matlab," *International Journal of Information and Electronics Engineering*, vol. 5, no. 4, p. 311, 2015.

[7] D. Lewandowski, "The creation and exploration of the pneumatic and hydraulic simulation models," 2000: Scientific books of Kielce University of Technology, XII National Conference ….

[8] C. E. Molina, J. Heijman, and D. Dobrev, "Differences in left versus right ventricular electrophysiological properties in cardiac dysfunction and arrhythmogenesis," *Arrhythmia & electrophysiology review*, vol. 5, no. 1, p. 14, 2016.

[9] W. Parandyk, D. Lewandowski, and J. Awrejcewicz, "Mathematical Modeling of the Hydro-Mechanical Fluid Flow System on the Basis of the Human Circulatory System," *Nonlinear Dynamics and System Theory*, vol. 15, no. 1, 2015.

[10] B. Baumgartner, A. Mendoza, S. Eichhorn, U. Schreiber, and A. Knoll, "A comparative study on extra-corporal circulation control," in *2011 Annual International Conference of the IEEE Engineering in Medicine and Biology Society*, 2011: IEEE, pp. 4287-4290.

[11] C. Vlachopoulos, M. O'Rourke, and W. W. Nichols, *McDonald's blood flow in arteries: theoretical, experimental and clinical principles*. CRC press, 2011.

[12] P. Salvi, "Pulse waves," *How vascular hemodynamics affects Blood pressure*, 2012.

[13] J. Blacher, R. Asmar, S. Djane, G. M. London, and M. E. Safar, "Aortic pulse wave velocity as a marker of cardiovascular risk in hypertensive patients," *Hypertension*, vol. 33, no. 5, pp. 1111-1117, 1999.

[14] D. J. Korteweg, *Over voortplantings-snelheid van golven in elastische buizen*. Van Doesburgh, 1878.

[15] A. Tijsseling and A. Anderson, "CASA-Report 12-42 December 2012," 2012.

[16] G. Androutsos, M. Karamanou, and C. Stefanadis, "William Harvey (1578-1657): discoverer of blood circulation," *Hellenic J Cardiol*, vol. 53, no. 1, pp. 6-9, 2012.
[17] K. H. Parker, "A brief history of arterial wave mechanics," *Medical & biological engineering & computing*, vol. 47, no. 2, pp. 111-118, 2009.
[18] M. Capoccia, "Development and Characterization of the Arterial W indkessel and Its Role During Left Ventricular Assist Device Assistance," *Artificial organs*, vol. 39, no. 8, pp. E138-E153, 2015.
[19] M. Żyliński *et al.*, "Individualization of the parameters of the three-elements Windkessel model using carotid pulse signal," in *Photonics Applications in Astronomy, Communications, Industry, and High-Energy Physics Experiments 2015*, 2015, vol. 9662: International Society for Optics and Photonics, p. 96621N.
[20] S. Kamoi *et al.*, "Accuracy of stroke volume estimation via reservoir pressure concept and three element Windkessel model," *IFAC Proceedings Volumes*, vol. 47, no. 3, pp. 5647-5652, 2014.
[21] P. Charlton, J. Smith, L. Camporota, R. Beale, and J. Alastruey, "Optimising the Windkessel model for cardiac output monitoring during changes in vascular tone," in *2014 36th Annual International Conference of the IEEE Engineering in Medicine and Biology Society*, 2014: IEEE, pp. 3759-3762.
[22] J. Ruel and G. Lachance, "Mathematical modeling and experimental testing of three bioreactor configurations based on windkessel models," *Heart international*, vol. 5, no. 1, 2010.
[23] M. Hlaváč and J. Holčík, "Windkessel model analysis in matlab," in *Proceedings of 10th conference STUDENT EEICT*, 2004, no. 3, p. 5.
[24] A. Tsanas *et al.*, "The Windkessel model revisited: a qualitative analysis of the circulatory system," *Medical engineering & physics*, vol. 31, no. 5, pp. 581-588, 2009.
[25] A. D. Choudhury, R. Banerjee, A. Sinha, and S. Kundu, "Estimating blood pressure using Windkessel model on photoplethysmogram," in *2014 36th Annual International Conference of the IEEE Engineering in Medicine and Biology Society*, 2014: IEEE, pp. 4567-4570.
[26] D. Guan, F. Liang, and P. A. Gremaud, "Comparison of the Windkessel model and structured-tree model applied to prescribe outflow boundary conditions for a one-dimensional arterial tree model," *Journal of biomechanics*, vol. 49, no. 9, pp. 1583-1592, 2016.
[27] G. Ortiz-León, M. Vílchez-Monge, and J. J. Montero-Rodríguez, "Simulations of the cardiovascular system using the cardiovascular simulation toolbox," in *5th Workshop on Medical Cyber-Physical Systems*, 2014: Schloss Dagstuhl-Leibniz-Zentrum fuer Informatik.
[28] N. Stergiopulos, J.-J. Meister, and N. Westerhof, "Determinants of stroke volume and systolic and diastolic aortic pressure," *American Journal of Physiology-Heart and Circulatory Physiology*, vol. 270, no. 6, pp. H2050-H2059, 1996.
[29] N. Fazeli and J.-O. Hahn, "Estimation of cardiac output and peripheral resistance using square-wave-approximated aortic flow signal," *Frontiers in physiology*, vol. 3, p. 298, 2012.

[30] I. Kokalari, T. Karaja, and M. Guerrisi, "Review on lumped parameter method for modeling the blood flow in systemic arteries," *Journal of biomedical science and engineering,* vol. 6, no. 01, p. 92, 2013.
[31] E. Maksuti, N. Westerhof, B. E. Westerhof, M. Broomé, and N. Stergiopulos, "Contribution of the arterial system and the heart to blood pressure during normal aging–a simulation study," *PloS one,* vol. 11, no. 6, p. e0157493, 2016.
[32] O. Ghasemalizadeh, M. R. Mirzaee, B. Firoozabadi, and K. Hassani, "Exact modeling of cardiovascular system using lumped method," *arXiv preprint arXiv:1411.5337,* 2014.
[33] B. Chen *et al.*, "A simplified computer model of cardiovascular system with an arm branch," *Bio-medical materials and engineering,* vol. 24, no. 6, pp. 2555-2561, 2014.
[34] T. Du, D. Hu, and D. Cai, "Outflow boundary conditions for blood flow in arterial trees," *PLoS One,* vol. 10, no. 5, p. e0128597, 2015.
[35] V. de los Reyes, "A mathematical model for the cardiovascular system with a measurable pulsatile pressure output," PhD thesis, University of Graz, Institute for Mathematics and Scientific …, 2010.
[36] Y. Wu, P. E. Allaire, G. Tao, and D. Olsen, "Modeling, estimation, and control of human circulatory system with a left ventricular assist device," *IEEE transactions on control systems technology,* vol. 15, no. 4, pp. 754-767, 2007.
[37] T. Parlikar, T. Heldt, G. Ranade, and G. Verghese, "Model-based estimation of cardiac output and total peripheral resistance," in *2007 Computers in Cardiology,* 2007: IEEE, pp. 379-382.
[38] R. Gul, C. Schütte, and S. Bernhard, "Mathematical modeling and sensitivity analysis of arterial anastomosis in the arm," *Applied Mathematical Modelling,* vol. 40, no. 17-18, pp. 7724-7738, 2016.
[39] R. Roy, D. N. Riahi, and N. Carrasquero, "Mathematical Modeling of Blood Flow in an Artery with an Unsteady Stenosis using Power-Law Fluid Model," *SOP Transactions on Applied Mathematics,* vol. 1, no. 1, pp. 2373-8480.
[40] V. Srivastava, S. Mishra, and R. Rastogi, "Non-Newtonian arterial blood flow through an overlapping stenosis," *Applications and Applied Mathematics,* vol. 5, no. 1, pp. 225-238, 2010.
[41] S. R. Shah and S. Siddiqui, "Two-phase model for the study of blood flow through stenosed artery," *International Journal of Pharmacy and Biological Sciences,* vol. 1, no. 3, pp. 246-254, 2011.
[42] N. Manring, "The effective fluid bulk-modulus within a hydrostatic transmission," *Journal of dynamic systems, measurement, and control,* vol. 119, no. 3, pp. 462-466, 1997.
[43] W. Tsai and Ö. Savaş, "Flow pumping system for physiological waveforms," *Medical & biological engineering & computing,* vol. 48, no. 2, pp. 197-201, 2010.
[44] T. Chen, M. Diciolla, M. Kwiatkowska, and A. Mereacre, "A simulink hybrid heart model for quantitative verification of cardiac pacemakers," in *Proceedings of the 16th international conference on Hybrid systems: computation and control,* 2013: ACM, pp. 131-136.
[45] L. Taura, I. Ishiyaku, and A. Kawo, "The use of a continuity equation of fluid mechanics to reduce the abnormality of the cardiovascular system: A control

mechanics of the human heart," *Journal of Biophysics and Structural Biology*, vol. 4, no. 1, pp. 1-12, 2012.
[46] J. R. Gohean, M. J. George, T. D. Pate, M. Kurusz, R. G. Longoria, and R. W. Smalling, "Verification of a computational cardiovascular system model comparing the hemodynamics of a continuous flow to a synchronous valveless pulsatile flow left ventricular assist device," *ASAIO journal (American Society for Artificial Internal Organs: 1992)*, vol. 59, no. 2, p. 107, 2013.
[47] V. Creigen *et al.*, "Modeling a heart pump," *European Study Group Mathematics with Industry*, vol. 7, 2007.
[48] A. Pironet, P. C. Dauby, S. Paeme, S. Kosta, J. G. Chase, and T. Desaive, "Simulation of left atrial function using a multi-scale model of the cardiovascular system," *PloS one*, vol. 8, no. 6, p. e65146, 2013.
[49] A. Aurelio, "Dynamics of a cardiovascular model obtaining measurable pulsatile pressure output," *World Journal of Modelling and Simulation*, vol. 11, no. 1, pp. 20-32, 2015.
[50] A. de los Reyes V and F. Kappel, "Modeling pulsatility in the human cardiovascular system," 2010.
[51] S. Gregory, N. Greatrex, D. Timms, N. Gaddum, M. J. Pearcy, and J. F. Fraser, "Simulation and enhancement of a cardiovascular device test rig," *Journal of Simulation*, vol. 4, no. 1, pp. 34-41, 2010.
[52] R. Chaudhary, A. Prakash, and C. Gupta, "Comparison of Different ECG Signals on MATLAB," *International Journal of Electronics and Computer Science Engineering*, vol. 2, no. 2, 2013.
[53] J. S. Lillie, A. S. Liberson, and D. A. Borkholder, "Quantification of hemodynamic pulse wave velocity based on a thick wall multi-layer model for blood vessels," *Journal of Fluid Flow, Heat and Mass Transfer*, vol. 3, 2016.
[54] P. D. Morris *et al.*, "Computational fluid dynamics modelling in cardiovascular medicine," *Heart*, vol. 102, no. 1, pp. 18-28, 2016.
[55] S. Petrescu and V. Enache, "Applying the Finite Speed Thermodynamics (FST) to the Human Cardiovascular System," in *National Conference of Thermodynamics (NACOT)*, 2013.
[56] R. C. Cascaval, C. D'Apice, and M. P. D'Arienzo, "Simulation of heart rate variability model in a network," in *AIP Conference Proceedings*, 2017, vol. 1863, no. 1: AIP Publishing, p. 560054.
[57] H. Gharahi, B. A. Zambrano, D. C. Zhu, J. K. DeMarco, and S. Baek, "Computational fluid dynamic simulation of human carotid artery bifurcation based on anatomy and volumetric blood flow rate measured with magnetic resonance imaging," *International journal of advances in engineering sciences and applied mathematics*, vol. 8, no. 1, pp. 46-60, 2016.
[58] P. Nithiarasu, "Robust Finite Element Approaches to Systemic Circulation Using the Locally Conservative Galerkin (LCG) Method," *Proceedings of the Indian National Science Academy*, vol. 82, no. 2, 2016.
[59] R. Gul and S. Bernhard, "Parametric uncertainty and global sensitivity analysis in a model of the carotid bifurcation: Identification and ranking of most sensitive model parameters," *Mathematical biosciences*, vol. 269, pp. 104-116, 2015.

[60] R. Gul and S. Bernhard, "Local sensitivity analysis of cardiovascular system parameters," *WIT Trans Biomed Health*, vol. 17, pp. 155-167, 2013.
[61] K. Cameron, D. H. Freed, and D. S. Nobes, "Time-resolved PIV of the pulsatile flow from an ex vivo heart perfusion model."
[62] F. He, L. Hua, and L.-j. Gao, "A computational model for biomechanical effects of arterial compliance mismatch," *Applied bionics and biomechanics*, vol. 2015, 2015.
[63] N. Xiao, J. Alastruey, and C. Alberto Figueroa, "A systematic comparison between 1-D and 3-D hemodynamics in compliant arterial models," *International journal for numerical methods in biomedical engineering*, vol. 30, no. 2, pp. 204-231, 2014.
[64] P. Segers, P. Steendijk, N. Stergiopulos, and N. Westerhof, "Predicting systolic and diastolic aortic blood pressure and stroke volume in the intact sheep," *Journal of biomechanics*, vol. 34, no. 1, pp. 41-50, 2001.
[65] A. Campo *et al.*, "Comparison between multi-channel LDV and PWI for measurement of pulse wave velocity in distensible tubes: Towards a new diagnostic technique for detection of arteriosclerosis," *Optics and Lasers in Engineering*, vol. 97, pp. 41-51, 2017.
[66] H. Obeid, H. Khettab, L. Marais, M. Hallab, S. Laurent, and P. Boutouyrie, "Evaluation of arterial stiffness by finger–toe pulse wave velocity: optimization of signal processing and clinical validation," *Journal of hypertension*, vol. 35, no. 8, pp. 1618-1625, 2017.
[67] J.-J. Wang, S.-H. Liu, T. Kao, W.-C. Hu, and C.-P. Liu, "Noninvasive determination of arterial pressure-dependent compliance in young subjects using an arterial tonometer," *Biomedical Engineering: Applications, Basis and Communications*, vol. 18, no. 03, pp. 111-118, 2006.
[68] Z. Keshavarz-Motamed, J. Garcia, P. Pibarot, E. Larose, and L. Kadem, "Modeling the impact of concomitant aortic stenosis and coarctation of the aorta on left ventricular workload," *Journal of biomechanics*, vol. 44, no. 16, pp. 2817-2825, 2011.
[69] D. B. McCombie, A. T. Reisner, and H. H. Asada, "Adaptive blood pressure estimation from wearable PPG sensors using peripheral artery pulse wave velocity measurements and multi-channel blind identification of local arterial dynamics," in *2006 International Conference of the IEEE Engineering in Medicine and Biology Society*, 2006: IEEE, pp. 3521-3524.
[70] A. Benetos *et al.*, "A decrease in diastolic blood pressure combined with an increase in systolic blood pressure is associated with a higher cardiovascular mortality in men," *Journal of the American College of Cardiology*, vol. 35, no. 3, pp. 673-680, 2000.
[71] N. Manring, *Hydraulic control systems*. Wiley, 2005.
[72] M. ECOBICI and C. STOICESCU, "Arterial Stiffness and Hypertension–Which Comes First?," *Maedica*, vol. 12, no. 3, p. 184, 2017.
[73] A. P. Boresi, R. J. Schmidt, and O. M. Sidebottom, *Advanced mechanics of materials*. Wiley New York et al., 1985.
[74] G. F. Carrier and C. E. Pearson, *Partial differential equations: theory and technique*. Academic Press, 2014.

[75] D. Halpern, H. B. Wilson, and L. H. Turcotte, *Advanced mathematics and mechanics applications using MATLAB*. Chapman and Hall/CRC, 2002.
[76] S. i Carós and J. Maria, "Continuous non-invasive blood pressure estimation," ETH Zurich, 2011.
[77] T. G. Papaioannou *et al.*, "Total arterial compliance, estimated by a novel method, is better related to left ventricular mass compared to aortic pulse wave velocity: The SAFAR study," *Clinical and Experimental Hypertension*, vol. 39, no. 3, pp. 271-276, 2017.
[78] O. Vardoulis, T. G. Papaioannou, and N. Stergiopulos, "On the estimation of total arterial compliance from aortic pulse wave velocity," *Annals of biomedical engineering*, vol. 40, no. 12, pp. 2619-2626, 2012.
[79] J. C. Bramwell and A. V. Hill, "The velocity of pulse wave in man," *Proceedings of the Royal Society of London. Series B, Containing Papers of a Biological Character*, vol. 93, no. 652, pp. 298-306, 1922.
[80] N. Westerhof and D. R. Gross, *Vascular dynamics: physiological perspectives*. Springer Science & Business Media, 2013.
[81] A. International, *ASTM D638-14, Standard Test Method for Tensile Properties of Plastics*. ASTM International, 2015.
[82] Z. Zi, "Sensitivity analysis approaches applied to systems biology models," *IET systems biology*, vol. 5, no. 6, pp. 336-346, 2011.
[83] A. M. Dart, "Should pulse pressure influence prescribing?," *Australian prescriber*, vol. 40, no. 1, p. 26, 2017.
[84] T. Girum, T. Shumbej, and M. Shewangizaw, "Burden of malaria in Ethiopia, 2000-2016: findings from the Global Health Estimates 2016," *Tropical Diseases, Travel Medicine and Vaccines*, vol. 5, no. 1, p. 11, 2019.
[85] Å. Hjalmarson, "Heart rate: an independent risk factor in cardiovascular disease," *European Heart Journal Supplements*, vol. 9, no. suppl_F, pp. F3-F7, 2007.
[86] H. J. White and J. Borger, "Anatomy, Abdomen and Pelvis, Aorta," in *StatPearls [Internet]*: StatPearls Publishing, 2019.
[87] G. G. Belz, "Elastic properties and Windkessel function of the human aorta," *Cardiovascular Drugs and Therapy*, vol. 9, no. 1, pp. 73-83, 1995.
[88] H.-L. Kim and S.-H. Kim, "Pulse wave velocity in atherosclerosis," *Frontiers in cardiovascular medicine*, vol. 6, 2019.
[89] E. J. Benjamin, P. Muntner, and M. S. Bittencourt, "Heart disease and stroke statistics-2019 update: a report from the American Heart Association," *Circulation*, vol. 139, no. 10, pp. e56-e528, 2019.
[90] G. Burnstock and S. G. Griffith, *Nonadrenergic Innervation of Blood Vessels: Regional Innervation*. CRC Press, 2019.
[91] N. Stergiopulos, J. Meister, and N. Westerhof, "Evaluation of methods for estimation of total arterial compliance," *American Journal of Physiology-Heart and Circulatory Physiology*, vol. 268, no. 4, pp. H1540-H1548, 1995.
[92] G. A. Holzapfel, G. Sommer, C. T. Gasser, and P. Regitnig, "Determination of layer-specific mechanical properties of human coronary arteries with nonatherosclerotic intimal thickening and related constitutive modeling," *American Journal of Physiology-Heart and Circulatory Physiology*, vol. 289, no. 5, pp. H2048-H2058, 2005.

[93] S. Laurent *et al.*, "Expert consensus document on arterial stiffness: methodological issues and clinical applications," *European heart journal,* vol. 27, no. 21, pp. 2588-2605, 2006.
[94] R. Asmar *et al.*, "Assessment of arterial distensibility by automatic pulse wave velocity measurement: validation and clinical application studies," *Hypertension,* vol. 26, no. 3, pp. 485-490, 1995.
[95] C. Ting, M. Chang, S. Wang, B. Chiang, and F. C. Yin, "Regional pulse wave velocities in hypertensive and normotensive humans," *Cardiovascular research,* vol. 24, no. 11, pp. 865-872, 1990.
[96] E. Kazanavicius, R. Gircys, A. Vrubliauskas, and S. Lugin, "Mathematical methods for determining the foot point of the arterial pulse wave and evaluation of proposed methods," *Information Technology and control,* vol. 34, no. 1, 2005.
[97] J. Sola, S. F. Rimoldi, and Y. Allemann, "Ambulatory monitoring of the cardiovascular system: the role of pulse wave velocity," *New Developments in Biomedical Engineering,* pp. 391-424, 2010.
[98] J. Radhakrishnan, "Changes in arterial stiffness and other cardiovascular risk variables following specific exercise programmes," Buckinghamshire New University, 2013.
[99] S. Laurent *et al.*, "Aortic stiffness is an independent predictor of all-cause and cardiovascular mortality in hypertensive patients," *Hypertension,* vol. 37, no. 5, pp. 1236-1241, 2001.

VITA

The author Mouayed Hassan Ziada AL-Toki was born in April 1970 in Baghdad, Iraq. The focus of Mouayed's Ph.D. research was how to estimate the arterial compliance (elasticity of arteries) of the cardiovascular system, and he supported his work with many of experiments by using a simulator machine for the cardiovascular system. Mouayed achieved his Ph.D. research under the guidance of Professor Noah D. Manring at the Mechanical & Aerospace Engineering Department in the University of Missouri-Columbia.

His primary interest is in hydraulic systems, and he worked for years as a maintenance engineer for the hydraulic machines. Earlier he received his B.Sc. in Mechanical Engineering/Air-conditioning & Refrigeration in University of Technology-Baghdad in 1992, and then his M.Sc. in Mechanical Engineering in University of Technology-Baghdad in 2004. In December 2017, he got his Master of Engineering (in Mechanical & Aerospace Engineering) from University of Missouri – Columbia College of Engineering.